

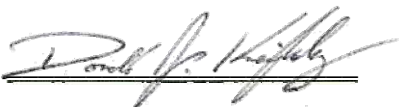
**P-WAVE TIME-LAPSE SEISMIC DATA INTERPRETATION
AT RULISON FIELD, PICEANCE BASIN, COLORADO**


by
Donald J. Keighley

A thesis submitted to the Faculty and the Board of Trustees of the Colorado School of Mines in partial fulfillment of the requirements for the degree of Master of Science (Geophysics).

Golden, Colorado

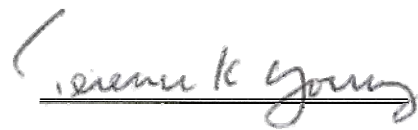
Date 5/10/06

Signed: 
Donald J. Keighley

Approved: 
Dr. Thomas L. Davis
Thesis Advisor

Golden, Colorado

Date May 15, 2006


Dr. Terence K. Young
Professor and Head,
Department of Geophysics

ABSTRACT

Two dedicated P-wave time-lapse seismic surveys, shot by the Reservoir Characterization Project in the fall of 2003 and 2004, at Rulison Field, Piceance basin, Colorado, exhibit production induced changes in this tight gas reservoir over the period of one year. Time shifts measured at the base of this reservoir indicate velocity increases near some producing wells. An initial simple model of the time-lapse response due to pressure decline in the Williams Fork, based on ultrasonic core measurements and diagnostic fracture initiation tests, is consistent with these observed shifts. Negative time shifts are also present and may be the result of noise or a mechanism of time-lapse change that was not included in modeling. Impedance changes of nearly ten percent are measured in the Cameo Coal interval of the Williams Fork Formation. These changes indicate production from this interval. The large magnitude of these changes is related to the presence of coal in this part of the reservoir, and indicates production from or stress changes in the coals. Faults, located near these anomalies, appear to act as conduits for production from this deeper zone. Few changes are observed in tight sands and shales of the Upper Williams Fork, indicating that the Lower Williams Fork may be the more productive and better connected member of the formation. In all, this study shows that high repeatability 4D seismic can monitor tight gas reservoirs, to a limited extent, over a short period of time. Repeat surveys and integration with engineering data are necessary to tie the time-lapse response to production and reservoir pressure change, so that seismic may be used as a tool to predict well performance prior to drilling.

TABLE OF CONTENTS

ABSTRACT.....	iii
TABLE OF CONTENTS.....	iv
LIST OF FIGURES	vi
LIST OF TABLES.....	xi
CHAPTER 1: INTRODUCTION	1
1.1 Introduction.....	1
1.2 Objective	3
1.3 Background.....	3
1.4 Rulison Field.....	6
1.4.1 Geologic setting	6
1.4.2 Production history and practices.....	10
1.5 Methodology	13
CHAPTER 2: SEISMIC DATA	15
2.1 Survey Design.....	15
2.2 Processing	23
CHAPTER 3: DATA PREPARATION.....	27
3.1 Introduction.....	27
3.2 Correlation Time Shift	29
3.3 Shaping Filter.....	35
3.4 Comparison Gain	43
3.5 Time-variant Time Shift	48
3.6 Inversion	52
3.6.1 Considerations.....	52
3.6.2 Colored Inversion.....	53

CHAPTER 4: MODELING	61
4.1 Introduction	61
4.2 Input Data	61
4.3 Methodology	66
4.4 Results	69
4.5 Model Assumptions and Shortcomings	72
CHAPTER 5: INTERPRETATION	75
5.1 Time Shift Analysis	75
5.1.1 Repeatability	76
5.1.2 Observations and Interpretation	80
5.1.3 Conclusions	89
5.2 Amplitude Analysis	90
5.2.1 Repeatability	91
5.2.2 Observations and Interpretation	95
CHAPTER 6: CONCLUSIONS AND FUTURE WORK	105
6.1 Conclusions	105
6.2 Future Work	106
REFERENCES	109

LIST OF FIGURES

Figure 1.1 - The Piceance basin is located in northwestern Colorado. The edges of the basin are noted by the maroon outline. The top of the Rollins is contoured. Rulison field is shown in bright red (Koepsell et al., 2003).....	6
Figure 1.2 - This paleogeographic map of the Piceance basin area during the late Cretaceous shows the distribution of environments that produced various formations (Cumella and Ostby, 2003) (Blakey, 2003).	7
Figure 1.3 - A generalized stratigraphic column for Rulison field with the seismic reflectors of the UMV shale and the upper Cameo coal denoted (Cole and Cumella, 2003).	9
Figure 1.4 - An idealized cross section of the Piceance basin shows the gently dipping southwestern flank and the steeply dipping northeastern flank. It also indicates the distribution of water and gas in this basin-centered gas accumulation (Cumella and Ostby, 2003).....	11
Figure 1.5 - The workflow used for interpretation is shown above.....	14
Figure 2.1 - The locations of many different pieces of information relative to the RCP seismic survey area.....	16
Figure 2.2 - The I/O Vectorseis sensor is inserted into a hole drilled in the ground for maximum coupling (adapted from (I/O, 2006).	18
Figure 2.3 - The locations of the source and receiver positions were repeated very closely in both 2003 (green) and 2004 (red).....	19
Figure 2.4 - The RCP survey has very high maximum fold (225) but it quickly diminishes toward the edges of the survey.	20
Figure 2.5 - The distribution of the differences between the source and receiver positions quantifies how repeatable the geometry was.	21
Figure 2.6 - Raw field station 1038 indicates the severity of the drilling noise in the 2004 survey at some locations.....	22
Figure 2.7 - The final source and receiver statics are relatively consistent between years.....	25
Figure 3.1 - The correlation values calculated from the cross-correlation time shift process.....	30
Figure 3.2 - The calculated correlation time shifts.	30

Figure 3.3 - Difference sections before and after the application of the cross correlation time shift indicate that the step is effective in reducing differences.	32
Figure 3.4 - The NRMS maps over the static section before and after the application of the cross-correlation time shift are shown above.	33
Figure 3.5 - The histograms of the NRMS maps in Figure 3.4 before and after the application of the cross-correlation time shift are shown above.	34
Figure 3.6 - The 2003 volume has more high frequency content before the application of the shaping filter. After the shaping filter the two are closely matched.	36
Figure 3.7 - The areal extent of the traces used in designing the shaping filter is shown above.....	38
Figure 3.8 - The global shaping filter applied to the 2003 seismic volume is shown above.....	38
Figure 3.9 - The difference sections before and after the application of the shaping filter are shown above. They indicate that the shaping filter was effective in reducing differences between the volumes.	40
Figure 3.10 - The NRMS maps before and after the application of the shaping filter are shown above. They indicate that the shaping filter reduced differences between the surveys.	41
Figure 3.11 - The histograms of the NRMS maps show that the repeatability of the data has been improved by the shaping filter.....	42
Figure 3.12 - The calculated comparison gain factors vary considerably. The edges and the two zones in the north show significant variations. The source and receiver positions are overlaid in the lower two maps to indicate that a lack of fold and offsets in the north may have caused this....	44
Figure 3.13 - The difference section after the application of the comparison gain appears to show lower difference between the two volumes.	45
Figure 3.14 - The NRMS maps of the static section indicate that the static section repeatability improved with the application of the comparison gain.	46
Figure 3.15 - The histograms of the NRMS maps indicate that the comparison gain improved the repeatability in the static section.	47
Figure 3.16 - A cross section before and after the application of the time-variant time shift indicate a slight improvement in repeatability at depth after the application of the shift.....	49
Figure 3.17 - NRMS maps of the static section before and after the application of the time-variant time shift indicate very slight improvements after the application of the shift.	50
Figure 3.18 - The histograms of the NRMS maps indicate very slight improvements in the static section after the application of the time-variant time shift.	51

Figure 3.19 - The log impedance log frequency crossplot indicates that the relationship is very linear. The derived colored inversion operator is shown on top and it basically resembles a -90 ° phase shifted wavelet.	56
Figure 3.20 - This figure illustrates the fact that the seismic data lacks low frequencies. This is compensated for in the inversion process by adding information from wells. The blue curve indicates the information that is added to the idealized seismic amplitude spectrum in red.	57
Figure 3.21 - The smoothed acoustic impedance model that was added to the seismic to provide low frequency information was derived from well RWF 332-21.	57
Figure 3.22 - The inversion is very consistent with the original seismic data. There is almost no difference between the real data and the synthetic data derived from the inverted volume.	58
Figure 3.23 - The inverted seismic data falls within the range of impedance values found in the logs; however, due to a lack of high frequencies, it cannot resolve thin beds.	59
Figure 3.24 - A tuning curve indicates that in the Cameo coal zone the tuning thickness is approximately 30-ft.	60
Figure 4.1 - The mini-frac data from two wells at Rulison is shown above. The blue lines indicate virgin pore-pressure and the red line indicates 35% depletion. The well on the left is assumed to be virgin while the well on the right is depleted from production	64
Figure 4.2 - Above wellhead pressure is shown in black and production is shown in red for well RWF 443-20. The time-lapse interval is shaded. The pressure drop is nearly 1800 psi over only a few months.	65
Figure 4.3 - P-wave velocity vs. effective-pressure as measured by Eugenia Rojas is shown above. The black line is an exponential relationship fitted to the data (Rojas, 2005).	65
Figure 4.4 - The calculated values of α for every perforated sand in well RWF 332-21. The average value, $\alpha = 0.55$, is shown in red.	67
Figure 4.5 - The scaled and unscaled modeled changes of effective-pressure are shown above for two values of α	68
Figure 4.6 - The calculated cross-correlation time shifts between the modeled data and the original data. The results indicate that time shifts will be very small and cannot indicate individual producing zones.	70
Figure 4.7 -The percent impedance change between the modeled and original data. The results indicate that impedance changes will be very small but will be able to identify large individual or groups of producing zones.	71
Figure 5.1 -Difference maps of the statics corrections between years indicate that the solutions are generally consistent, but that there are isolated differences up to 5 ms.	79

Figure 5.2 - The source and receiver statics crossplots indicate that the statics are consistent between the two years even though they were calculated independently.	79
Figure 5.3 - A section through the time-variant time shift volume indicates that there is an accumulated positive shift of nearly 0.7-ms. An overlay of one of the modeled scenarios shows that it is consistent with modeling where the shifts are positive.	81
Figure 5.4 - A map of the derived cross-correlation time shifts shows that within the region of high fold, the time shift is predominantly positive.....	82
Figure 5.5 - The shift does not appear to be the result of low correlation values as the correlation values are nearly all above 0.95.	83
Figure 5.6 - The time shift at the RC-2 with a 0.5-ms mask indicates that there are very few shifts over 0.5-ms. All wells that produced in the time-lapse interval are shown. The high fold zone is shown in green. The wells associated with anomalies are circled.	84
Figure 5.7 - The production at each well in the high fold zone during the time-lapse interval shows that the four wells associated with the largest time-shift anomalies (black arrows) are not the highest producers.	86
Figure 5.8 - The time shift at the Cameo with the total production during the time-lapse period indicated in red dots. There is a general correlation, but there is not a direct correlation between high production and high time shifts.....	87
Figure 5.9 - A cross plot of production vs. the time shift averaged over a 350-ft radius around each well location shows that there is no relationship between the two.....	88
Figure 5.10 - The calculated time shifts for varying sums of producing sand thickness for different pore pressure declines indicate that time shift interpretation is complicated at Rulison.	88
Figure 5.11 - The maximum absolute impedance changes over the static section indicate the noise level to be approximately 4% in the highest fold portion of the survey. The solid black line indicates the low noise zone. The black and blue dashed circles indicate the approximate locations of the oil-shale plant and garbage dump respectively.....	93
Figure 5.12 - The percent seismic amplitude difference maps at the UMV and the Cameo before the application of the comparison gain process.	94
Figure 5.13 - The maximum absolute percent impedance change from the UMV to the Cameo is very similar to the same map over the static section indicating that the changes are at or below the noise level. There is one significant anomaly at the Clough-19 well (circled in black).	95
Figure 5.14 - The anomaly at the Clough-19 is associated with perforations. The perforations are the black lines perpendicular to the wellbore.	96
Figure 5.15 - The maximum absolute percent impedance change from the UMV to the Cameo has no relationship to production.	97

Figure 5.16 - The maximum absolute impedance changes in the Lower Williams Fork are significantly larger than the changes in the Upper Williams Fork. The black circles indicate wells that began production during the time-lapse interval.....	99
Figure 5.17 - An impedance change map from the RC3 level of the Lower Williams Fork is shown above. The dashed black circle indicates a possible real anomaly.....	100
Figure 5.18 - Cross sections through the impedance volumes between years 2003 and 2004 indicate some impedance changes in the Lower Williams Fork.....	101
Figure 5.19 - The impedance changes in the RC3 coal are located near faults interpreted from coherency volumes.	101
Figure 5.20 - Image logs indicate that the coals can be fractured or unfractured.	103

LIST OF TABLES

Table 2.1 -The specifications of the data recording system are shown below (Input/Output, 2005)....	17
Table 2.2 - The P-wave processing flow is shown below. Independent indicates that the process was calculated separately for each volume.	23
Table 3.1 - The parameters used in the design of the shaping filter are shown in this table.	37

CHAPTER 1: INTRODUCTION

1.1 Introduction

The Reservoir Characterization Project (RCP) focuses on incorporating multi-component and time-lapse seismic data with conventional reservoir characterization techniques to see a more complete and dynamic picture of the reservoir. Phases X and XI, of which this thesis is a part, are no different. The objective of Phases X and XI is to monitor and explain the production at Rulison field so that it can be produced more effectively. However, Rulison field is quite different than past fields studied by the RCP and poses new and difficult challenges (Davis, 2003).

For instance, Rulison is not imaged well by conventional seismic. It consists primarily of a large interval of stacked tight fluvial sandstones and shales. These beds are below seismic resolution and are not always well-defined. Also, the sands are not clean and therefore have impedances similar to the shales. This leads to low impedance contrasts and poor seismic imaging in the reservoir. The thickness of the interval, nearly 3000 feet makes traditional horizon-based interpretation methods difficult.

The low permeability of the sandstones within the reservoir complicates the picture. Natural and artificial fracturing is necessary to achieve economic flow rates. Also, very tight well spacing (20-acres or less) must be implemented to drain the reservoir (Cumella and Ostby, 2003). Therefore, to effectively produce the field, natural fracture networks must be identified along with drained and undrained reservoir compartments. Current practice involves using 3D seismic to identify structures that could indicate fracturing. Unfortunately, this method does not directly find natural

fractures or indicate where production has already occurred. For this type of information unconventional data, like multi-component and time-lapse seismic, must be used.

To improve understanding of Rulison, the RCP, in cooperation with Williams Production RMT Company, the field operator, acquired two multi-component seismic surveys that encompass part of Williams' 10-acre pilot program and about 75 wells. The surveys were acquired in November of 2003 and September of 2004 by Solid State and are processed for time-lapse purposes by Veritas DGC. The 2003 data are also processed for time-lapse comparison with a 1996 Department of Energy (DOE) P-wave survey. A multi-component vertical seismic profile (VSP) and dipole sonic logs were acquired in order to calibrate the seismic. In addition to these new data, the study area is near a DOE-funded study known as the Multi-Well Experiment (MWX) that drilled, cored, and analyzed three very closely-spaced wells. These data aid in the characterization of the field.

Techniques like shear-wave seismic data interpretation can indicate the presence of fracture swarms and their orientation. Geomechanical modeling based on log, core, and microseismic analysis can give important information on the current and paleo-stress states of the reservoir. These can be used for production modeling, the placement of wells, and frac-job design. Conventional seismic interpretation, combined with outcrop study and geologic modeling, can provide the distribution and structure of the different reservoir lithologies.

Time-lapse seismic is the only source of field-scale information about physical changes occurring in the reservoir over time. It is sensitive to fluid and pressure changes, therefore making it an excellent tool for monitoring production or injection. Knowing the extent of pressure changes within the reservoir is not only important from the standpoint of locating new wells, it is also important in that it can serve as a check for reservoir simulation models. Time-lapse synthetic seismic models based on reservoir simulation models should not result in changes bigger or smaller than what is seen in the actual data.

Also, if the model is run over the same time interval as the time-lapse field acquisition then changes in the model should be in the same locations as changes in the real data.

Thus, time-lapse data can be used for more than simply locating extracted or injected fluids. It can be used as an input into other reservoir characterization processes, and can therefore serve as a way of checking other interpretations of field properties. It is for these reasons that I have decided to interpret the time-lapse P-wave seismic data at Rulison.

1.2 Objective

The objective of this research is to interpret the P-wave time-lapse survey taken at Rulison field in the fall of 2003 and 2004. A realistic model of expected time-lapse change at Rulison is used to estimate the seismic response of production. Time shifts and amplitude changes in reflectors between years are used to interpret the time-lapse data.

1.3 Background

At this point you may be saying to yourself, "This sounds a lot like other time-lapse work that I've seen. What's new about this project?" It is true that this workflow is similar to many other time-lapse projects that have been done. However, most of those projects are carried out in the deep water basins of the Gulf of Mexico and the North Sea. They are generally looking at very porous and relatively soft rocks. Often there are drastic fluid saturation changes, phase changes, pressure changes, or a combination of all three. Fluid saturation and phase changes are often the key to success in these studies since they yield faster larger changes than pressure alone. In many cases, a specific well-defined reservoir is targeted.

For instance, time-lapse seismic monitoring of the Draugen field in the North Sea was used to map water encroachment into oil zones (Gabriels et al., 1999). The Nelson, field, also in the North Sea, successfully integrated forward models, based on rock physics measurements, to image oil water contact movement (Boyd-Gorst et al., 2001). In the Lena field, a Gulf of Mexico oil field composed of a series of separated thick well imaged turbidite sandstones, Exxon was able to monitor gas cap expansion and water movement (Eastwood et al., 1998). SEG distinguished instructor Rodney Calvert offers many examples of successful time-lapse applications in his short course, but nearly all are North Sea examples with large signals due to fluid injection or gas coming out of solution. The land cases he does mention are simply repeatability studies (Calvert, 2005). There has in fact been a good deal of time-lapse work done on land. It has been used to successfully aid in using steam to recover heavy oil (Eastwood et al., 1994). The RCP has used it on land to monitor carbon dioxide injection in fields like Vacuum and Weyburn. Crosswell time-lapse data have even been used to prove the concept of monitoring primary production from coal in the Powder River Basin in Wyoming (Akintunde, 2005).

This, however, is the first case of a dedicated time-lapse survey being used to image production in a tight gas reservoir. Prior to my work, Mahendra Kusuma, another RCP student, used a legacy P-wave survey to monitor production regionally and from individual sand bodies. His work focused on a Department of Energy survey from 1996 and the 2003 RCP survey used in this study. After parallel processing of the two surveys and cross-equalization, he found velocity anomalies at individual sandstones, though the increase was on the order of 50%. Even over a period seven years, a fifty-percent velocity increase is unrealistic (Kusuma, 2005). Therefore, more accurate estimates of the changes are necessary so that the time-lapse data may be used in reservoir simulation.

Another time-lapse survey of a tight gas reservoir was performed by Hall et al. using legacy data over the Southern Gas Basin in the North Sea. As at Rulison, the permeability in the Southern Gas Basin is low, 20-40 μD , and the only expected change

in the reservoir is pressure depletion of approximately 1800 psi. Forward modeling indicated that only 2-6% impedance decreases were expected at the top of the reservoir. The surveys, shot in 1992 and 1999, were not intended for time-lapse purposes, and therefore underwent reprocessing and rigorous cross-equalization. The matching process involved a spatial warping procedure to correct for mispositioning. Interpretation of the equalized volumes indicated mixed results. Some modest negative anomalies were found that corresponded to zones of pressure depletion. However, the areas of largest pressure decline showed almost no response, while other areas even showed positive anomalies. Time shifts of approximately 2.4-ms were also found, though it was unclear how to correctly interpret them. The authors concluded that time-lapse showed promise for monitoring production in tight gas sandstones, but that dedicated surveys are necessary.

The time-lapse study at Rulison is also unique in that it is not targeting a well-defined reservoir unit. Instead it targets a nearly 3000-ft thick interval of thin interbedded sandstones, shales, and coals that are at or below the lower limits of seismic resolution. In addition, the beds, as determined through outcrop study and seismic observations, are not laterally continuous throughout the reservoir for long distances.

Therefore, this work is research. The methods applied are not new, and in fact are standard time-lapse techniques. However, monitoring of tight gas sandstone reservoirs, using land dedicated 4D seismic surveys, has never before been done.

It is the intent of this work to improve upon previous work to assess the feasibility of short period time-lapse monitoring in tight gas sandstones, and if successful, contribute to the characterization of Rulison field. Interpreting the time-lapse data at Rulison is important because it works to answer several questions that could improve understanding of the field. These are questions like: "Can production in tight gas reservoirs be monitored?", "Where are the depleted reservoir units?", "What lithologies produce gas?", and "What are the controls on production?" The work presented in this thesis provides partial answers to these questions and provides a foundation for future work that can fully do so.

1.4 Rulison Field

This data for this study come from Rulison Field in the Piceance Basin of Colorado. Background information about the field are given in this section.

1.4.1 Geologic setting

Rulison field is a basin-centered gas accumulation located in the Piceance Basin of northwest Colorado (Figure 1.1). It is one of many fields in the basin and is located near the town of Rifle. Estimated to contain approximately 300 TCF of natural gas, the Piceance basin produces almost exclusively from tight discontinuous sandstones in the 1,700- to 2,400-ft-thick Cretaceous Mesaverde Group. These fluvial sandstones extend laterally approximately 500-800-ft and exhibit matrix permeabilities of less than a millidarcy (Cumella and Ostby, 2003).

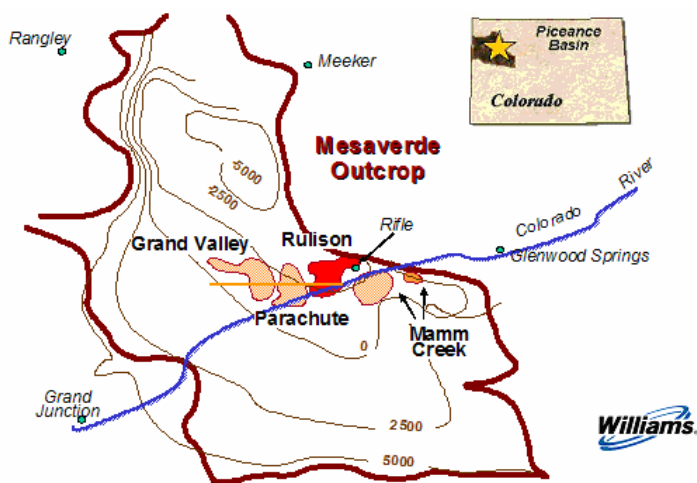


Figure 1.1 - The Piceance basin is located in northwestern Colorado. The edges of the basin are noted by the maroon outline. The top of the Rollins is contoured. Rulison field is shown in bright red (Koepsell et al., 2003).

The Piceance basin is located in northwestern Colorado and is adjacent to the Uinta basin which is very similar. During the Late Cretaceous it was located near the western edge of the Cretaceous interior seaway (Figure 1.2). Throughout the Late Cretaceous the seaway transgressed and regressed over the area depositing marine shales and shoreface sandstones. At its maximum extent it reached to central Utah. During this time, fluvial sandstones and shales, sourced by the Sevier orogeny to the West, slowly accumulated in the coastal plains. Sediments that would eventually become coals were also deposited in these wet lowlands. Eventually, the seaway slowly receded as tectonic uplift began to elevate the basins (Hettinger and Kirschbaum, 2002).



Figure 1.2 - This paleogeographic map of the Piceance basin area during the late Cretaceous shows the distribution of environments that produced various formations (Cumella and Ostby, 2003) (Blakey, 2003).

This Late Cretaceous cycle of seaway encroachment and subsequent period of fluvial deposition deposited what is now known as the Mesaverde Group. The Mesaverde Group overlies the Mancos Shale, a nearly 5400-ft thick Upper Cretaceous shale deposited in the open marine environment of the Cretaceous Interior Seaway (Hettinger and Kirschbaum, 2002). The Mesaverde Group is broken into two formations: the Iles Formation and the Williams Fork Formation (Cumella and Ostby, 2003).

The Iles Formation was produced from a series of transgressions and regressions that ultimately created three widespread sandstone members: the Corcoran, the Cozzette, and the Rollins. These members are separated by tongues of the Mancos Shale. Apparent shoreline reorientations and increases in accommodation space during the deposition of the Rollins indicate that tectonism, possibly due to the beginning of the Laramide Orogeny, was present at this time (Cumella and Ostby, 2003).

The Williams Fork Formation overlies the Rollins and consists first of the Cameo coal zone. This is a zone of relatively continuous coal beds separated by fluvial sandstones and shales deposited by meandering streams. The presence of the coals indicates a rise in the water table that created favorable conditions for the formation of peat swamps. Eventually, the sea level fell enough that deposition above the Cameo coal zone became almost entirely fluvial (Cumella and Ostby, 2003).

The majority of the upper Williams Fork Formation is therefore composed of stacked meandering stream deposits. The sand bodies in this part of the formation are lenticular, laterally discontinuous, and chaotic in distribution. Some sandstones are more laterally continuous than others, and this can be attributed to changes in accommodation space. These changes caused channel deposits to either amalgamate as the channel moved back and forth, as in periods of low accommodation space, or form as isolated bodies, as in periods of high accommodation space. The most upper part of the Williams Fork is comprised of thick laterally continuous sandstones that may have been formed as braided stream deposits. At the very top of the Williams Fork is an approximately 20-ft thick laterally extensive shale known as the upper Williams Fork shale marker. It is an

excellent seismic reflector and is often called the UMV shale. It is overlain by the approximately 5-ft thick Price Coal (Cumella and Ostby, 2003).

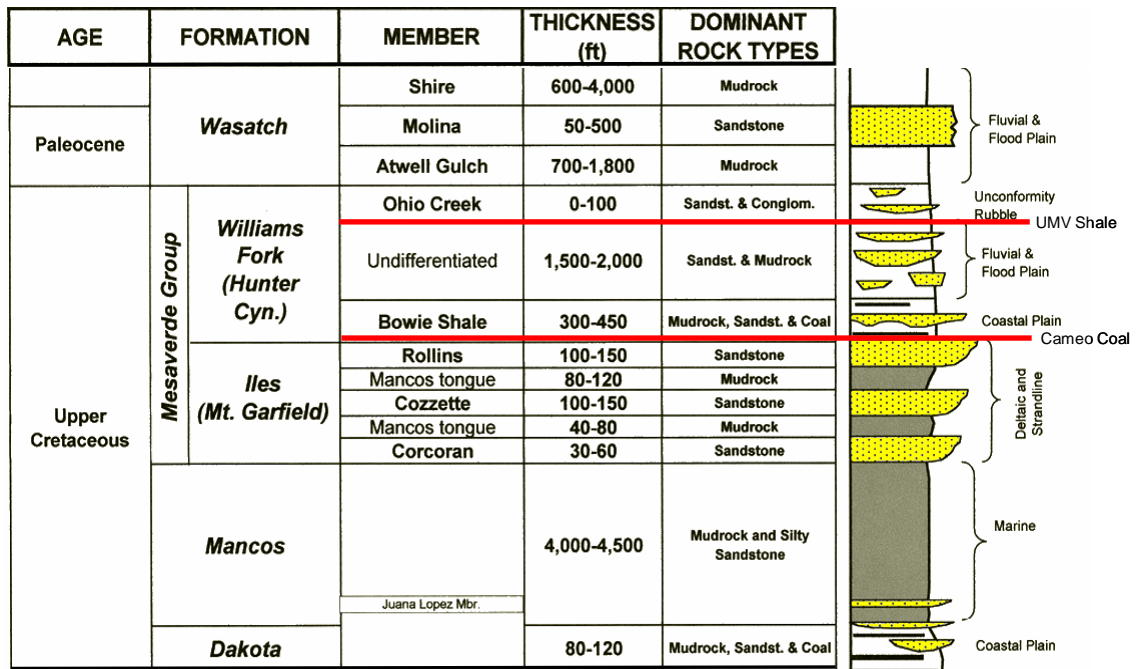


Figure 1.3 - A generalized stratigraphic column for Rulison field with the seismic reflectors of the UMV shale and the upper Cameo coal denoted (Cole and Cumella, 2003).

The regional structure of the Piceance is captured by a conventional P-wave seismic survey acquired by Seitel. It shows that the Piceance is an asymmetric basin. Its southwestern flank dips gently to the northeast and the center of the basin. The opposite flank dips more steeply in the other direction. Rulison is near the center of the basin close to an antiformal feature known as the Rulison nose. The axis of the Rulison nose is approximately north-northwest. The seismic also shows two styles of faulting. One style strikes approximately N45W, has near vertical dips, and has left lateral slip. The other style strikes about N20W, dips between 30 ° and 60 °, and has reverse movement. East-

west compression, indicated by fractures identified from borehole image logs and other sources of data, probably caused the left-lateral and reverse slips along these faults. Generally, the faults are large and easily identified at the Dakota sandstone level, below the Mancos shale, but at the level of the Williams Fork they appear to branch and decrease in offset. The faults are difficult to see in the Mancos, but thickening of the Mancos is associated with faults in the Dakota indicating that the faults are syndepositional (Cumella and Ostby, 2003).

The gas in the Piceance basin is part of a basin-centered gas accumulation. In this type of reservoir water overlies highly pressured gas with a transition zone in between. For this type of accumulation to occur, the reservoir units must have low permeability. In the Williams Fork, the porosity and permeability of the sandstones are reduced to approximately 6%-12% and 0.1 to 2 microdarcies respectively after regional diagenesis. The reservoir must also have an abundant source of gas. The coals and shales of the Williams Fork served this purpose as they were buried by the addition of progressive layers of overburden. As gas is produced from these sources, it attempts to accumulate in the overlying tight sandstones, but due to the low permeability the process is slow. Pressure builds up and eventually expels the free water upward. The reservoirs in the Piceance generally still have high water saturations, from 40-60%, due to their high clay content. In Rulison the pressure built up into an overpressure situation, probably due to the presence of the laterally continuous sealing UMV shale. Finally, in the Piceance, the downcutting of the Colorado River unloaded some of the accumulated overburden. (Cumella and Ostby, 2003).

1.4.2 Production history and practices

Rulison field is currently operated by Williams Production RMT and has undergone multiple phases of development. Initially produced in the 1960's, major

operations at Rulison did not begin until the mid 1980's (Cumella and Ostby, 2003). Tax credits from the federal government spurred development in the early nineties. The credits were given for drilling and producing natural gas from coals; thus until 1996, when the program was discontinued, the coals were preferentially targeted. After this time, the low permeability sandstones were preferentially targeted (Evans, 2006). The low permeability of the reservoir sandstone matrix was, and still is, overcome by extensive artificial hydraulic fractures and natural fractures. At one time, near Rulison, a nuclear device was even used in an attempt to increase fracturing in the tight sandstones of the Williams Fork Formation; however, the program was unsuccessful (Cumella and Ostby, 2003).

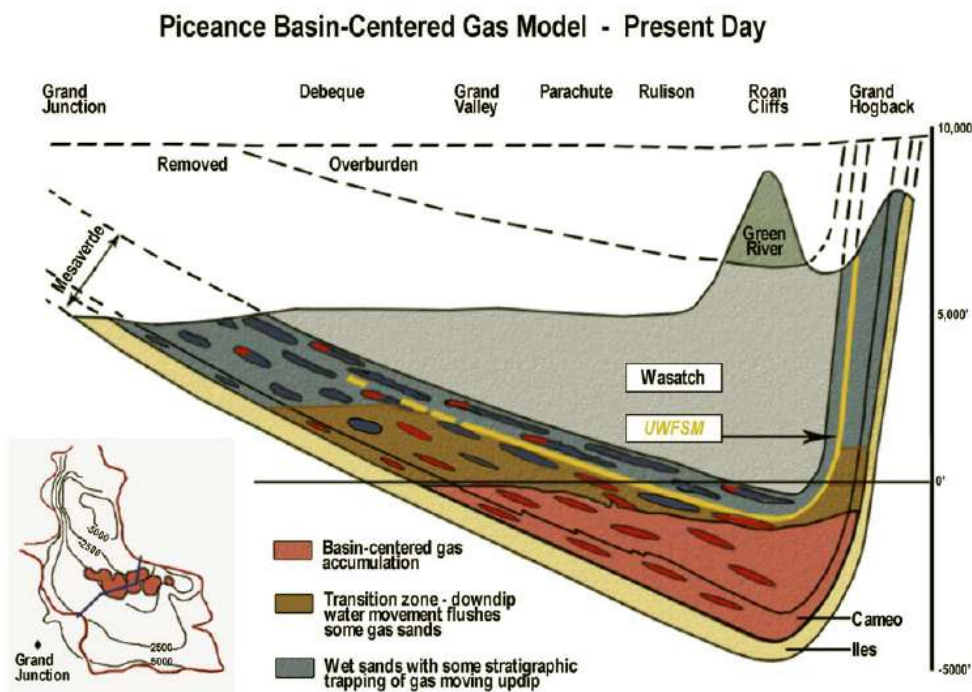


Figure 1.4 - An idealized cross section of the Piceance basin shows the gently dipping southwestern flank and the steeply dipping northeastern flank. It also indicates the distribution of water and gas in this basin-centered gas accumulation (Cumella and Ostby, 2003).

Though the sandstones are thin and low permeability, the reservoir is economic for several reasons. First, it contains an incredible amount of gas due to the sheer thickness of the reservoir and the fact that much of it is overpressured with gas. Also, the gas it produces is virtually water free, so little money is wasted on disposing of huge volumes of water (Cumella and Ostby, 2003). Finally, the recent increase in natural gas prices has increased the economic life of these wells making them more profitable to drill and produce.

There is, however, a large variability in the productivity of individual wells; thus, improved understanding of the reservoir may lead to more efficient production of the field. The variability of the wells is attributed to several factors. First, due to the seemingly chaotic distribution of channel deposits within the reservoir, different sand bodies are intersected by each well. Second, the permeability of the matrix of all these sandstones is very low. This is overcome with natural fractures that can be connected to the wellbore initially or through artificial fractures. The fracture networks allow more potential reservoir to be connected to each wellbore, and therefore increase the productivity of individual wells. Unfortunately, the distribution of natural fractures is poorly understood. Finally, there is a varying degree of success in completing the sandstones in any given well. Artificial fractures are often not as large as intended. This can be attributed to an inability to predict the variation of the geomechanical properties of the reservoir.

Rulison field is produced in a relatively simple fashion. Currently, three to four wells are drilled horizontally out from one surface location, and are eventually steered vertically throughout the bulk of the reservoir. The bottomhole locations of each well are located in a rough grid pattern based on 20-acre spacing. Recently, permission was granted to decrease the well spacing to 10-acres. After drilling and logging, the largest sandstones intersecting the well are then completed with hydraulic fracturing. The well is then opened and the commingled gas is allowed to flow under its own pressure to the

surface. As with wells in most fields, production begins initially as a peak and then hyperbolically declines to an essentially flat producing rate.

1.5 Methodology

I interpreted the migrated P-wave time-lapse seismic data at Rulison using a relatively conventional workflow (Figure 1.5). First, I cross-equalized the volumes. Cross-equalization is necessary to remove post-stack differences that arise despite the best efforts at consistently acquiring and processing the data. I applied a fairly standard cross-equalization flow using the Hampson-Russell PRO4D software package (version 2.2 CE7/R2) (Rickett and Lumley, 2001).

Following the cross-equalization, I modeled the time-lapse response that would be expected at Rulison. Unfortunately, there are no direct measurements of in situ impedance change due to production at Rulison. There are also no measurements of in situ pressure change at the field. Thus, I made due with wellhead pressure data and pore-pressure depletion inferred from mini-fracture tests. I also used an ultrasonic P-wave effective-pressure relationship and made several assumptions about the effective-pressure coefficient.

Finally, I interpreted the data based on changes that I observed in the model. First, I calculated the time shift between the volumes at every sample in the data and compared it to the modeling. Next, I applied these time shifts and inverted the data for acoustic impedance. I then looked at sections, difference volumes, and percent-change volumes and slices to find amplitude-based changes in the data. By comparing these to the model, well locations, production information, and fault locations, I was able to create a coherent picture of the time-lapse changes that I observed.

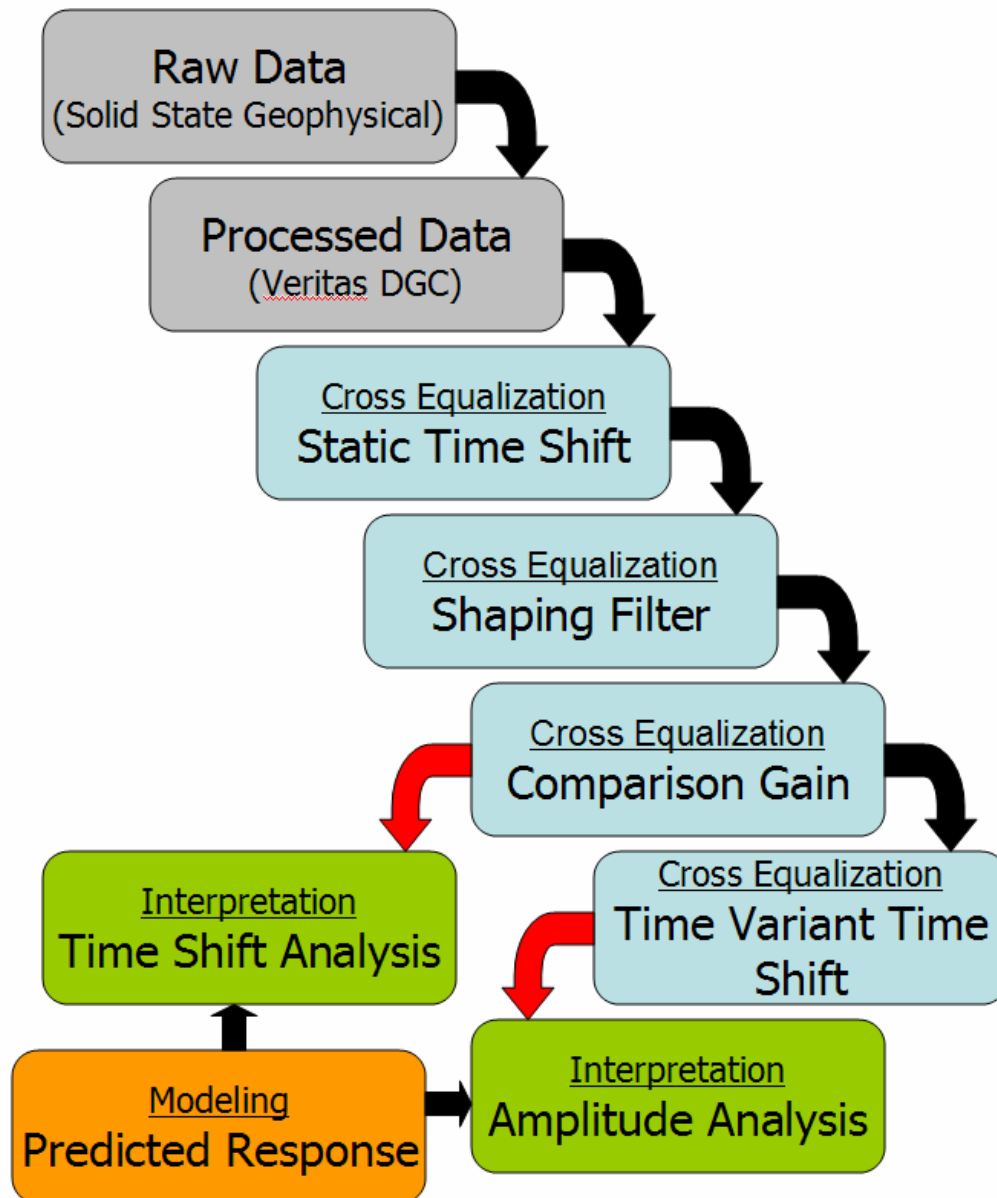


Figure 1.5 - The workflow used for interpretation is shown above.

CHAPTER 2: SEISMIC DATA

2.1 Survey Design

The RCP 4-D survey is located in a data-rich area just north of Interstate 70 (Figure 2.1). The base survey was shot in November of 2003 and the monitor survey was shot in September of 2004. The RCP survey encompasses nearly 80 wells of varying ages, production rates, and log suites that include: diagnostic fracture initiation tests (DFIT), image logs, dipole sonic logs, and even a multi-component VSP. Also, it includes a 10-acre well spacing pilot project initiated by Williams Production RMT, the field's operator. The aim of the pilot project is to test the production rates and communication of wells at 10-acre spacing. Overlapping the east side of the RCP survey is a 1996 DOE P-wave seismic survey. This survey was used with the RCP 2003 survey for a time-lapse experiment done by Mahendra Kusuma (Kusuma, 2005). Nearly 2 miles south of the RCP survey is the Department of Energy's (DOE) multi-well experiment (MWX). The MWX is a set of three closely-spaced cored wells that were used in a multitude of geologic, geophysical, and engineering related experiments. Unfortunately, the northern part of the RCP survey also includes the edge of the Roan Cliffs. Vibrators cannot operate and phones cannot be planted in this area; thus, this it has poor data quality due to a lack of near offsets and low fold. This effect is seen in Figure 2.3.

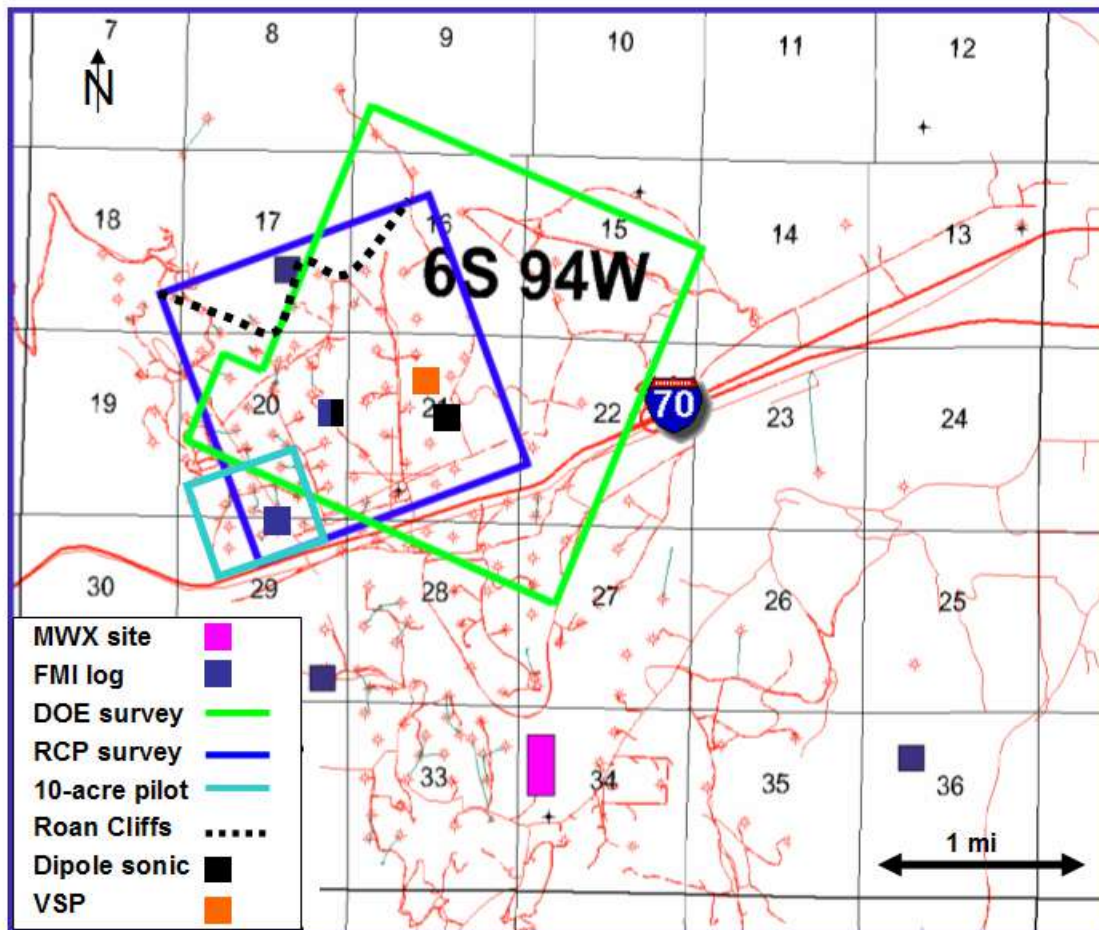


Figure 2.1 - The locations of many different pieces of information relative to the RCP seismic survey area.

The survey is approximately 7260-ft by 8250-ft. Nearly 1500 receivers were placed with an inline spacing of 110-ft and a crossline spacing of 330-ft (Figure 2.3). All receivers were live for every shot and connected to the recording system via radio telemetry. 709 source points were spaced 110-ft inline and 660-ft crossline. The 12 source lines are perpendicular to the 26 receiver lines (Figure 2.3). This geometry gives a maximum fold of 225 that is highest in the center of the survey and decreases rapidly toward the edges (Figure 2.4). A P-wave shot consists of six 5-120 Hz sweeps over 10

seconds while a S-wave sweep is only 5-50 Hz. This geometry is repeated closely in the 2004 survey such that the standard deviation of position differences was only 2.15-ft for the receivers and 3.39-ft for the sources (Figure 2.5). This is important because repeating the geometry is one of the most crucial factors in acquiring repeatable seismic data (Calvert, 2005).

The latest equipment and technology was employed to acquire the seismic data. Solid State Geophysical, who acquired the survey, used A Mertz 18 vibrator as the P-wave source and an IVI Tri-Ax as the S-wave source. Pelton VibPro 3X electronics controlled the vibrators. I/O VectorSeis System Four single sensor digital multi-component receivers were surveyed into location using ground based techniques and GPS. These receivers are excellent for time-lapse applications because they do not use an array. This lowers the number of receivers and allows more care to be taken with their placement. Each receiver is inserted into a hole drilled into the ground and roughly oriented with a compass Figure 2.2. This maximizes ground coupling, minimizes wind noise, and makes shear-wave results more consistent. In addition, the survey was shot with a live receiver at every location at all times. This not only increases fold, but ensures that coupling and placement are not compromised by a need to constantly move and plant geophones in order to keep up with the shooting (I/O, 2006). The specifications of these receivers are shown in Table 2.1.

Table 2.1 -The specifications of the data recording system are shown below (Input/Output, 2005).

Sampling Rate	2-ms
Instantaneous Dynamic Range	118 dB
Bits	24 bit
Time Break Accuracy	+/- 8 μ s
Inclination Resolution	+/- 0.5 °

I/O Vectorsis System Four Sensors

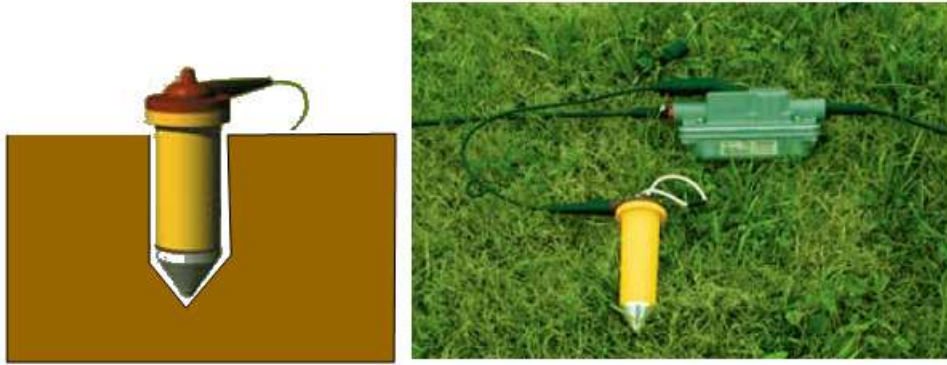


Figure 2.2 - The I/O Vectorsis sensor is inserted into a hole drilled in the ground for maximum coupling (adapted from (I/O, 2006).

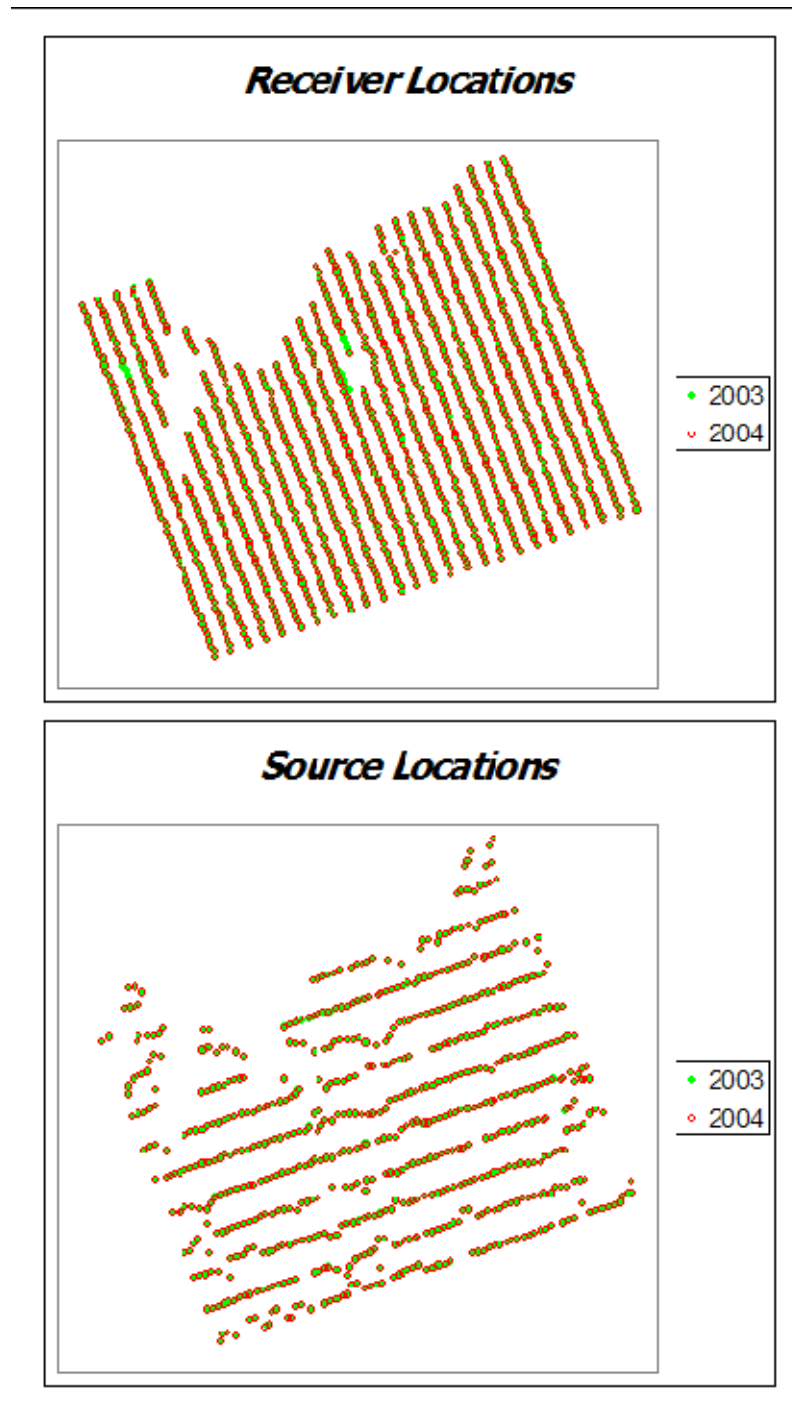


Figure 2.3 - The locations of the source and receiver positions were repeated very closely in both 2003 (green) and 2004 (red).

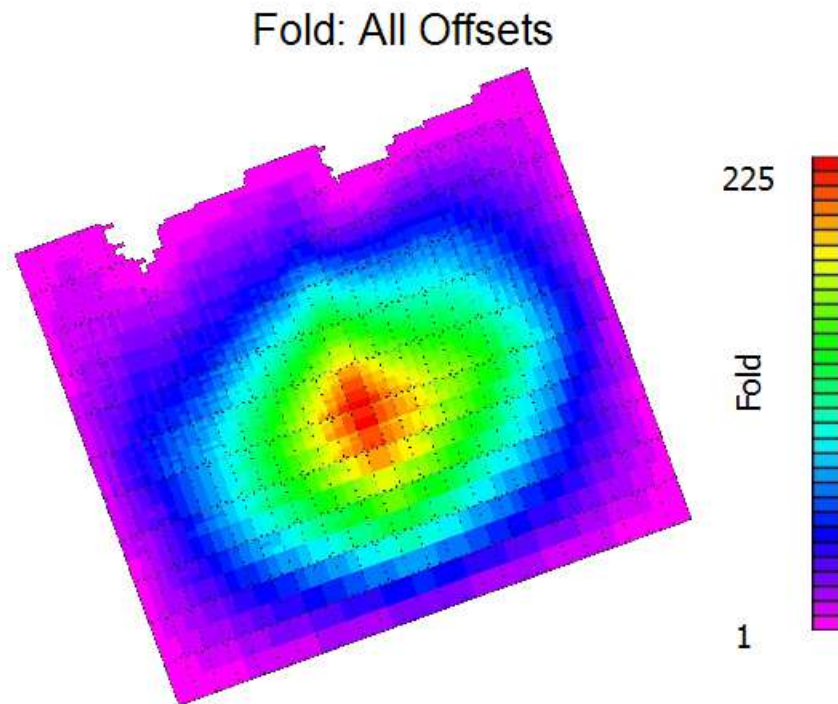


Figure 2.4 - The RCP survey has very high maximum fold (225) but it quickly diminishes toward the edges of the survey.

While the equipment and geometry were best suited to maximize time-lapse repeatability, the environment was not. The fall of 2003 was dry and well suited to seismic acquisition. Unfortunately, the fall of 2004 was very rainy. This changed the level of the water table and introduced near surface static differences between the data sets. Also, the fall of 2004 saw increased drilling activity: specifically in the northwest corner of the RCP survey. The drilling caused increased noise and ultimately the removal of some station gathers from the data set (Figure 2.6). All traces removed from one data set were removed the other prior to processing (Winarsky, 2006).

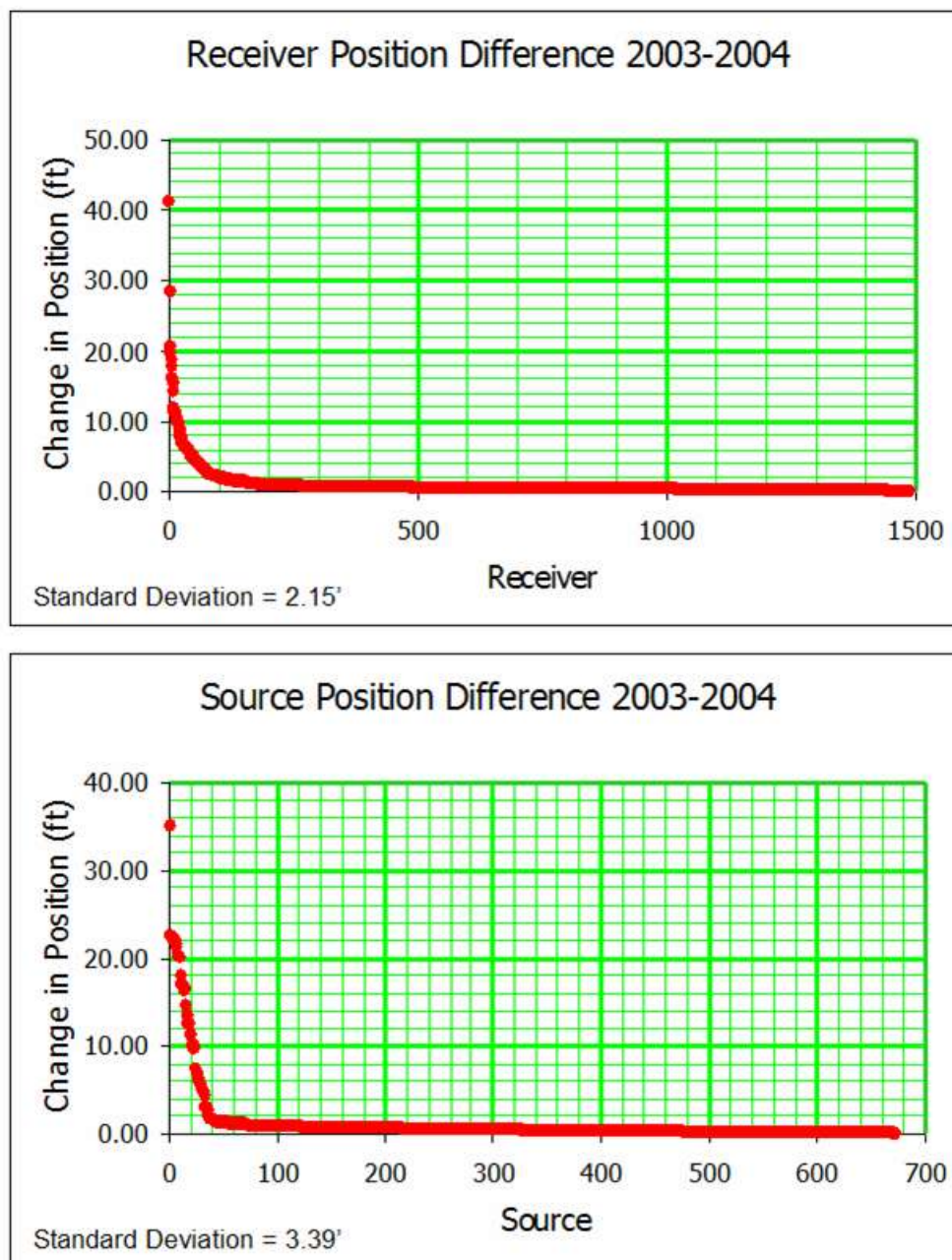


Figure 2.5 - The distribution of the differences between the source and receiver positions quantifies how repeatable the geometry was.

P-P Raw station gather – Field Station 1038

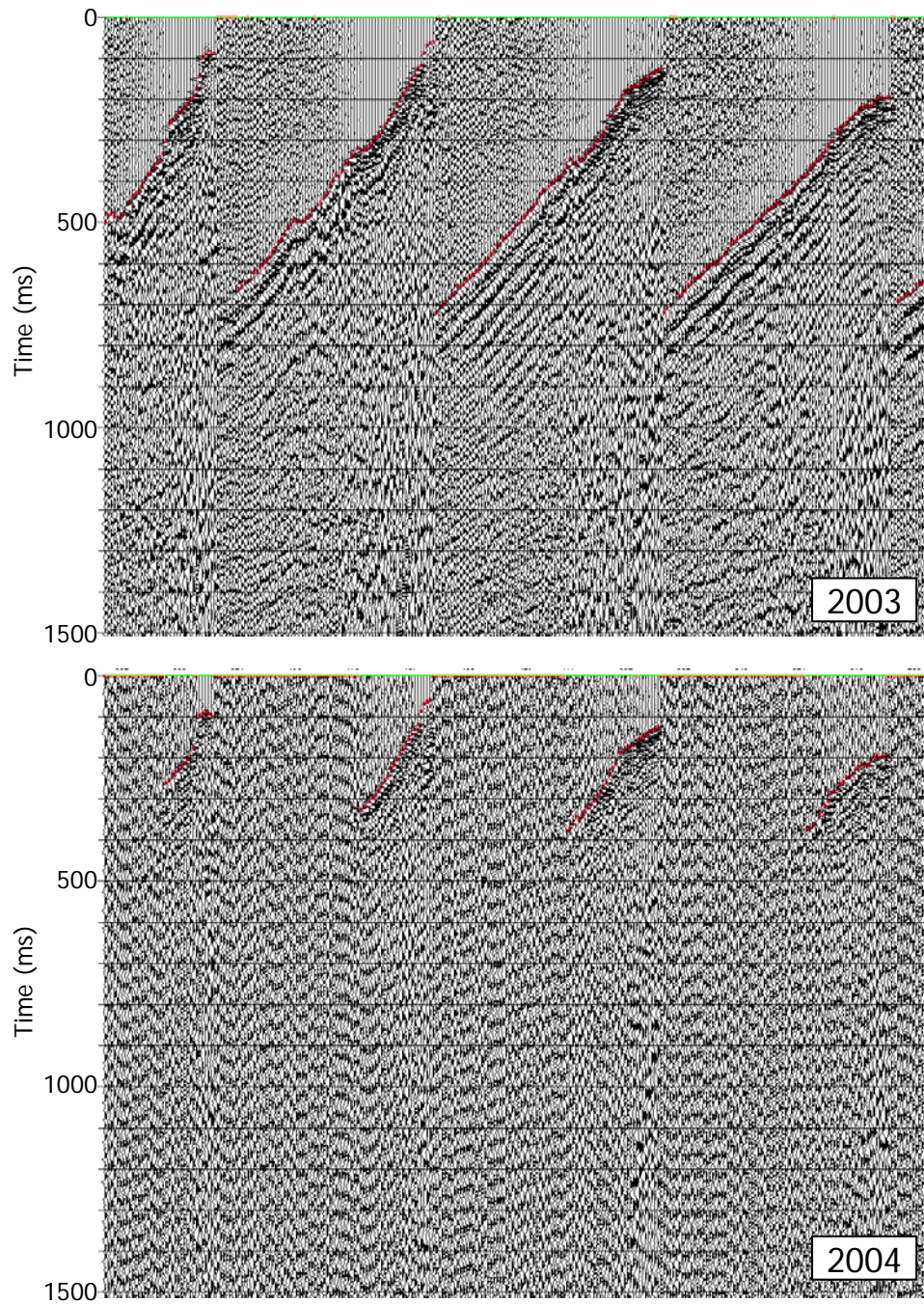


Figure 2.6 - Raw field station 1038 indicates the severity of the drilling noise in the 2004 survey at some locations.

2.2 Processing

The data is processed by Veritas DGC. Processing is carried out on both volumes simultaneously in order to maximize repeatability. The processing flow is given in Table 2.2.

Table 2.2 - The P-wave processing flow is shown below. Independent indicates that the process was calculated separately for each volume.

Vectorseis tilt correction (applied in the field)
Demultiplex, Geometry, First break picks
Refraction Tomography Statics
Manual Trace Edits, Amplitude Recovery - T^2
Surface Consistent Amplitude Equalization and Deconvolution (independent)
Velocity Analysis (Preliminary)
Surface Consistent Statics (Preliminary, independent)
Velocity Analysis (Final)
Surface Consistent Statics (Final, independent)
First Break Mutes
Trim Statics
Amplitude Equalization (Mean Scaling)
Stack
Noise Attenuation (FXY Deconvolution)
Post Stack Migration (Kirchhoff)
Frequency Filter
Amplitude Equalization (Mean Scaling)

In order to make sure that observed time-lapse changes are not due to processing artifacts both volumes are treated exactly the same when possible. In this case, the NMO mutes, NMO velocities, and migration velocities are the same for both volumes. Statics, surface consistent amplitude equalization, and deconvolution are applied independently to each volume because of near surface variations. The final source and receiver statics solutions are shown in Figure 2.7 (Winarsky, 2006).

Only the most repeatable traces are included in the final volumes. This is accomplished by removing trace pairs that have significant differences. A trace pair is a set of two traces, one from each volume, that have the same source and receiver position as each other. To maximize repeatability, if one trace is removed from the data, its pair is also removed. In this data, several noisy receiver gathers and traces are removed prior to stacking. Also, traces derived from sources or receivers that did not reoccupy their original position to within 55' (half the inline source and receiver spacing) are removed (Winarsky, 2006).

I use the data immediately after migration rather than the migrated filtered scaled data set. The reason for this is that filtering and amplitude scaling have the aim of making the image better. While this is good for geologic interpretations, it is not necessarily good for time-lapse interpretations unless it is consistently applied. Not knowing the parameters used in filtering and scaling, I use the data without those processes applied.

Thus, the data are acquired and processed to maximize time-lapse repeatability. Though, as future chapters show, differences still exist. Cross-equalization is necessary to lessen these differences. Also, investigations of the noise level are required to interpret the time-lapse data.

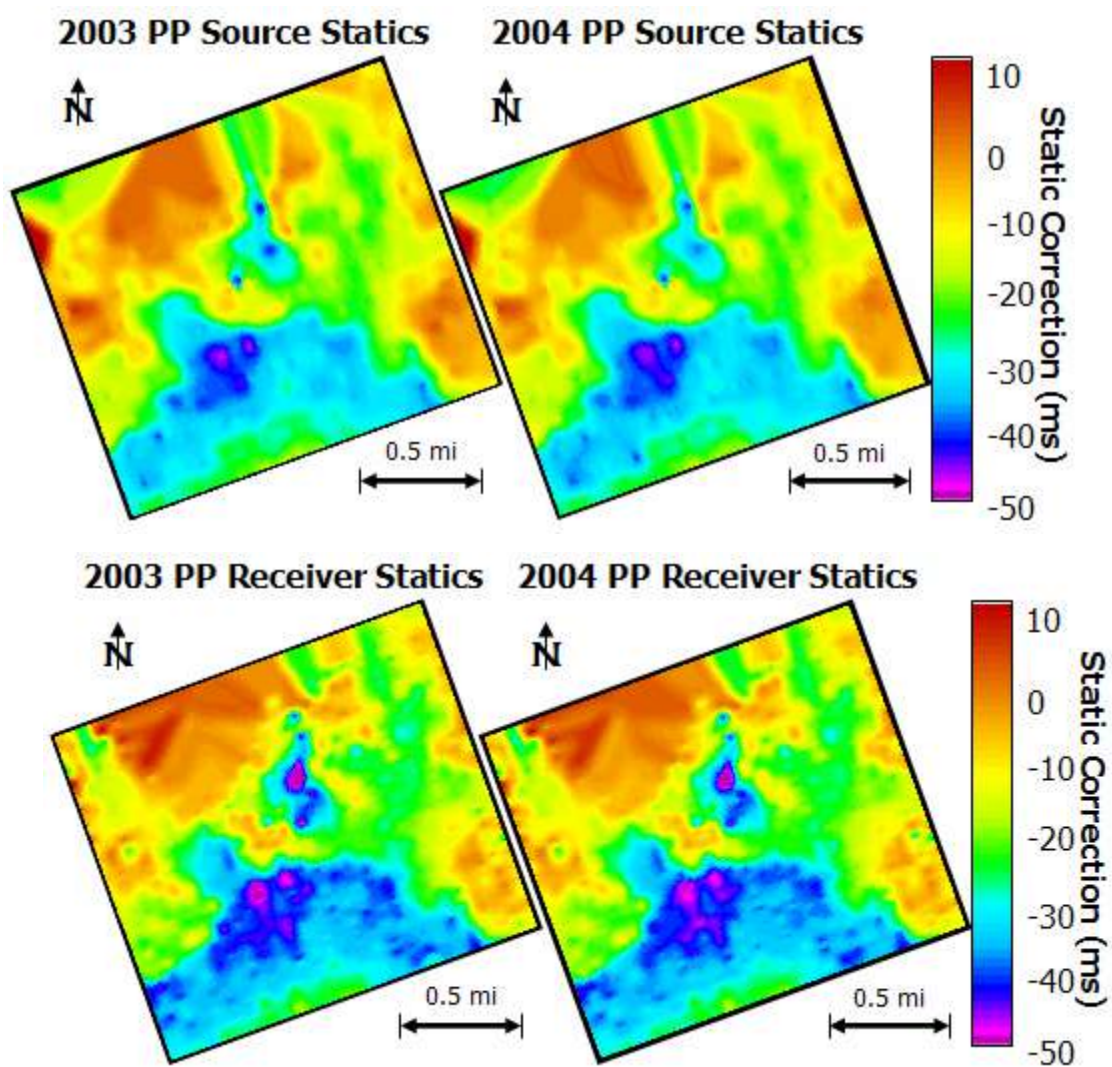


Figure 2.7 - The final source and receiver statics are relatively consistent between years.

CHAPTER 3: DATA PREPARATION

3.1 Introduction

Despite our best efforts to acquire and process two seismic data sets in the same way, systematic differences arise that must be removed through a process called cross-equalization. Most cross-equalization flows work to correct time shifts, spectral differences, and amplitude differences in either the pre or post-stack domains. I applied cross-equalization on the post-stack data, though ideally it would have been applied on the pre-stack data.

Cross-equalization works with common trace pairs, or a pair of traces that occupy the same position in space but are from volumes acquired at different times. The idea is to remove timing and wavelet differences in common trace pairs that occur where no difference is expected. The zone where no change is expected is often called the static section. At Rulison, I chose this zone to be from 700-ms to 925-ms because it includes two strong reflectors, the Mesaverde and the UMV Shale. While no change is expected above 700-ms fold decreases drastically above that point due to pre-stack muting. Thus, if that shallower zone was included, the equalization corrections would be corrupted by the presence of a large amount of noise due to low fold. Below 925-ms gas is produced from the Williams Fork formation, so to avoid removing the expected signal, I kept the static window above this zone. Since corrections designed in the static window are applied to the whole volume, the process of cross-equalization implicitly assumes that these corrections should not vary with time.

My flow applied four corrections in the following order: a correlation time shift, a shaping filter, comparison gain, and a time-variant time shift. The first step, correlation time shift, attempts to correct for static, or time invariant, time shifts that occur between

seismic traces. These are probably caused by near surface velocity variations that are not completely corrected by the prestack statics. The second step, a shaping filter, tries to make the wavelet of each data set the same. In doing so it removes spectral and phase differences. The third step, comparison gain, tries to scale the traces of the common trace pairs to have the same amplitude. The final step, a time-variant time shift, attempts to perfectly time align the data volumes for all time. The application of the time-variant time shift is only necessary for amplitude based interpretation and therefore the data after the application of the comparison gain are used for time interpretation. These steps are described later in detail.

Amplitude interpretation is accomplished using an acoustic impedance volume derived from the seismic data. This is necessary because when interpreting changes in seismic amplitude, especially for a large stacked reservoir like Rulison, it is good to have a volume based attribute that can indicate relative changes throughout the reservoir. A volume showing the difference of sections can serve this purpose, but it is skewed toward showing larger differences at higher amplitude reflectors. Unfortunately, because seismic data contains zero crossings, a seismic amplitude difference volume cannot be divided by the original volumes because the result will go to infinity at the zero values. Acoustic impedance values, however, do not go to zero, or even vary by orders of magnitude. For this reason converting to acoustic impedance is a stable way to create a normalized difference volume. I transform the seismic data to acoustic impedance through a process called colored inversion in order to create a percent difference volume. This process, and the cross-equalization processes are described in detail in the following sections.

3.2 Correlation Time Shift

The first step I applied was a correlation-based time shift. This step computes a single time shift for each trace in an attempt to align the base and monitor volumes in time. The correlation-based time shift algorithm, a part of Hampson Russell's PRO4D software package, uses cross-correlation to determine the time shift. The user simply tells the algorithm over what time window and range of lag values to calculate the cross-correlation. Since the correlation value should be largest when the traces are aligned, the lag value at maximum correlation is considered the time shift that should be applied. Of course, if the maximum value of the correlation is small, then the calculated time shift is often unreliable. To counter this effect an optional filter can be applied that removes time shifts associated with low correlation and replaces them with values interpolated from the surrounding area.

The correlation time shift was not very sensitive to the parameters used to determine it. I tried several different calculation windows and correlation cutoff values, but the results were always consistent. Eventually, I settled on a 225-ms long window that started at 700-ms. I chose this window because it included the Mesaverde and UMV shale, both strong seismic reflectors, but the window remained above the top of gas in all the wells. I filtered out time shifts with correlations lower than 0.85; however, only the extreme edges of the data had correlations that low (Figure 3.1). The final calculated time shifts reveal that the 2003 volume was on average 2-ms earlier in time than the 2004 volume (Figure 3.2). The data slices in Figure 3.1 and Figure 3.2, and in the rest of this document, are accompanied to the left by a seismic time or depth section that is marked to indicate the zone over which the data slice was calculated.

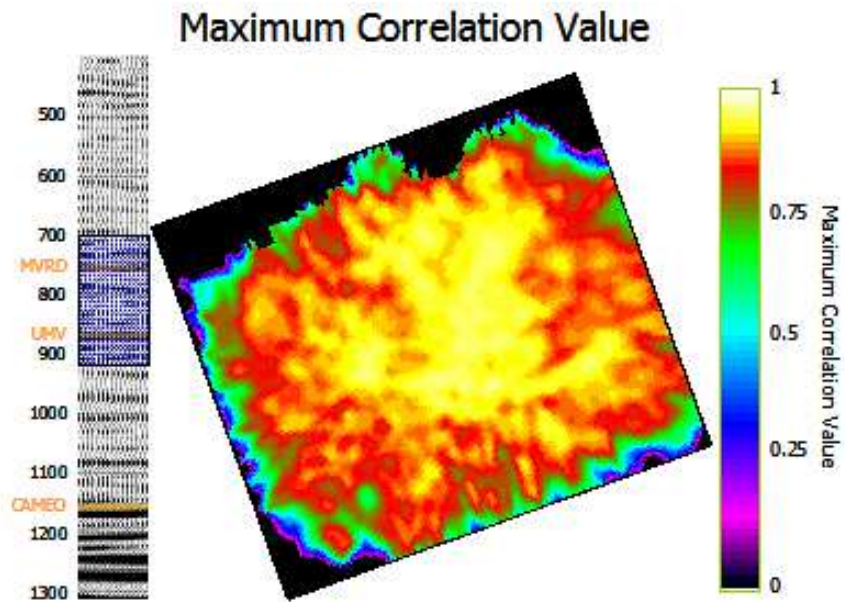


Figure 3.1 - The correlation values calculated from the cross-correlation time shift process.

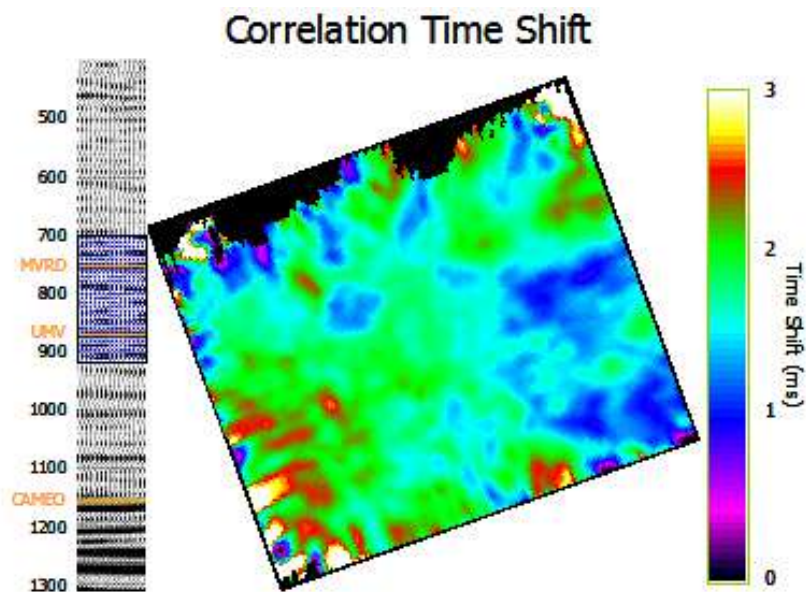


Figure 3.2 - The calculated correlation time shifts.

Quality control measures show that the cross-correlation time shift is reducing timing differences between the volumes. Differences between the volumes before and after the cross-correlation time shift indicate that the cross-correlation time shift is working to the degree that the differences after the cross-correlation time shift are much smaller than the differences before Figure 3.3.

Normalized root mean square of the difference (NRMS) maps over the static window before and after the cross-correlation time shift also show reduced difference. The NRMS of two traces a_t and b_t over a specified time window is calculated using the following equation (Kragh and Christie, 2002):

$$NRMS = \frac{2 \times RMS(a_t - b_t)}{RMS(a_t) + RMS(b_t)}$$

Perfectly repeatable data would have a NRMS value of zero and anti-correlated data would have a NRMS value of two; thus, cross-equalization procedures should lower the NRMS values. NRMS maps before and after the application of the cross-correlation time shift are shown in Figure 3.4. They indicate that repeatability is highest in the center of the survey and lowest at the edges. This is probably due to low fold in those regions. This lowers signal to noise and makes statics determinations less reliable. Also, the NRMS maps indicate that the cross-correlation time shift decreased differences between the base and monitor volumes over the entire spatial extent of the survey.

The decrease in differences can perhaps be shown more effectively by the histograms of the maps in Figure 3.4 (Figure 3.5). These histograms show the percentage of the pixels in each map that have the values specified on the x-axis. In perfectly repeatable data, they would consist simply of a 100% spike at zero; therefore, each cross-equalization step should push the histograms of the NRMS maps closer to this ideal. Figure 3.5 shows that the cross-correlation time shift moves the peak closer to zero; thus it improves the repeatability of the data.

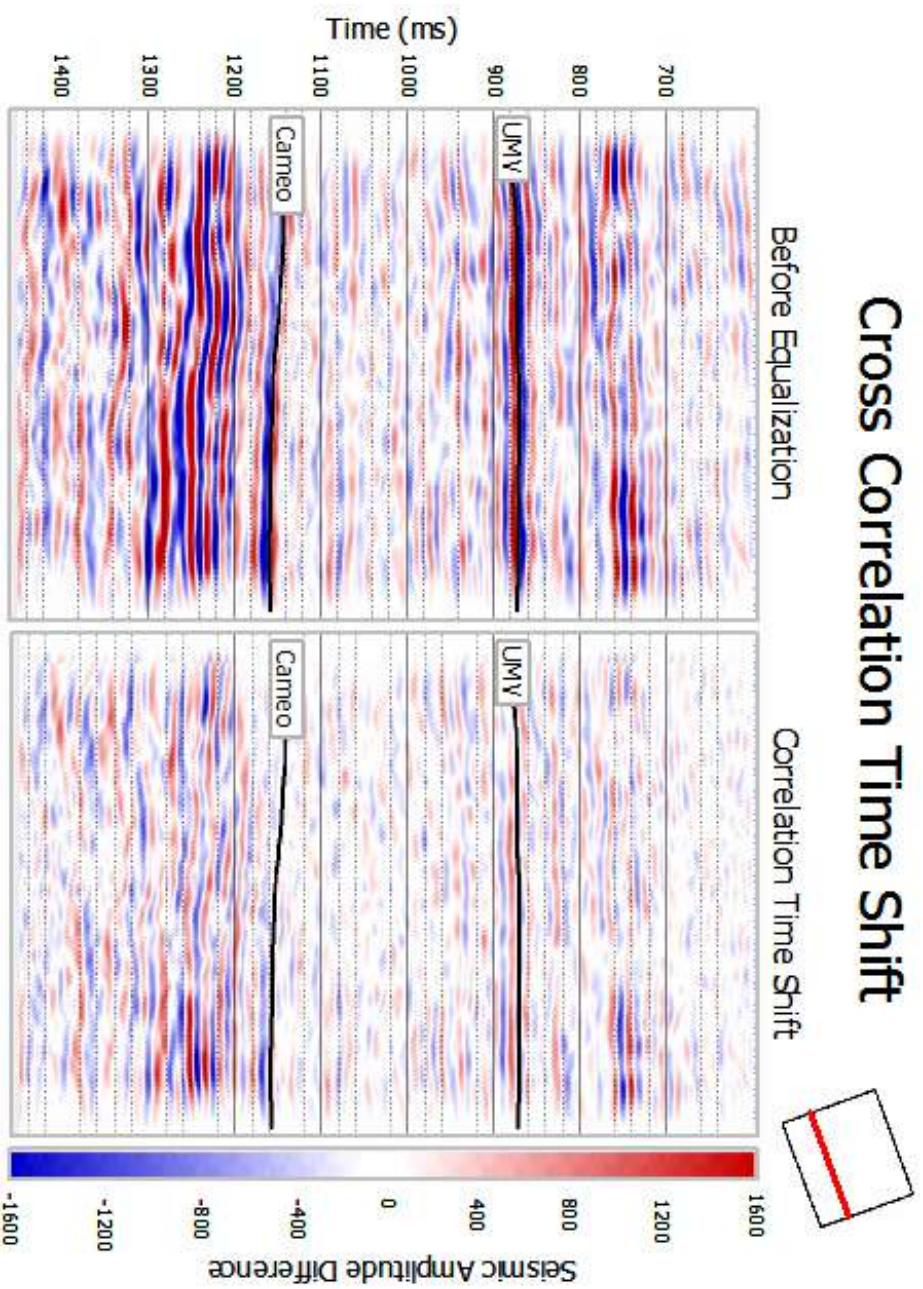
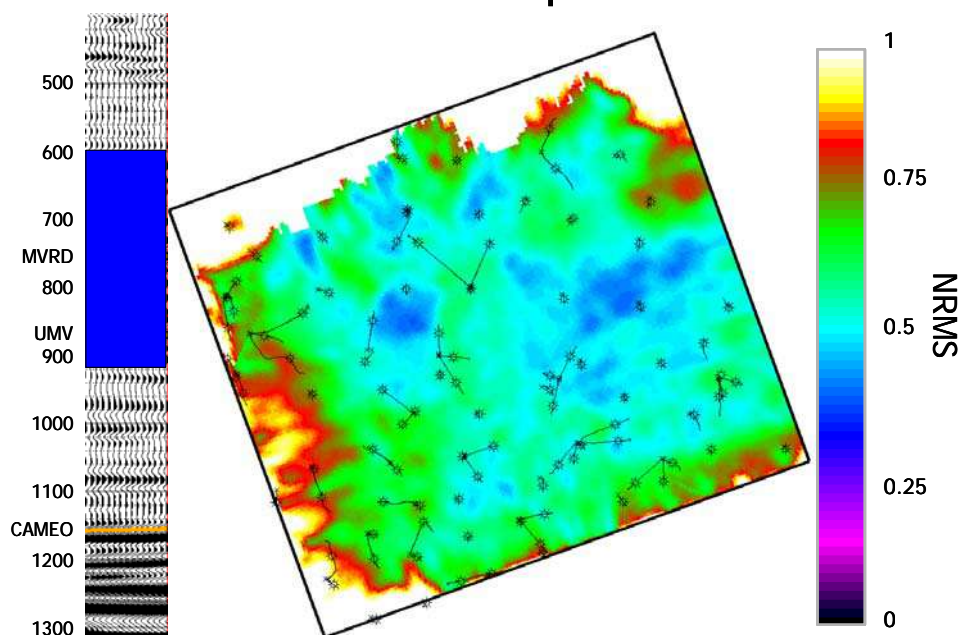


Figure 3.3 - Difference sections before and after the application of the cross correlation time shift indicate that the step is effective in reducing differences.

NRMS: No Equalization



NRMS: Correlation Time Shift

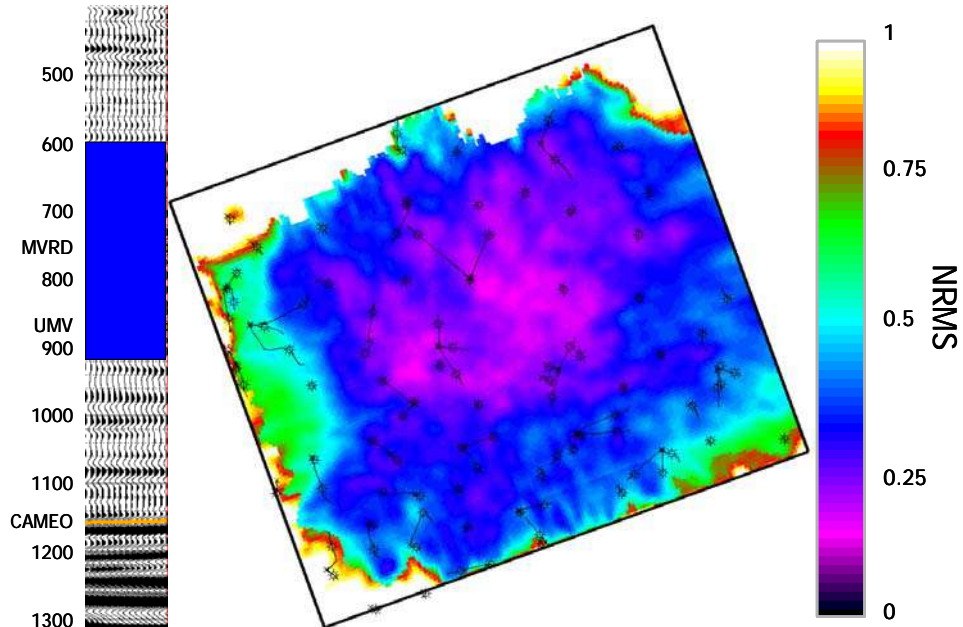
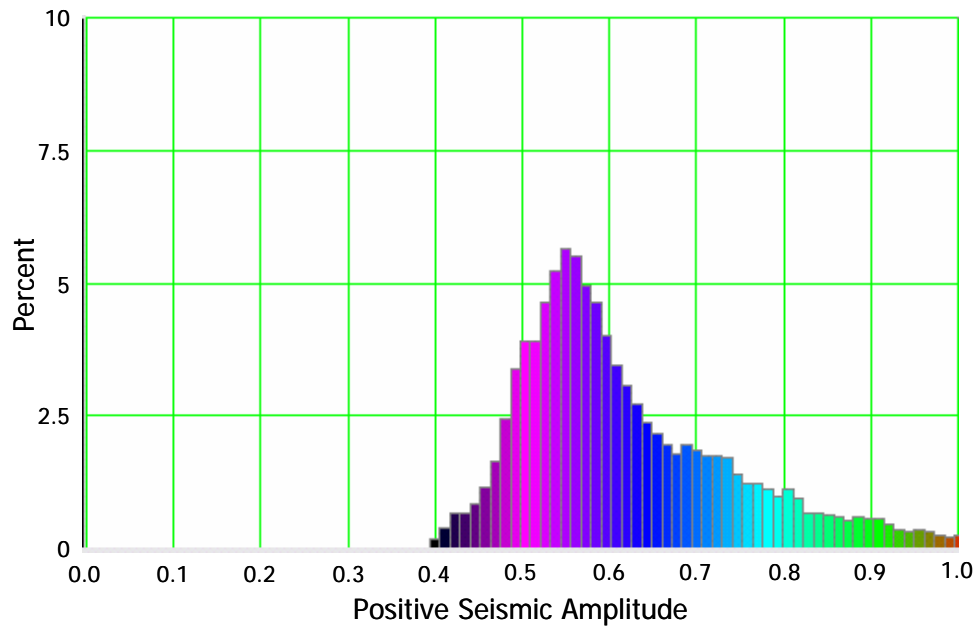


Figure 3.4 - The NRMS maps over the static section before and after the application of the cross-correlation time shift are shown above.

NRMS: No Equalization



NRMS: Correlation Time Shift

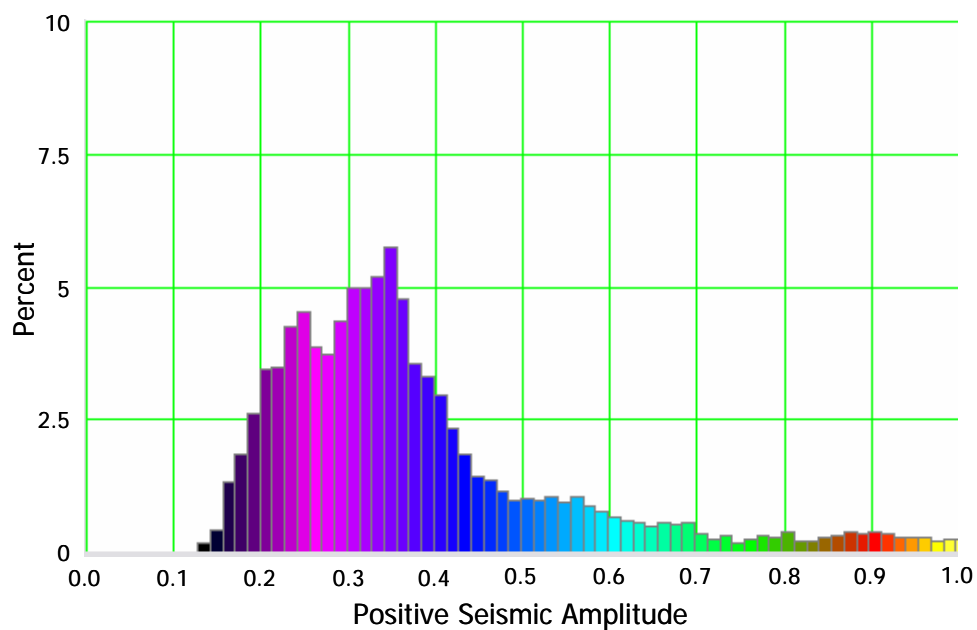


Figure 3.5 - The histograms of the NRMS maps in Figure 3.4 before and after the application of the cross-correlation time shift are shown above.

3.3 Shaping Filter

After the application of the cross-correlation based time shift, a Wiener-Levinson shaping filter is applied. The purpose of this filter is to "shape" one wavelet into another to the best approximation in a least squares sense. It does this using only the autocorrelation of the input wavelet and the cross-correlation of output or desired wavelet with the input wavelet (Yilmaz, 1987):

$$\begin{bmatrix} r_0 & r_1 & \dots & r_{n-1} \\ r_1 & r_2 & \dots & r_{n-2} \\ \dots & \dots & \dots & \dots \\ r_{n-1} & r_{n-2} & \dots & r_0 \end{bmatrix} \begin{bmatrix} a_0 \\ a_1 \\ \dots \\ a_{n-1} \end{bmatrix} = \begin{bmatrix} g_0 \\ g_1 \\ \dots \\ g_{n-1} \end{bmatrix}$$

In the above equation r_i is the autocorrelation of the input wavelet, a_i are the elements of the shaping filter, and g_i is the cross-correlation of the output wavelet with the input wavelet.

In cross-equalization, the shaping filter is designed over the static window and it attempts to convert the traces from one volume into the traces of another volume within that window with the constraint of a finite operator length. Effectively, since the two traces are assumed to be derived from the same subsurface, the filter is simply matching the phase and amplitude spectra of the wavelet from one volume to the other. This is done on a trace-to-trace basis, or the resulting filters can be averaged and applied globally. I use a global average. Assuming that the wavelet is consistent throughout time, the application of the shaping filter corrects differences in areas where change is expected without equalizing them away (Rickett and Lumley, 2001).

The necessity of this step is shown in Figure 3.6. It shows the amplitude spectra of the 2003 and 2004 volumes. The 2004 volume has attenuated high frequencies compared to the 2003 volume. This may be due to the fact that the ground was wet during the acquisition of the 2004 survey. Whatever, the cause, the spectra must be more closely matched in order for a detailed comparison of the two seismic volumes.

I applied the filter using an algorithm included in Hampson-Russell's PRO4D package. The algorithm first requires that one volume be chosen as the input and the

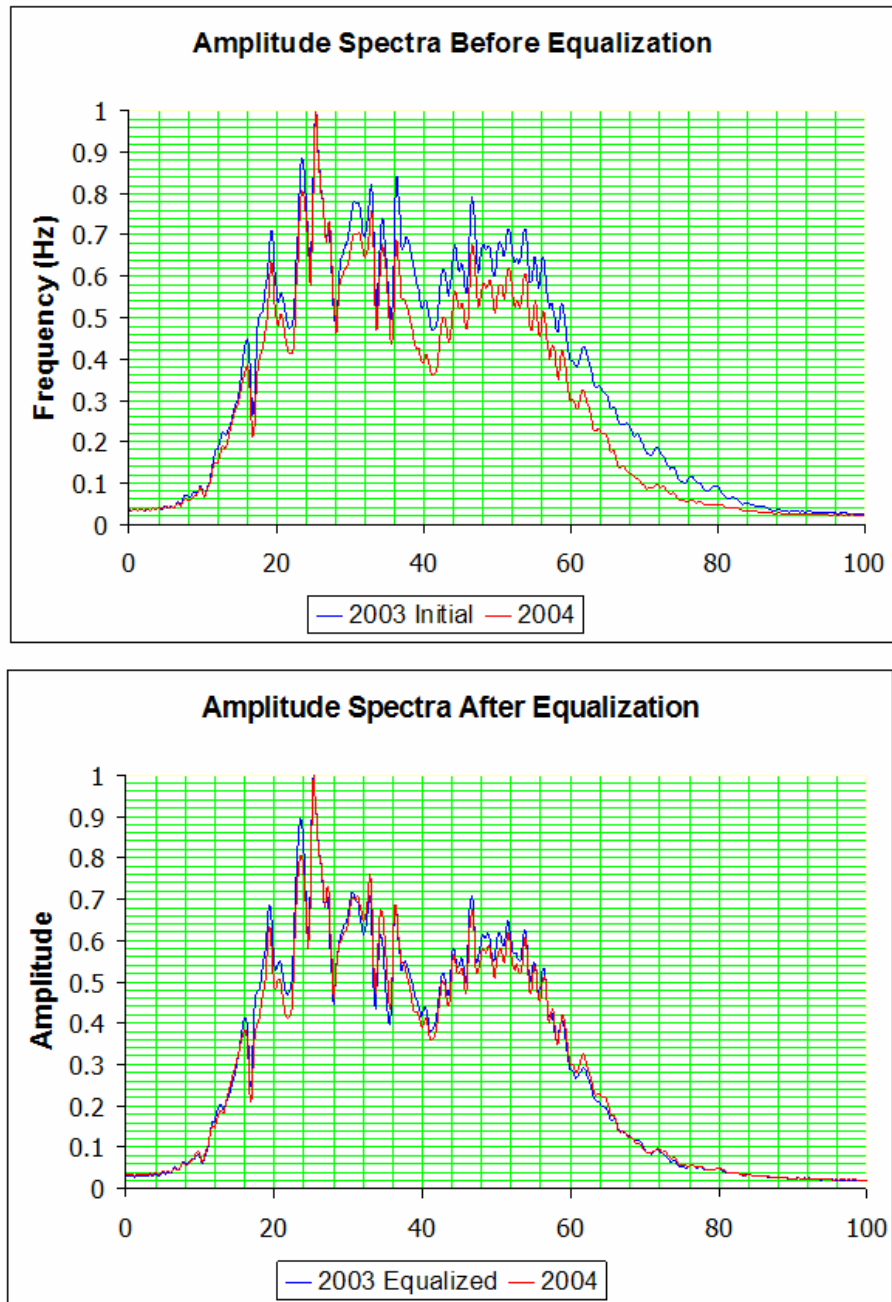


Figure 3.6 - The 2003 volume has more high frequency content before the application of the shaping filter. After the shaping filter the two are closely matched.

other as the reference. The input volume is the volume to which the filter is applied and the reference volume is the desired output of the shaping filter process. I filter the 2003 volume to avoid boosting high-frequency noise in the 2004 volume which was relatively deficient in high frequency signal.

Second, the algorithm requires a window over which to calculate the shaping filter. A design window of 700-ms to 925-ms is used for the Rulison data. Next, the number of filters is chosen. A filter can be created and applied to each common trace pair or a single global filter can be created and applied to the entire dataset. A global filter is used here because trace-to-trace filters produce unstable results. In order to keep edge effects from influencing the filter I allow only traces from the central portion of the data set to be included in the filter design(Figure 3.7). Also, only trace pairs with correlation values over 0.85 are used in the design of the filter. This keeps out the influence of noisy or highly unrepeatable traces. Fortunately, there are only a few of these. The other parameters used in designing the filter make little difference in the end result and are summarized in Table 3.1. The additive noise level is a factor that keeps division by zero from occurring in the frequency domain (Yilmaz, 1987). The shaping filter is shown in Figure 3.8.

Table 3.1 - The parameters used in the design of the shaping filter are shown in this table.

Parameter	Value
Design Window Start	700 ms
Design Window End	925 ms
Shaping Filter Length	321 samples (160.5 ms)
Correlation Threshold	0.85
Maximum Time Shift	40 ms
Global Shaping Filter	Yes
Additive Noise Level	0.001

Shaping Filter Design Zone

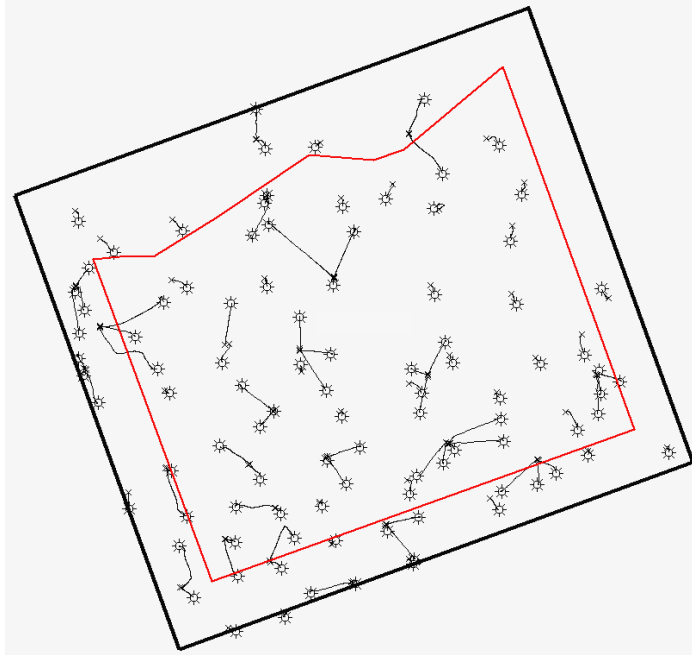


Figure 3.7 - The areal extent of the traces used in designing the shaping filter is shown above.

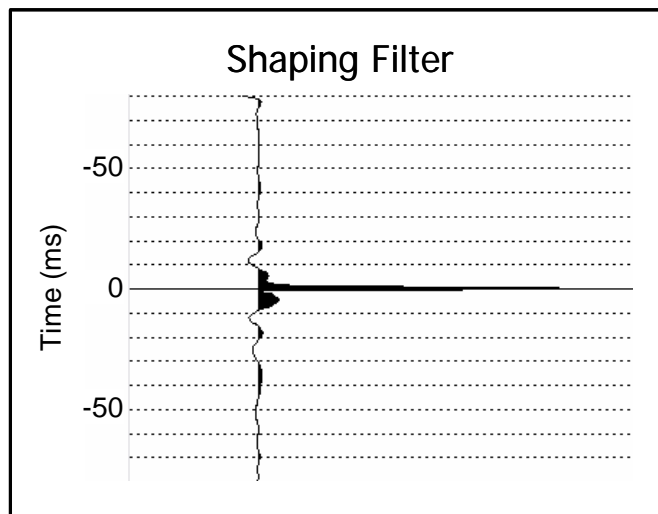


Figure 3.8 - The global shaping filter applied to the 2003 seismic volume is shown above.

The application of the shaping filter reduced differences between the volumes. Difference sections before and after the application of the filter clearly indicate this (Figure 3.9). NRMS maps of the static section show the areal extent of the improvements to the repeatability (Figure 3.10). Histograms of these maps indicate that the improvement was significant. Notice that the peak has tightened and shifted toward zero. Therefore, these measures of repeatability all indicate that the shaping filter was a productive step in cross-equalization.

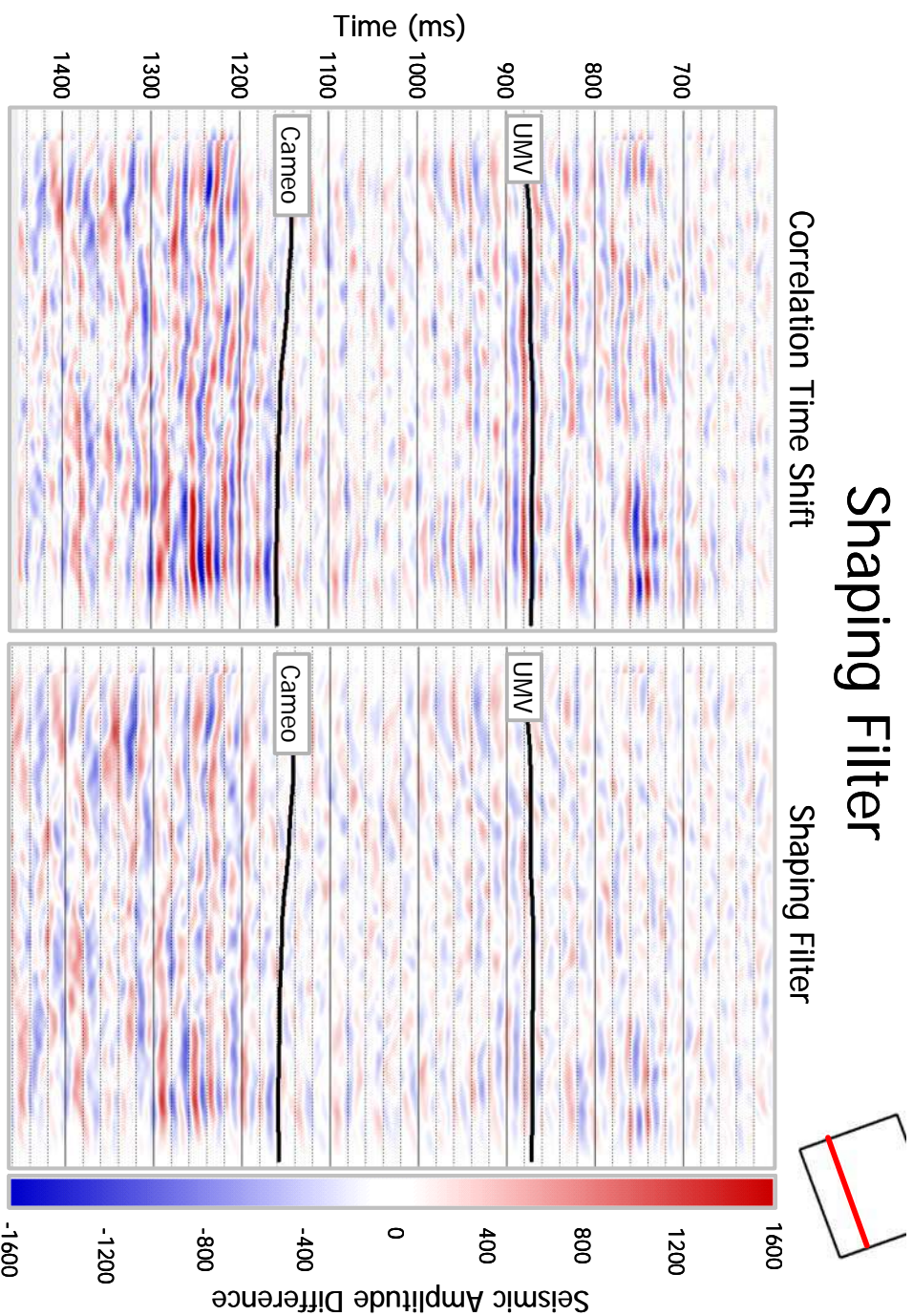
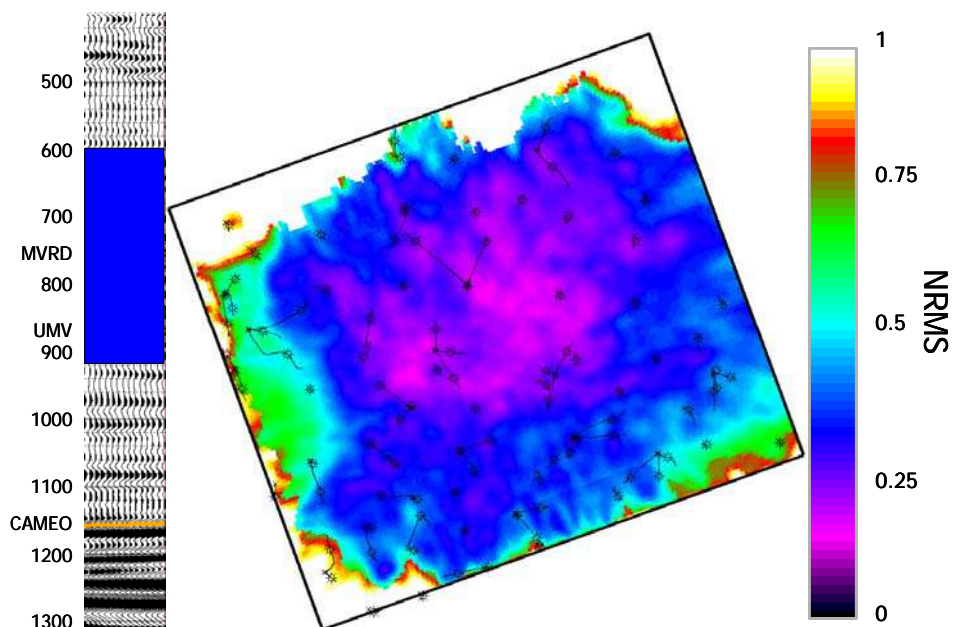


Figure 3.9 - The difference sections before and after the application of the shaping filter are shown above. They indicate that the shaping filter was effective in reducing differences between the volumes.

NRMS: Correlation Time Shift



NRMS: Shaping Filter

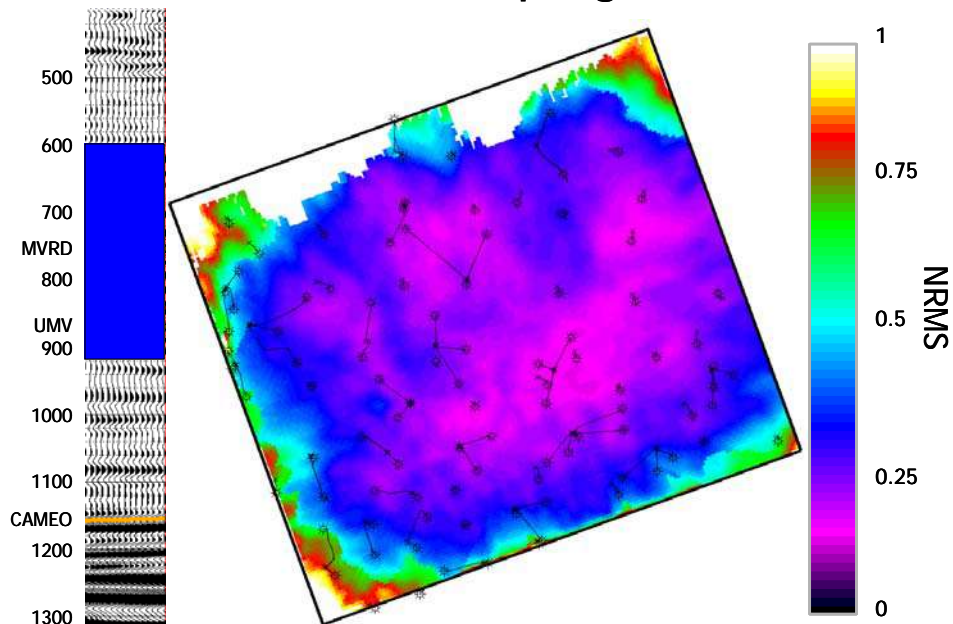
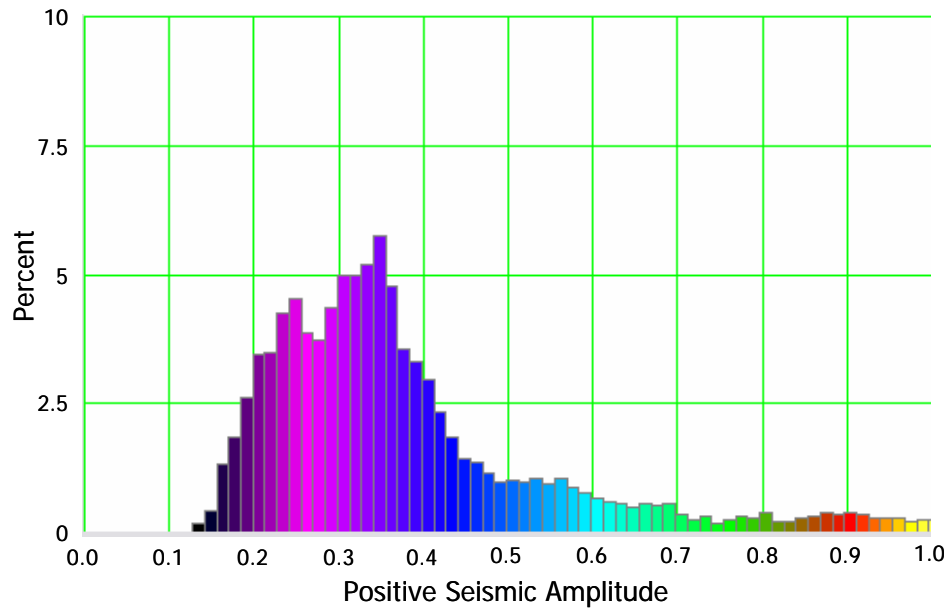


Figure 3.10 - The NRMS maps before and after the application of the shaping filter are shown above. They indicate that the shaping filter reduced differences between the surveys.

NRMS: Correlation Time Shift



NRMS: Shaping Filter

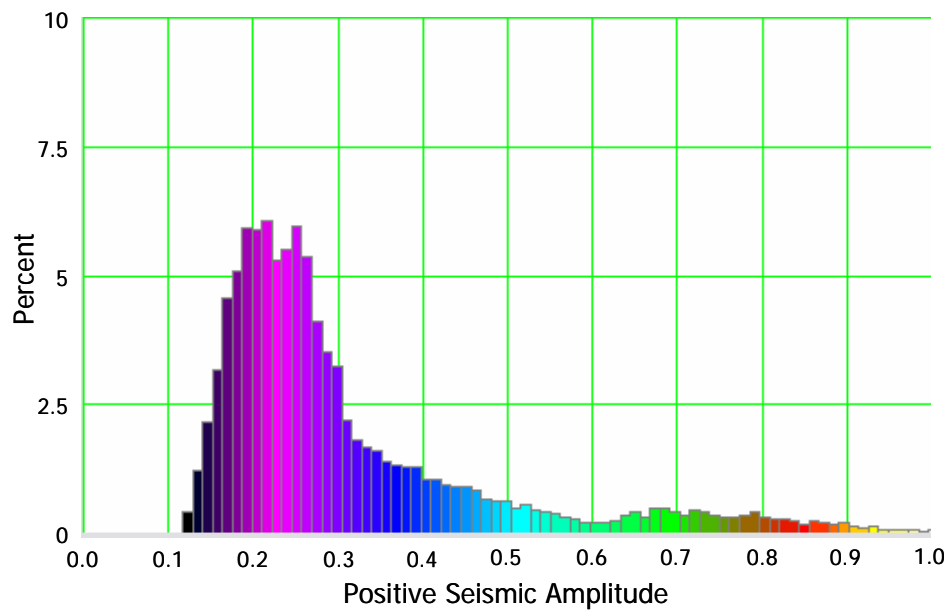


Figure 3.11 - The histograms of the NRMS maps show that the repeatability of the data has been improved by the shaping filter.

3.4 Comparison Gain

Comparison gain, or cross normalization, is a process that corrects for amplitude scaling differences between traces. It is a difficult step to perform properly because incorrect gain factors can create false anomalies and remove real ones. The process assumes that for each common trace pair, there is a single scaling factor that equalizes the amplitude of the traces. This assumes that the scaling factor is constant with time, essentially, that there is a high Q-factor. The scaling factors are calculated only from data in the static section. The factors are calculated by taking the ratio of the RMS values of each trace in a common trace pair over the static window. They therefore scale the ratio of the RMS values of every common trace pair to be one.

I applied this procedure to the Rulison data using the static window, 700-ms to 925-ms, as the window over which to calculate the comparison gain factors. The factors are shown in Figure 3.12. They indicate that the center of the survey needed less scaling than the edges. Unfortunately, there are severe scaling issues in the north, probably associated with the lack of source and receiver positions in that area (Figure 3.12).

The comparison gain lowers differences between the two volumes. A cross section through the data before and after the comparison gain process indicates this (Figure 3.13). It is also apparent that in the deeper section some anomalies are made a bit larger and others appear to be reversed. However, in the static section, as expected, there is no doubt that repeatability was increased. The NRMS maps of this section clearly show this (Figure 3.14). The histograms of these maps show that again the peak moved toward zero and tightened (Figure 3.15).

Ideally, this process matches the amplitude of the surveys without removing or creating large time-lapse differences. However, the scaling factor may be a function of time. In that case, while differences at the static section are reduced, differences later in time may be created or removed. As I show later, the comparison gain was unable to completely fix the severe problems in the north at later time.

Comparison Gain Factors

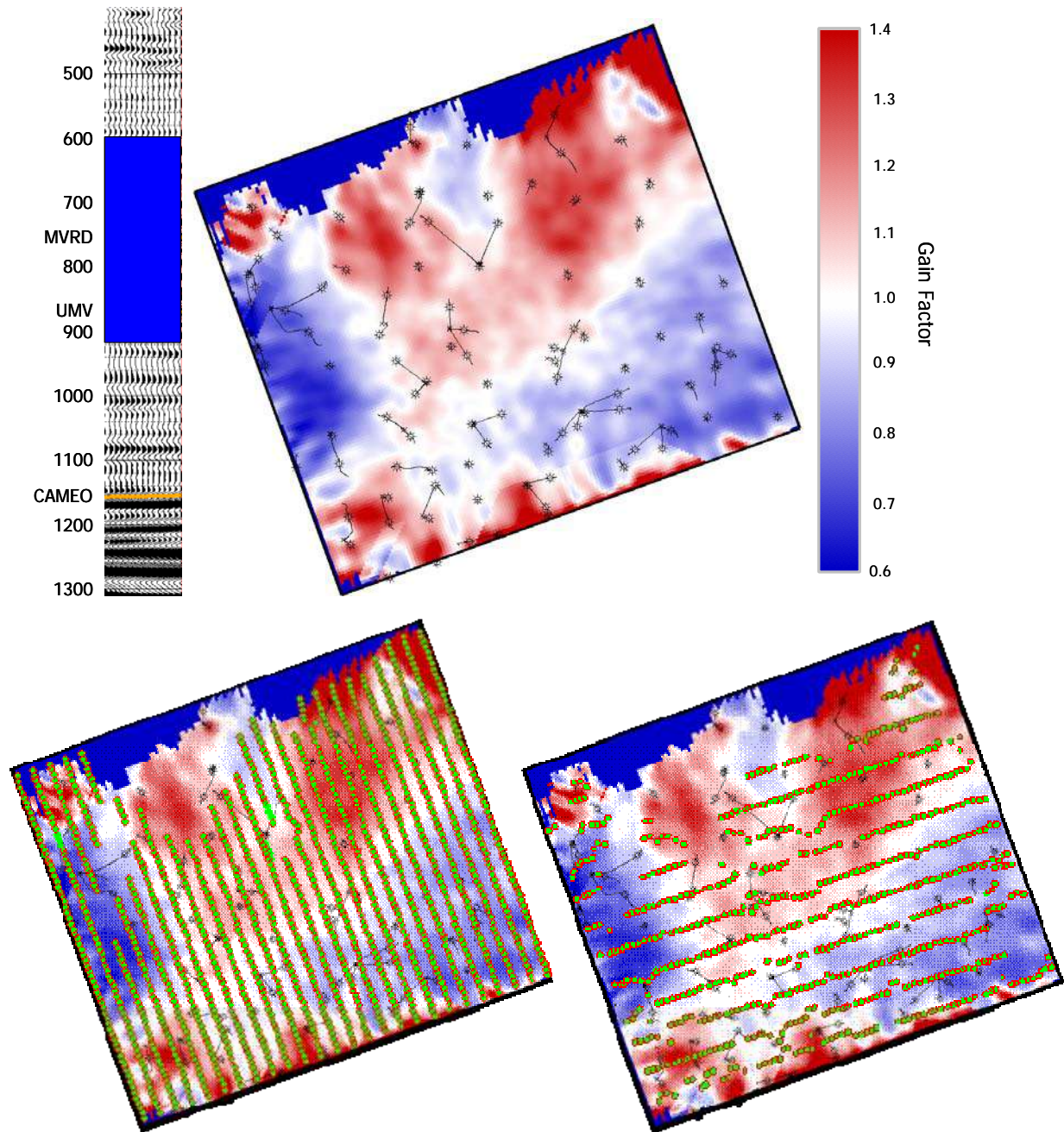


Figure 3.12 - The calculated comparison gain factors vary considerably. The edges and the two zones in the north show significant variations. The source and receiver positions are overlaid in the lower two maps to indicate that a lack of fold and offsets in the north may have caused this.

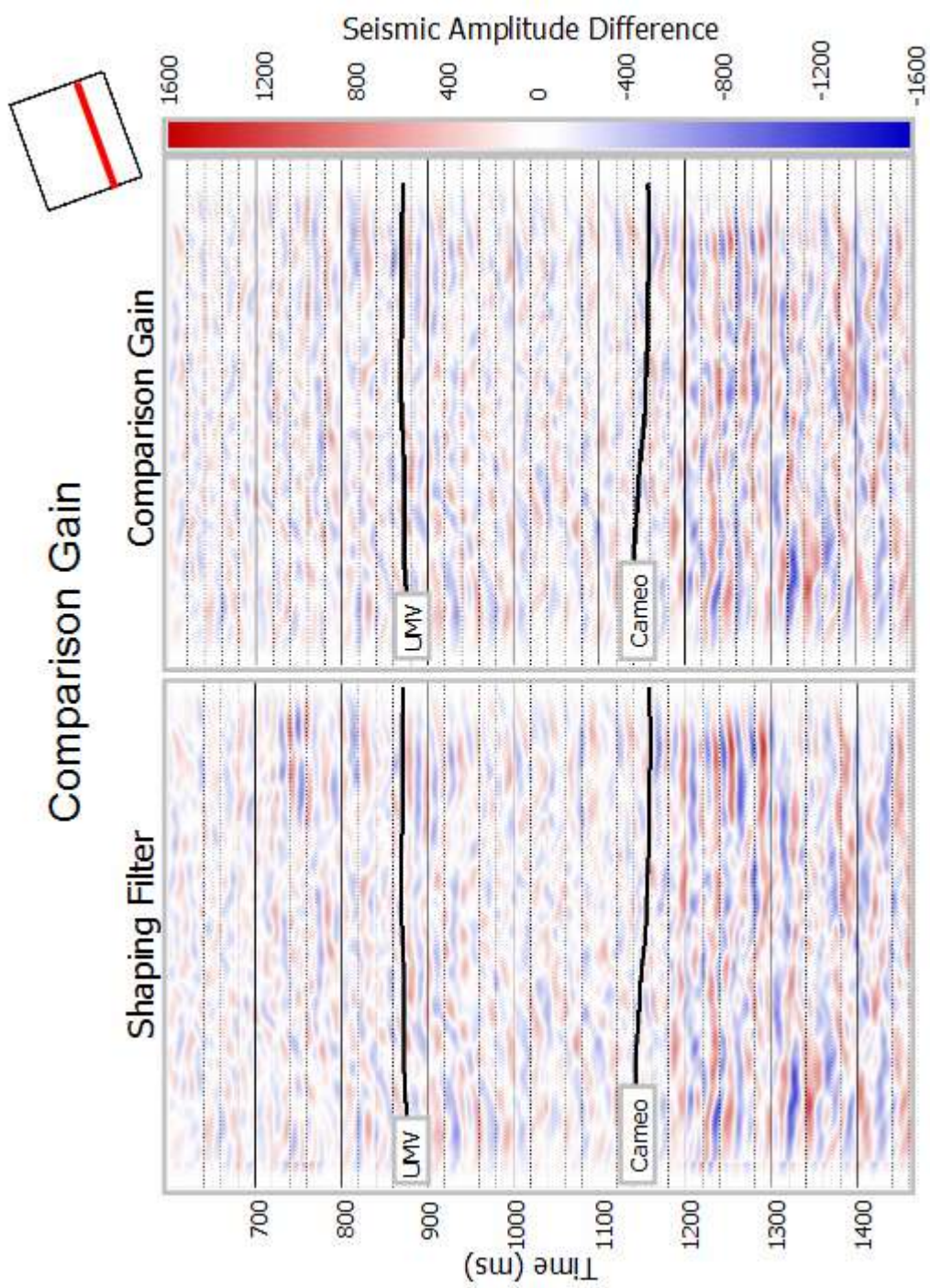
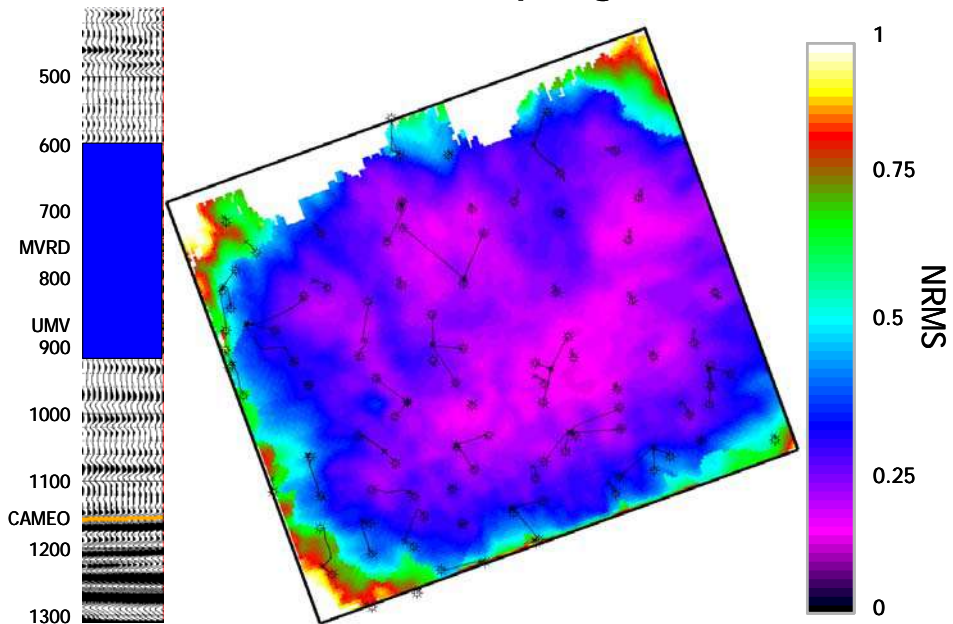


Figure 3.13 - The difference section after the application of the comparison gain appears to show lower difference between the two volumes.

NRMS: Shaping Filter



NRMS: Comparison Gain

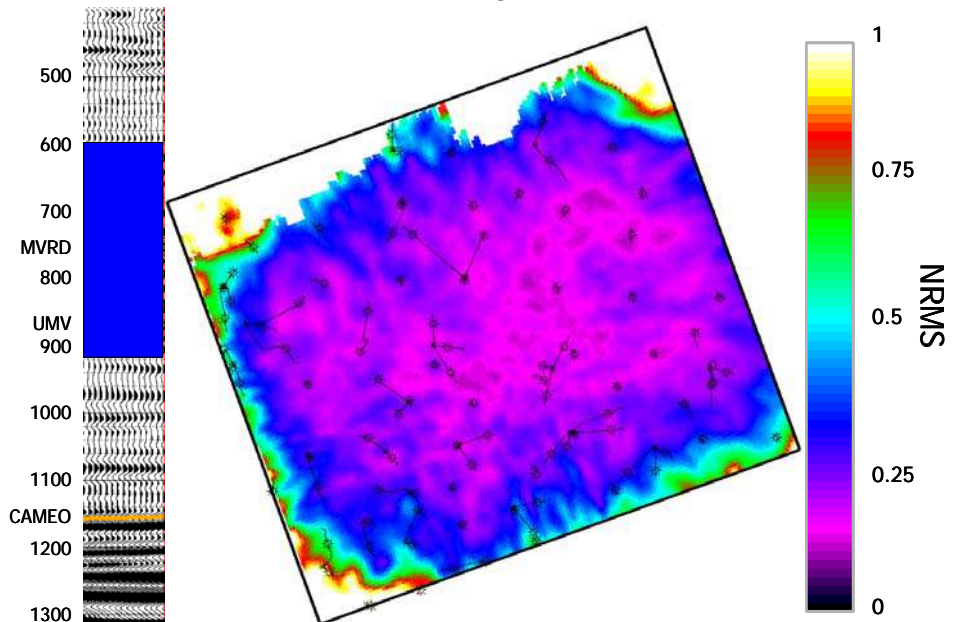
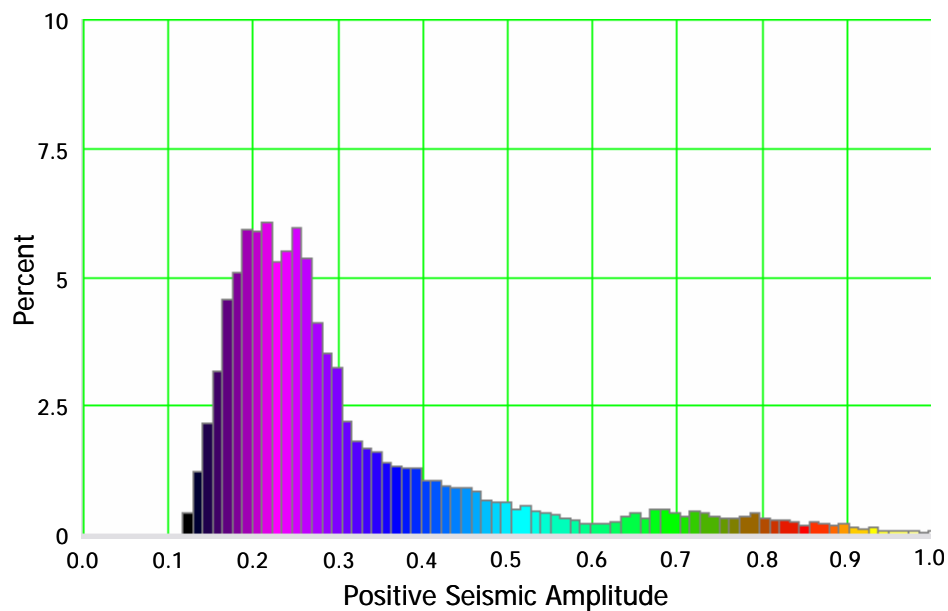


Figure 3.14 - The NRMS maps of the static section indicate that the static section repeatability improved with the application of the comparison gain.

NRMS: Shaping Filter



NRMS: Comparison Gain

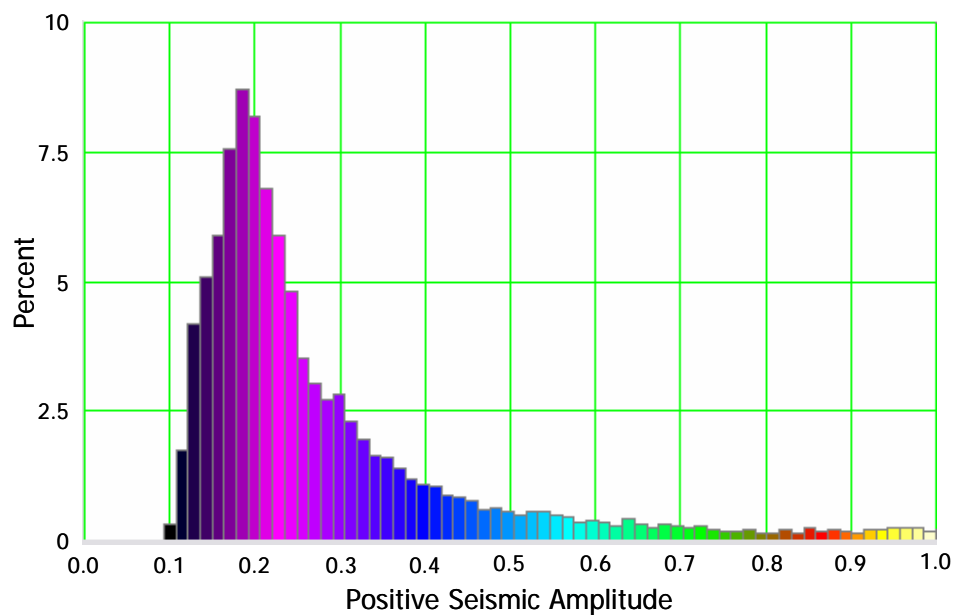


Figure 3.15 - The histograms of the NRMS maps indicate that the comparison gain improved the repeatability in the static section.

3.5 Time-variant Time Shift

The time-variant time shift process removes time shifts between corresponding reflectors. Unlike the static time shift, it removes shifts at all times rather than just one. If production increases effective-pressure and therefore velocity, then time shifts will occur in the seismic data, and these shifts will vary with time because the differences in velocities are depth dependent. These velocity-driven time shifts are a signal in that they indicate that a velocity change has occurred. They must however be removed for amplitude-based interpretation.

The shifts are calculated and removed through the same process that removes the static time shift: a correlation-based time shift. This process is based on a windowed cross-correlation that estimates the time shift between two traces by finding the lag of the maximum correlation value. Instead of calculating a time shift over one window, as in the estimation of the static time shift, the time-variant time shift calculation does this for multiple windows. Shifts at samples between the centers of consecutive windows are interpolated.

I implement the time-variant time shift using Hampson-Russell's PRO4D program. The algorithm is simple and requires only: the correlation window length, the maximum correlation lag, the number of correlation windows, and spacing of the windows. A 200-ms window, a 10-ms maximum time shift, and a window offset of one sample are used to calculate the shift for every data sample.

The volume of time shifts is a time-lapse attribute, but it is also used to precisely time align the two volumes for amplitude-based interpretation. The application of this time alignment reduces time-lapse differences. A cross section through the data after the time-variant time alignment was applied is shown in Figure 3.16. It shows differences are reduced slightly, more so at depth. NRMS maps and histograms of the static section indicate very slight improvements in repeatability with the application of the shift (Figure 3.17 and Figure 3.18).

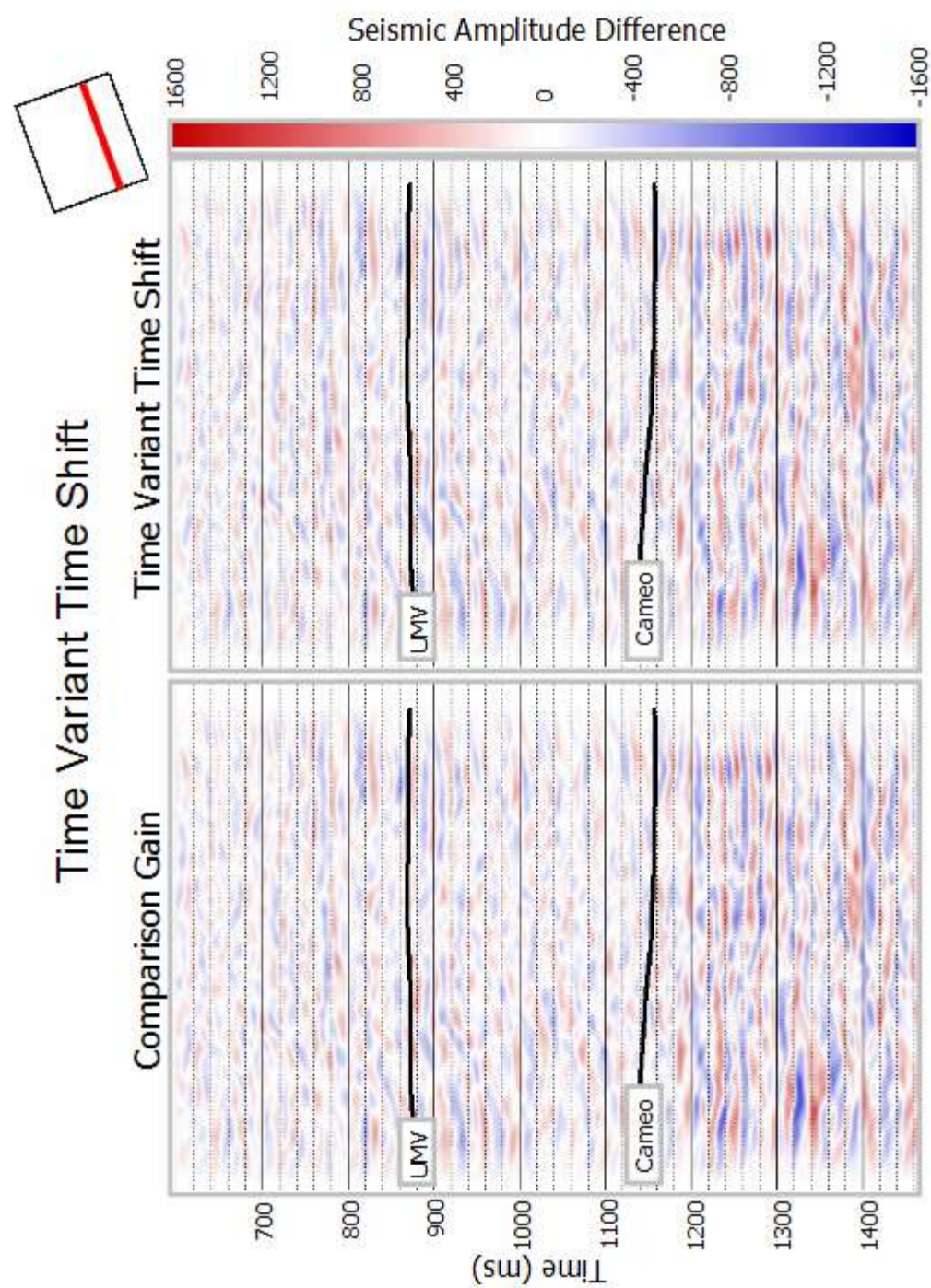
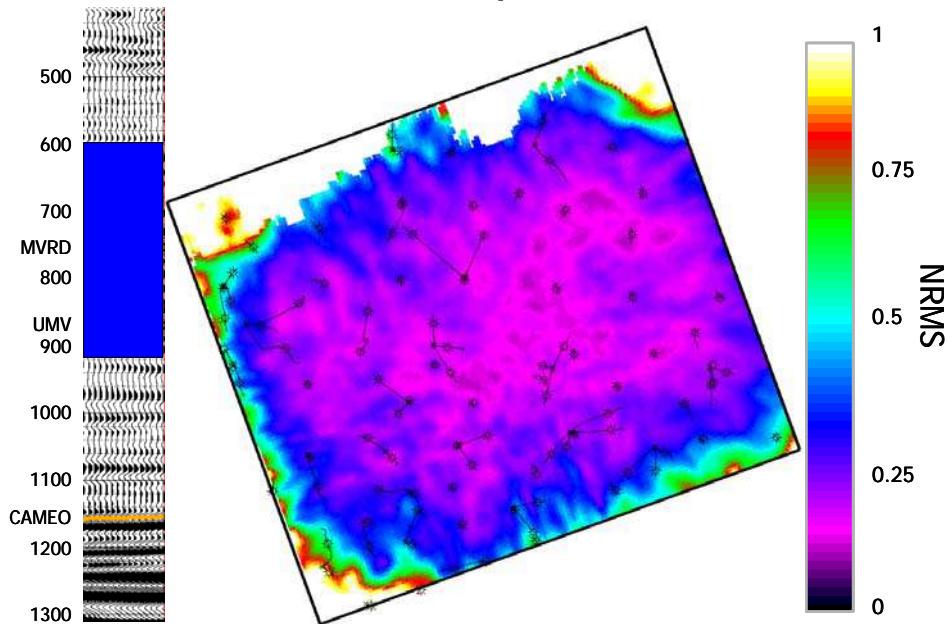


Figure 3.16 - A cross section before and after the application of the time-variant time shift indicate a slight improvement in repeatability at depth after the application of the shift.

NRMS: Comparison Gain



NRMS: Time Variant Time Shift

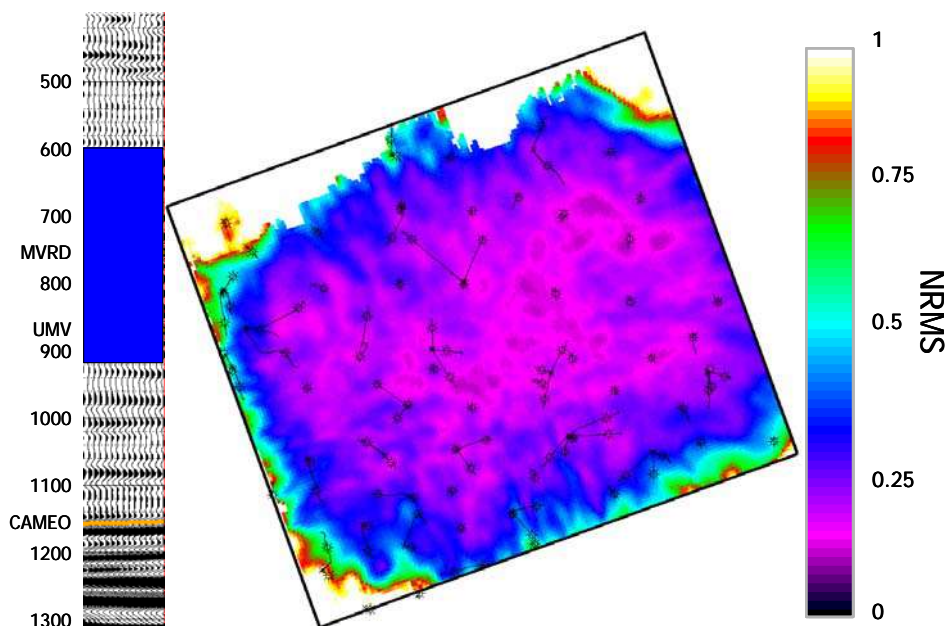
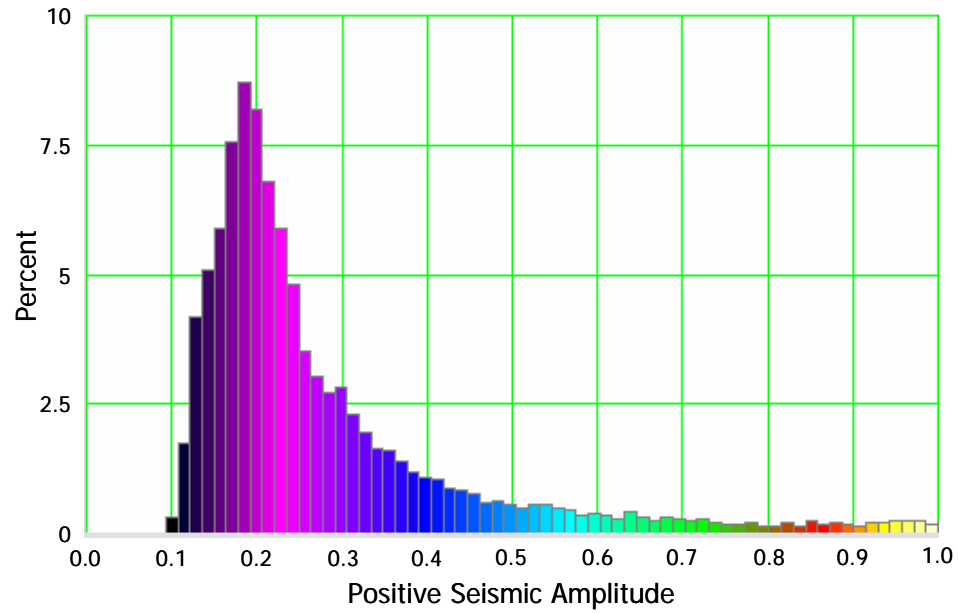


Figure 3.17 - NRMS maps of the static section before and after the application of the time-variant time shift indicate very slight improvements after the application of the shift.

NRMS: Comparison Gain



NRMS: Time Variant Time Shift

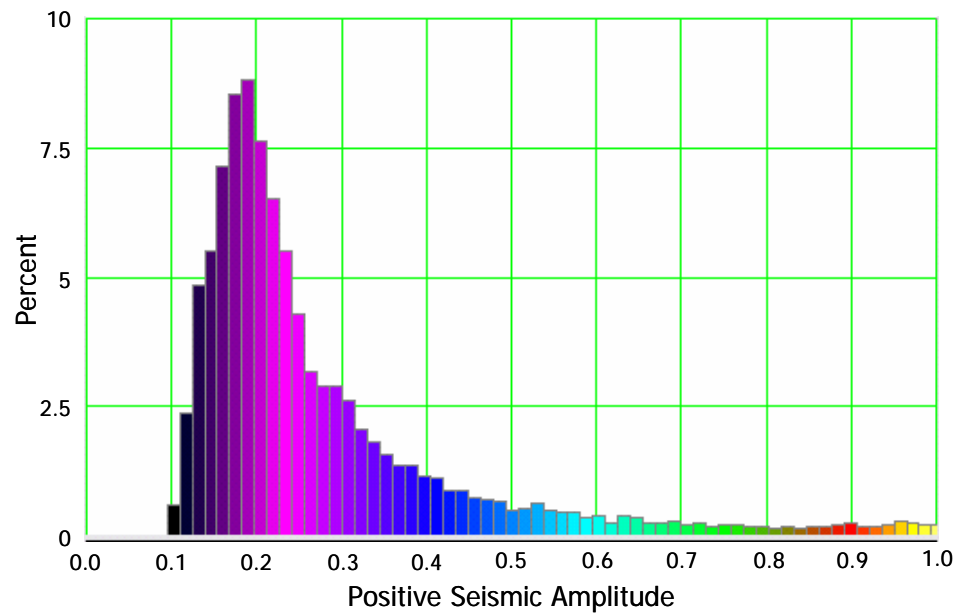


Figure 3.18 - The histograms of the NRMS maps indicate very slight improvements in the static section after the application of the time-variant time shift.

3.6 Inversion

Acoustic impedance inversions attempt to recover acoustic impedance from the seismic data. There are many ways to do this, and all are based on the amplitude of the reflections in the seismic data. Interpretations based on inverted data are essentially interpretations based on seismic amplitude, but acoustic impedance can give physical insights into the data that are difficult to draw with seismic amplitude data alone.

3.6.1 Considerations

There are two main reasons to interpret time-lapse changes from inverted data. First, impedance volumes are closer to an actual picture of the subsurface. Instead of reflectors that indicate impedance contrasts, impedance volumes are composed of bodies of impedance. Therefore, when amplitude changes are found, it is easier to interpret the lithology those changes are occurring in and whether those changes are acoustic impedance increases or decreases. The second reason for using inverted data is that it rescales conventional seismic so that there are no negative values. This may seem trivial, but in order to normalize the difference of two volumes to the original volume, it is important that there are no near-zero values. Otherwise, the normalization blows up and is meaningless.

Inversion is no different than any other transformation performed on time-lapse seismic data in that it must be consistently applied. If it is not consistently applied then there is a risk that artificial changes may be created and real changes may be inadvertently reduced. Therefore, I chose to apply the most consistent algorithm rather than the most accurate or advanced algorithm.

I judge colored inversion to be the most consistent method of inversion. First, it is not an iterative process like model based inversion. It is simply an operator, calculated

from well and seismic data that is convolved with every trace. This makes it very fast to apply. Also, while it may not be the most accurate method due to the fact that one simple operator is used for all traces, it is at least consistent and therefore won't introduce any trace-to-trace changes. Also, by this reasoning, it shouldn't change the relationship between common trace pairs between the volumes. Therefore, I used colored inversion.

Other, more accurate, methods of inversion may certainly be useful, though they must be applied carefully. For instance, model-based inversion can give more accurate results by accounting for the wavelet in the seismic data. However, it is an iterative method and has many parameters; therefore, it is a long and involved process to apply properly. For 4D applications, care must also be taken so that the inversion is consistent between surveys. This is easily done in colored inversion because the operator is the same, but this may not be the case in model-based inversion.

Sparse-spike inversion is another method that may be used. However, this method assumes sparse reflectivity. It attempts to fit the seismic data with the fewest number of reflectors possible. It also assumes simple layered geology. At Rulison, the reservoir is composed of chaotically arranged thin beds. Therefore, sparse-spike inversion may not be well suited for a field like Rulison. Also, this method is iterative and therefore takes longer to apply and refine than colored inversion.

3.6.2 Colored Inversion

Colored inversion is an inversion algorithm that was designed to be fast. It is based on empirical studies of the results of other more traditional inversion algorithms and is theoretically grounded. Basically, it uses the observation that the net result of the application of other inversion algorithms is the application of a -90° phase shift and a mapping of the amplitude spectrum of the acoustic impedance well logs to the seismic data (Lancaster and Whitcombe, 2000). Empirical observations also show that the

amplitude spectrum of the acoustic impedance log is relatively constant over most fields (Walden and Hosken, 1985). Therefore, it stands to reason that inversion can be approximated through the use of a single convolutional operator applied to all the traces in the volume (Lancster and Whitcombe, 2000).

The operator is relatively simple to determine. The amplitude spectra of acoustic impedance logs over a specific field are assumed to have the same general amplitude spectrum and are approximately described by the following equation:

$$Amp = f^{\alpha}$$

The value of α is estimated by fitting a straight line to a plot of logarithm frequency versus logarithm impedance. The slope of the fitted line determines the α value. The operator is then calculated by creating a convolutional operator that converts the amplitude spectrum of the seismic data to the estimated spectrum of the acoustic impedance log and rotates the phase -90 °. One benefit of this method is that the input wavelet does not need to be estimated since it gives rise to the amplitude spectrum of the seismic data (Lancster and Whitcombe, 2000). However, it does assume that the input wavelet is zero phase.

I created the inversion operator for the Rulison data using well RWF 332-21 since it had the best tie to the seismic. I tried using multiple wells, but the results were virtually identical. The determination of the α value is seen in Figure 3.19. It shows that the crossplot of the logarithm of the frequency versus the logarithm of the well log's impedance is very linear. The figure also shows the derived operator.

The colored inversion operator was designed and applied using Hampson-Russell's PRO4D software package. This version of the colored inversion algorithm allows the user to specify whether or not to add in the low-frequency impedance component that the seismic data is missing. Figure 3.20 illustrates this issue. The red curve indicates an idealized seismic amplitude spectrum. The blue curve indicates the frequencies that are added from well information by the inversion process. The real

amplitude spectrum at Rulison is shown in black, and it indicates that the frequencies ramp up linearly between 10 Hz and 20 Hz. Therefore, I chose to add low frequencies from the well information using this range as the ramp. This low frequency information is from well RWF 332-21 and is shown in Figure 3.21. It was extrapolated using the UMW and Cameo horizons to guide it structurally.

Quality control measures make sure that the inversion was well behaved. A comparison of the synthetic seismic data volume created from the inverted data with the real seismic data indicate that the two are virtually identical (Figure 3.22). This should quiet concerns that the colored-inversion process is not an “exact” inversion process. Inverted seismic data overlaid on logs of acoustic impedance at wells Clough-19, RMV 68-21, and RWF 332-21 is shown in Figure 3.23. The first observation to make from this figure is that the inverted data generally matches with the logs in that it falls within the range of the values in the log and thick layers agree well. Notice, however that most of the log is composed of very thin beds that aren't resolved by the inverted data because of the lack of high frequencies. Even in well RWF 332-21, for which the inversion operator was designed, the inverted data only captures the larger features of the impedance log well. A tuning curve for this data indicate that beds below 30-ft thick cannot be resolved Figure 3.24. Thus, we can infer from this that colored inversion is a process that is skewed towards relying on the seismic data rather than fitting the log data. This is ideal since I'm primarily looking for a way to consistently rescale the volumes to an impedance scale so that a percent difference volume can be created.

I created a percent impedance change volume using the following equation:

$$\% \Delta_{AI} = 100 \left(\frac{AI_{2004} - AI_{2003}}{AI_{2003}} \right)$$

The terms AI_{2003} and AI_{2004} denotes the acoustic impedance derived from the 2003 and 2004 surveys respectively. In interpretation I used this volume to find zones of apparent change for further study.

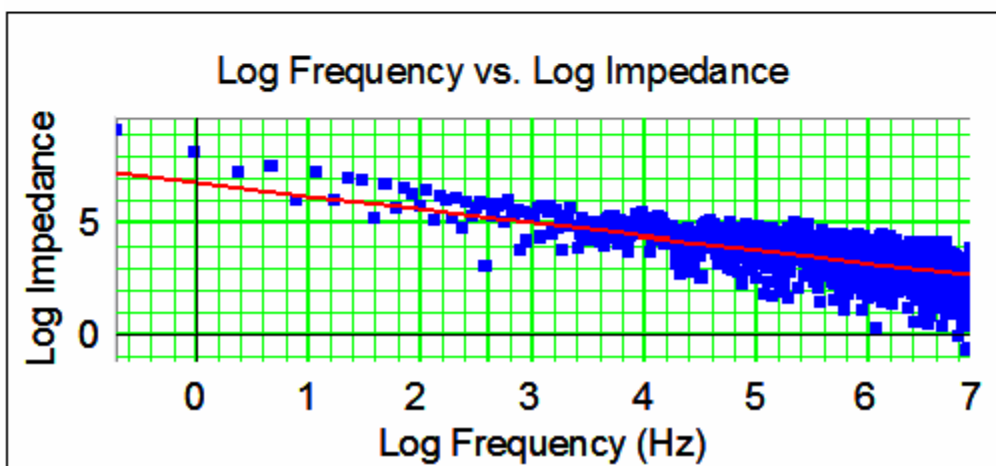
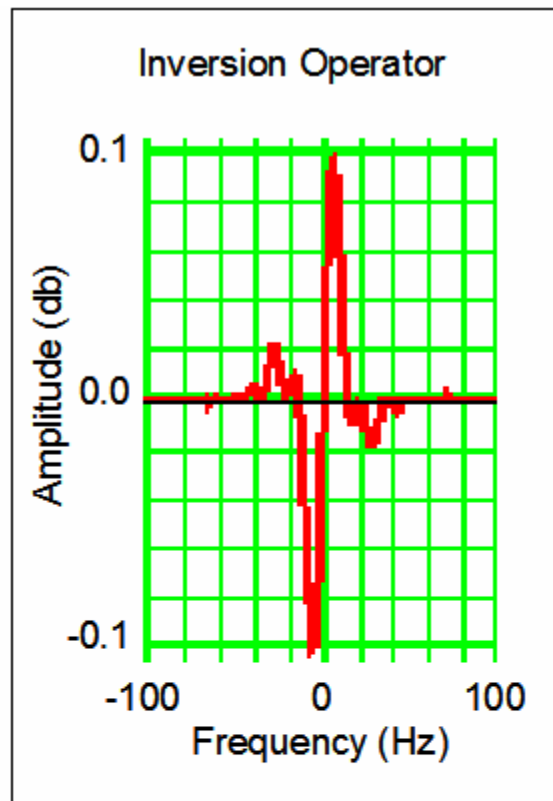


Figure 3.19 - The log impedance log frequency crossplot indicates that the relationship is very linear. The derived colored inversion operator is shown on top and it basically resembles a -90° phase shifted wavelet.

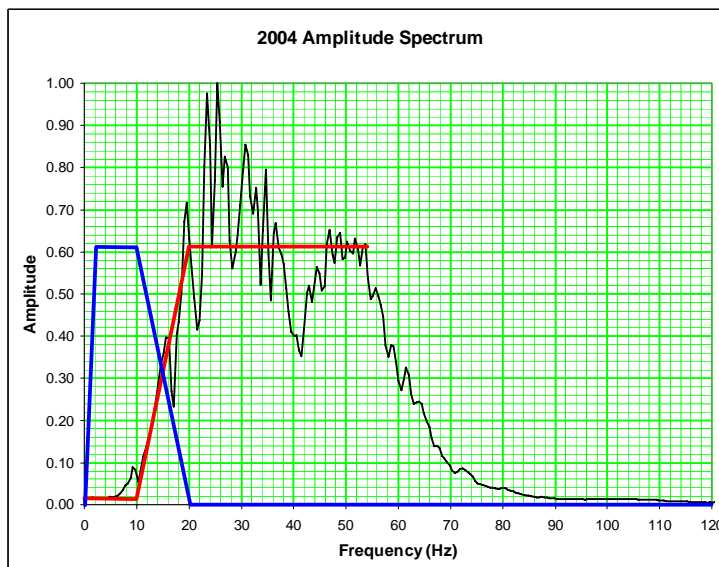


Figure 3.20 - This figure illustrates the fact that the seismic data lacks low frequencies. This is compensated for in the inversion process by adding information from wells. The blue curve indicates the information that is added to the idealized seismic amplitude spectrum in red.

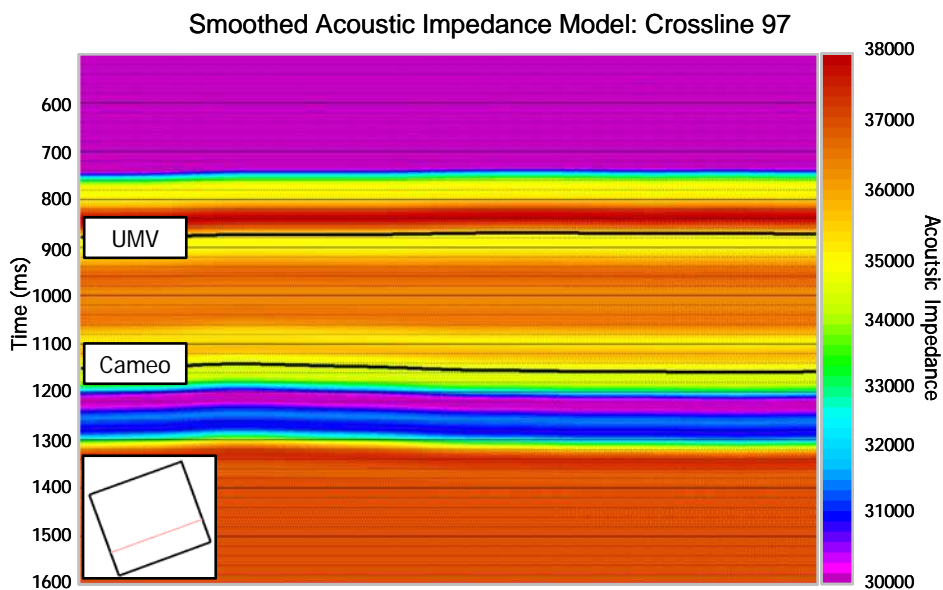


Figure 3.21 - The smoothed acoustic impedance model that was added to the seismic to provide low frequency information was derived from well RWF 332-21.

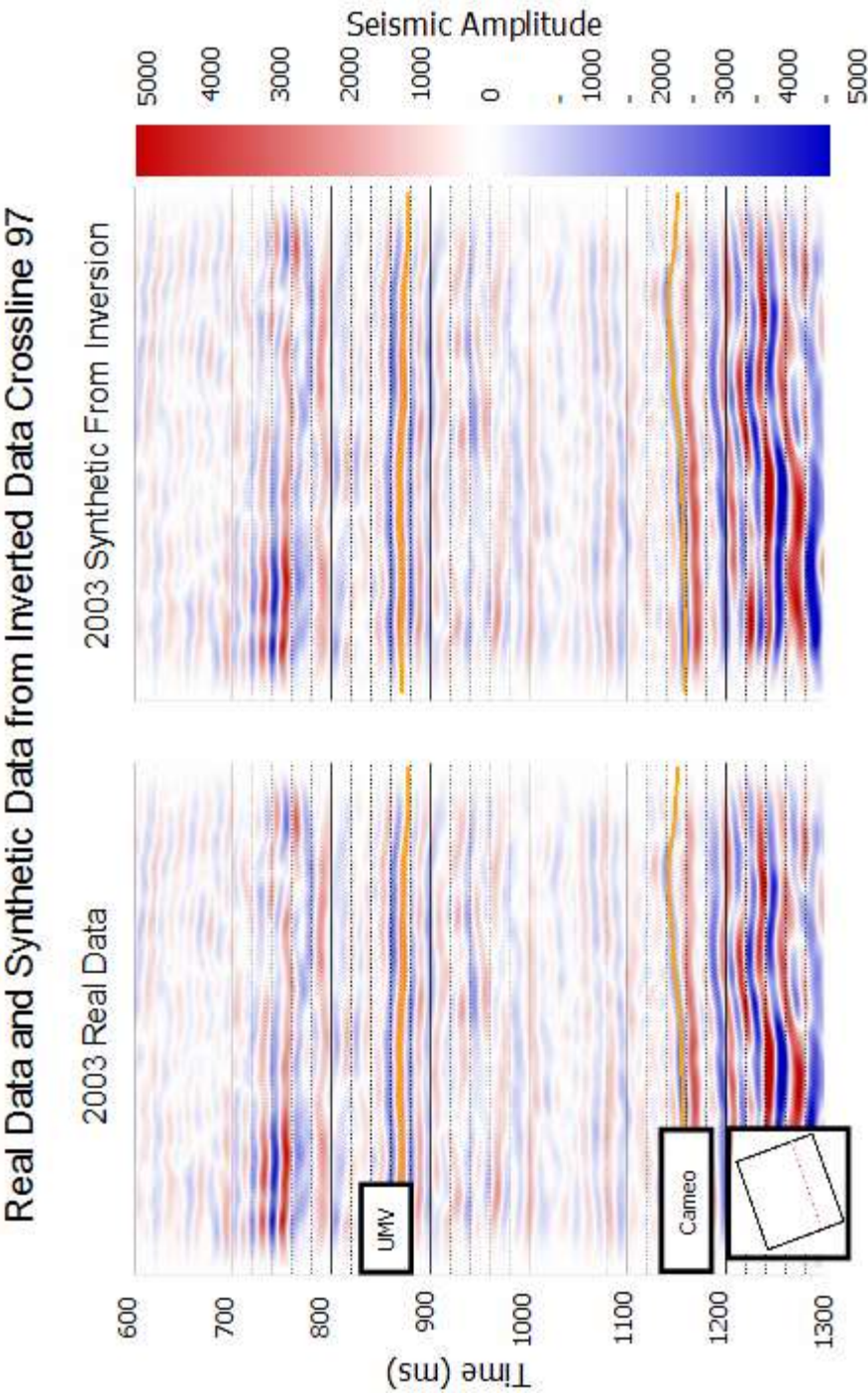


Figure 3.22 - The inversion is very consistent with the original seismic data. There is almost no difference between the real data and the synthetic data derived from the inverted volume.

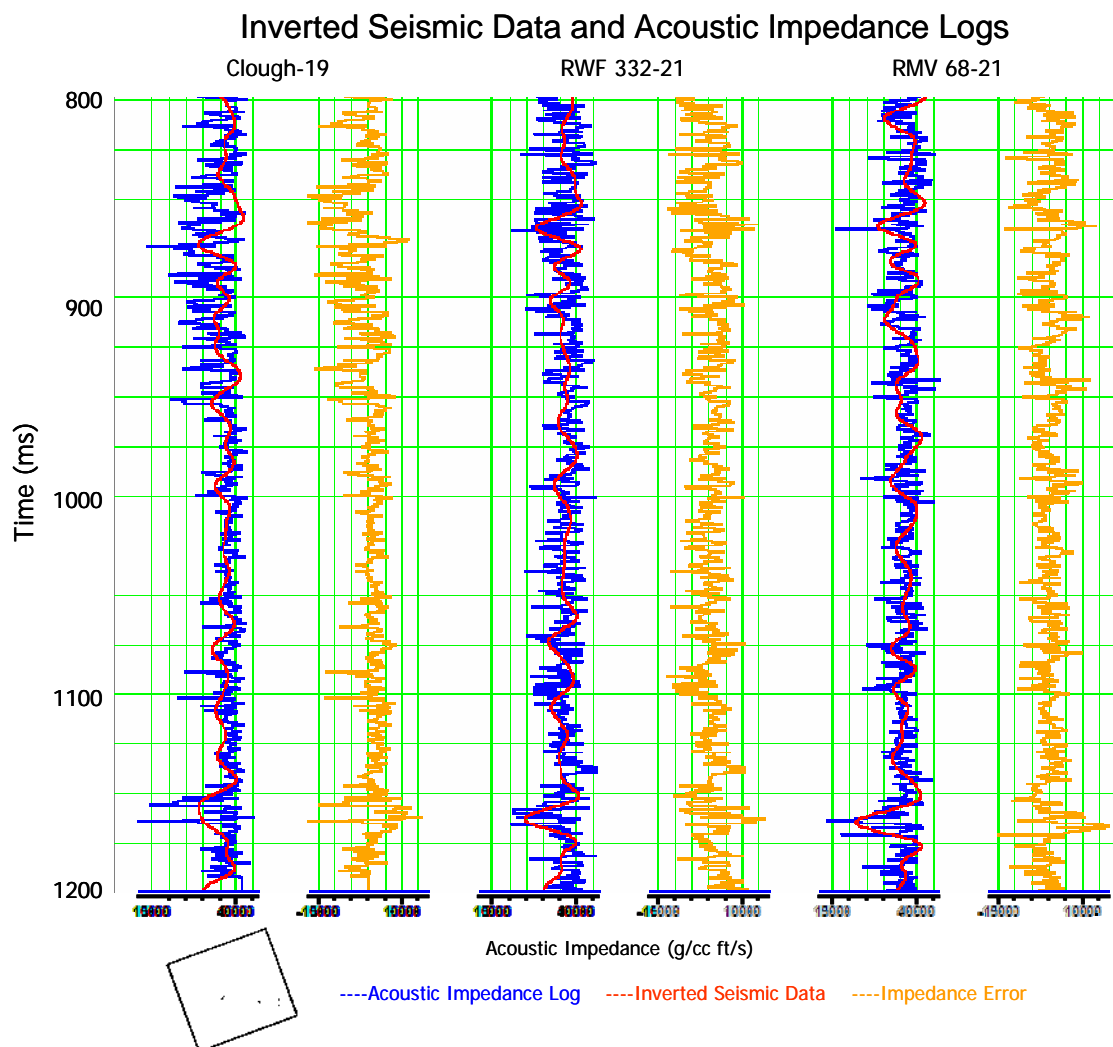


Figure 3.23 - The inverted seismic data falls within the range of impedance values found in the logs; however, due to a lack of high frequencies, it cannot resolve thin beds.

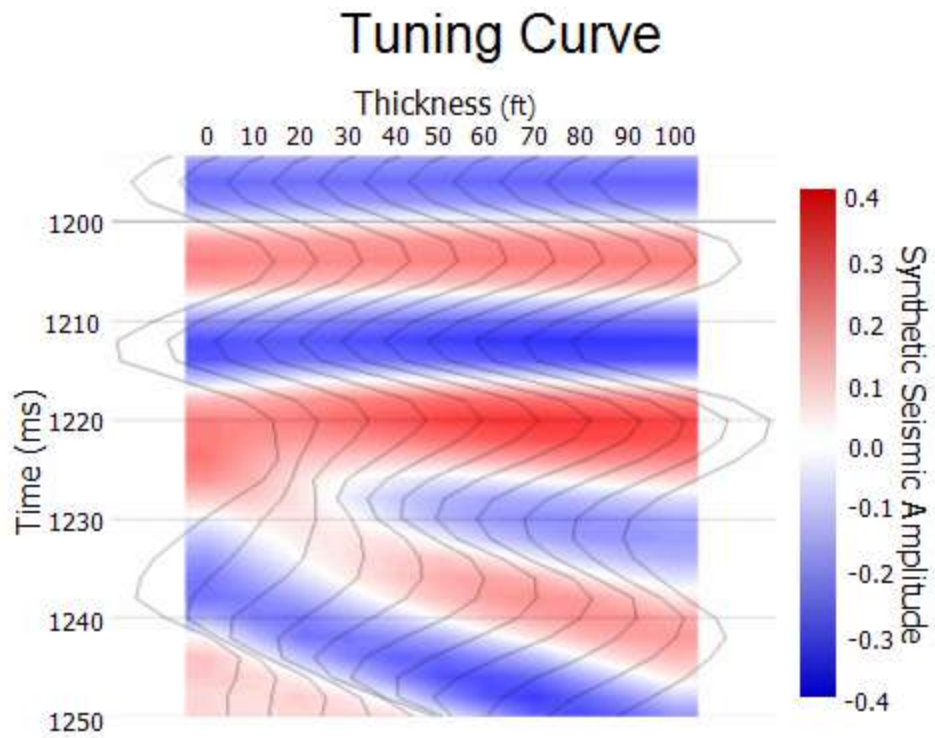


Figure 3.24 - A tuning curve indicates that in the Cameo coal zone the tuning thickness is approximately 30-ft.

CHAPTER 4: MODELING

4.1 Introduction

A realistic model is necessary for proper time-lapse seismic interpretation. First it can indicate the magnitude of the time-lapse signal in the real data. Knowing the magnitude of the expected signal, the necessary repeatability of the two surveys can be estimated and the statistical significance of anomalies can be judged. A model can also show what type of interpretation will best locate and characterize the changes. For instance, in the case of time-lapse seismic, will physical changes in the field best be seen by time shifts or amplitude changes in the seismic? It is primarily for the last reason that I decided to create a rigorous time-lapse model for Rulison field. In the words of Dr. Steve Hill, "If you're going on a turkey hunt, you better know what a turkey looks like."

4.2 Input Data

I chose to model the P-wave time-lapse response at well RWF 332-21 because it has a bulk density log and a real P-wave log. Sonic logs, unlike density logs, are rare at Rulison field, and it is important to use a real rather than a modeled sonic log. Also, RWF 332-21 has a cross-dipole sonic log; therefore, the modeling can be relatively easily extended to model S-waves in the future.

P-wave and bulk density logs are not enough to create a realistic time-lapse model. It is also necessary to know how those logs change with production of the field. Ideally, both logs would simply be run again after production to calculate impedance changes due to production. Unfortunately, that isn't economically feasible at Rulison. Thus, assumptions are made and relationships are used to create logs after production.

Rulison is a geologically complicated reservoir; however, the manner in which it is produced is not. This allows several assumptions to be made in the modeling. First I assumed that reservoir pressure decline is the only cause of 4D effects at Rulison. This is reasonable because only negligible amounts of water are produced at the field and no fluids are injected to maintain pressure. Also, the sandstones are very tight and stiff. Thus, it is reasonable to assume that we should expect little or no density change in producing sand intervals. As a result of these assumptions, it becomes clear that we simply need to know how production lowers effective-pressure and how P-wave velocity changes with effective-pressure.

The exact relationship between production and pressure at Rulison is poorly understood, because of a lack of data. Pressure buildup tests are time consuming and therefore expensive: especially when they must be carried out on up to 30 sandstones per well over a period of years. Fortunately, some pressure data exists at Rulison. Daily casing and tubing pressures are available for every well. Also, pore-pressure measurements at every perforated sand exist in several wells located in the 10-acre pilot area. These measurements are made with mini-frac tests.

Mini-frac tests work much like frac jobs: the interval of interest is packed off, fluids are pumped in, and fractures are created. These tests do the same thing, but once fracturing is initiated the pumping is stopped and the pressure is monitored. Based on the pressures over time pore-pressure can be estimated. At Rulison, these estimates are calibrated with a few pressure buildup tests taken at the same time. This data is good because it gives pore-pressures at every sand in the well in which it is run, but at Rulison the measurements were not repeated over time. Thus, there is no true measure of pore-pressure decline due to production at Rulison.

However, the mini-frac tests do give an idea of how large pore-pressure drops due to production can be. First, a "virgin" pore-pressure gradient must be assumed. The assumed gradient is derived from pore pressure measurements at the MWX site. The mini-frac data agree with this gradient. If this "virgin" pore-pressure gradient is correct,

then departures from it must be caused by some external factor. Because these tests were done in the 10-acre pilot area, where the wells are extremely close together and in close proximity to older producing wells, it is reasonable to assume, that even with very tight sandstones, communication could occur between wells. Thus, the difference between unusually low pore-pressure zones and the expected pore-pressure at that zone is the drop in pore-pressure due to production at a nearby well.

Mini-frac data indicate that pore-pressure depletion on the order of 35% of virgin pressure occurs (Figure 4.1). This gives a maximum pore-pressure drop of approximately 1500 psi. Unfortunately, it is difficult to tell how quickly these drops occur from mini-frac data. Because the wells are all so close it is unclear which wells are depleting each other and when the depletion occurred. Wellhead pressure data fills in that part of the story. Figure 4.2 shows a wellhead pressure curve at Rulison. It shows a pressure drop of approximately 1800 psi: a magnitude similar to that derived with mini-frac data. Perhaps more interesting is the fact that the drop occurs over only a period of months. So, pressure decline at Rulison is nearly 35% of virgin pressure and it occurs quickly, at least near the wellbore.

In order to turn pore-pressure changes into velocity changes, a relationship between the two is needed. This relationship was measured by another RCP student, Eugenia Rojas (Rojas, 2005). It was measured on dry core plugs from sandstones located in cores taken from the MWX site. In her experiments, the confining pressure was varied and the P-wave velocity was measured (Figure 4.3). An exponential fit to this data is used to calculate velocity changes from effective-pressure changes.

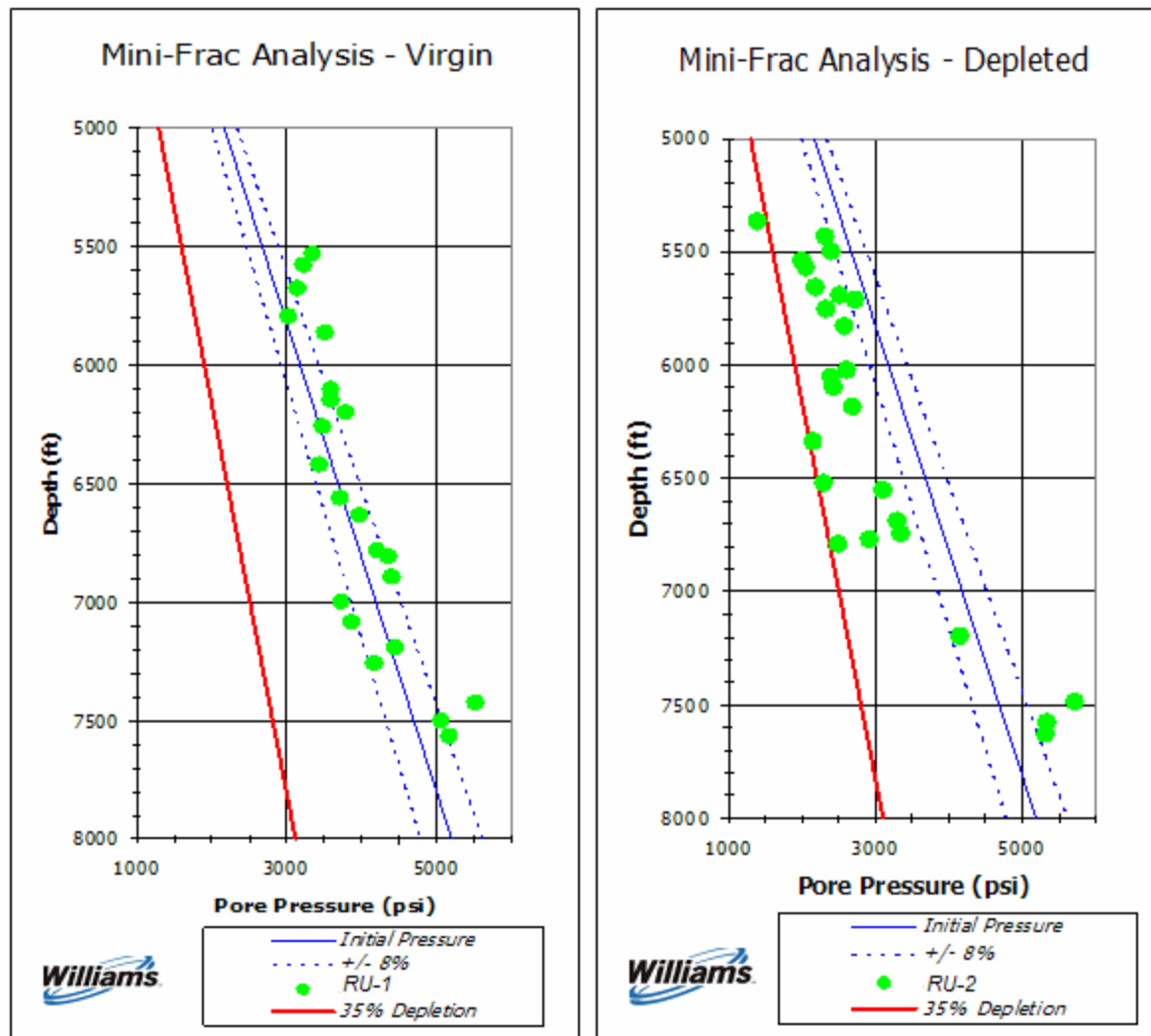


Figure 4.1 - The mini-frac data from two wells at Rulison is shown above. The blue lines indicate virgin pore-pressure and the red line indicates 35% depletion. The well on the left is assumed to be virgin while the well on the right is depleted from production

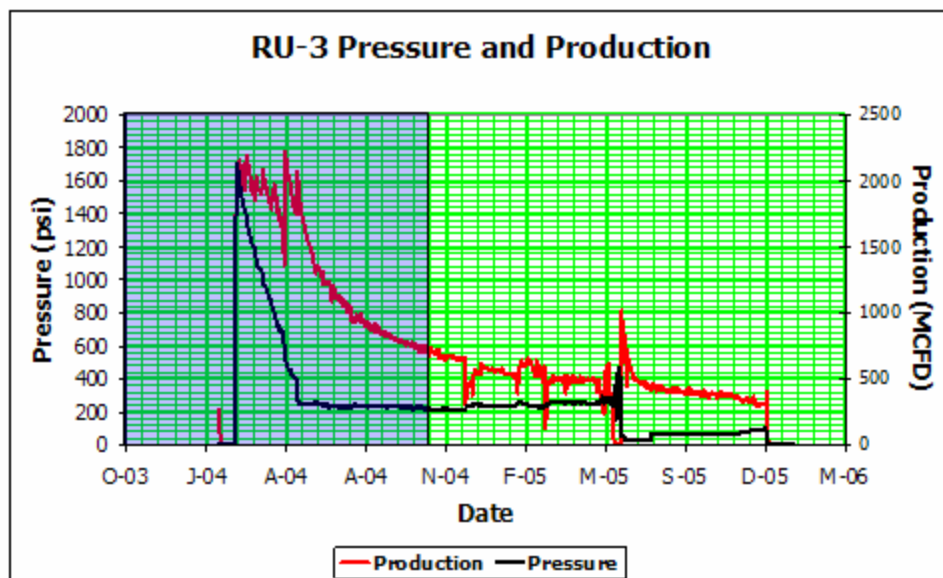


Figure 4.2 - Above wellhead pressure is shown in black and production is shown in red for well RWF 443-20. The time-lapse interval is shaded. The pressure drop is nearly 1800 psi over only a few months.

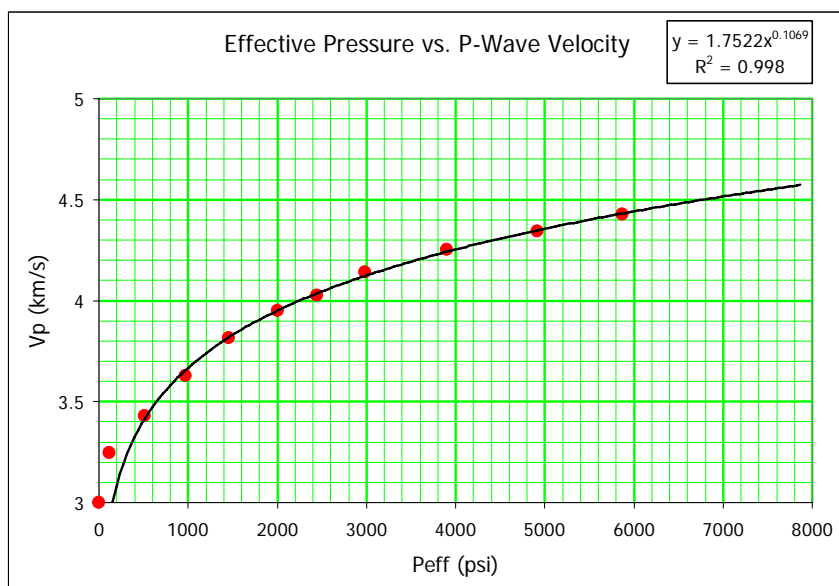


Figure 4.3 - P-wave velocity vs. effective-pressure as measured by Eugenia Rojas is shown above. The black line is an exponential relationship fitted to the data (Rojas, 2005).

4.3 Methodology

Modeling the time-lapse response at Rulison starts by creating an effective-pressure profile for well RWF 332-21. The virgin pore-pressure gradient from the MWX data is used as an estimate of the original pore pressure. A confining pressure profile is estimated by integrating the density log. Density is assumed to be constant at 2.5 g/cc in zones where there was no density log information. The density logs are not corrected for invasion effects, but since the formation is so tight and integration is insensitive to high frequency changes, it is not necessary. Finally, effective-pressure is calculated using the following equation:

$$P_{eff} = P_{confining} - \alpha P_{pore}$$

The term α is the coefficient of effective-pressure, and it has a large effect on the change in effective-pressure due to pore-pressure. Unfortunately, it is also very difficult to determine accurately. Using static bulk modulus logs (derived from the P-wave, S-wave, and density logs) and the following equation the effective-pressure coefficient is estimated (Hofmann et al., 2005):

$$\alpha = 1 - \frac{K_{eff}}{K_{matrix}}$$

K_{eff} = Effective bulk modulus of rock (derived from logs)

K_{matrix} = Bulk modulus of matrix (assumed to be quartz) ≈ 38 GPa

The resulting values of α for the perforated sandstones are quite scattered given that α must be between zero and one (Figure 4.4). The average is approximately 0.55, and that is the value used in modeling. As an upper bound cases where α was equal to

one are also modeled. The lower bound is of course when α is equal to zero, and in that case there is no effective-pressure change and no time-lapse signal.

To simulate production the effective pressure at every perforated sand is increased. Based on the mini-frac data, I assume that the maximum pore-pressure drop is 35% of virgin pore-pressure. This change is applied to the pore-pressure profile and the effective-pressure after production is calculated using equation 4.1 (Figure 4.5). This method, however, unrealistically assumes that every zone produces equally to depletion.

I also model a case where the pressure decline varies from zone to zone. Using a production log from a different well at Rulison, I assume that the production rate and pressure drop are linearly related. Dividing the production log by its maximum value and multiplying the result by the 35% yields a pore-pressure profile with variable pressure drops. Converting this new pore-pressure curve to effective-pressure gives an effective-pressure curve with varying pressure changes, or a production scaled curve (Figure 4.5).

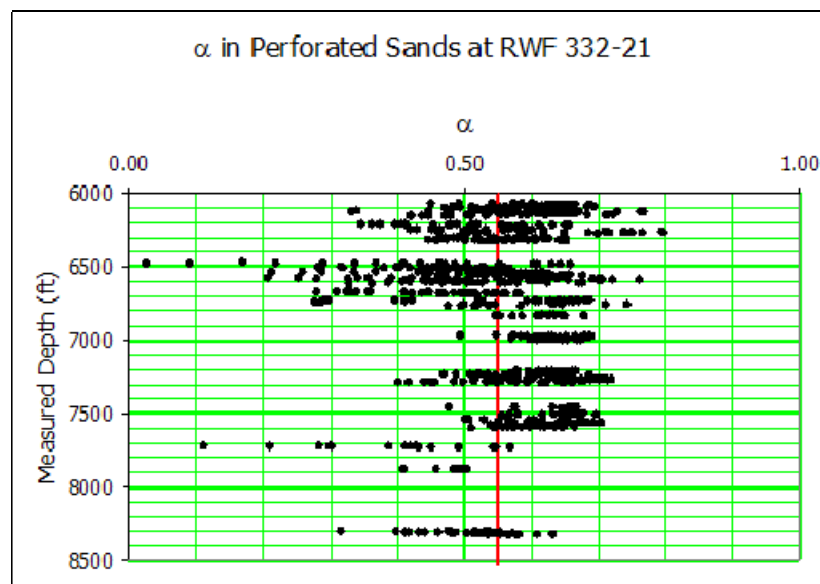


Figure 4.4 - The calculated values of α for every perforated sand in well RWF 332-21. The average value, $\alpha = 0.55$, is shown in red.

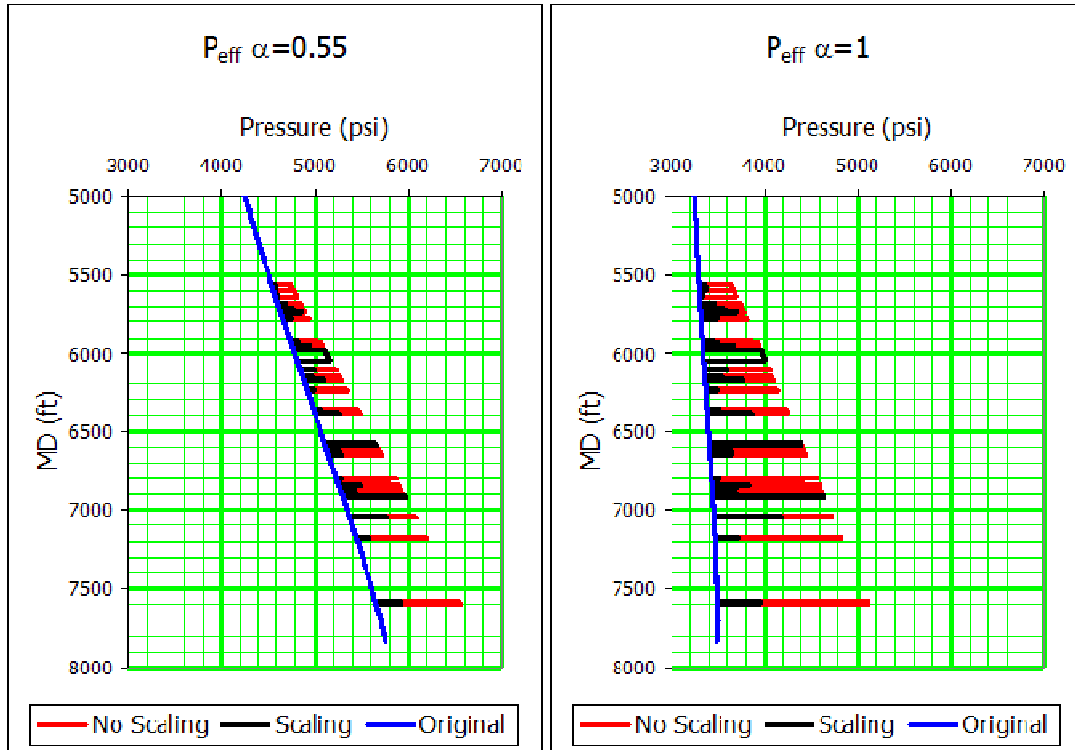


Figure 4.5 - The scaled and unscaled modeled changes of effective-pressure are shown above for two values of α .

The next step in modeling is to translate the changes in effective-pressure to changes in the P-wave sonic logs. This is done by fitting a curve to the ultrasonic P-wave velocity vs. effective-pressure measurements shown in Figure 4.3:

$$V_p = 1.7522P_{eff}^{0.1069} \quad (4.2)$$

Using equation 4.2 the increase in P-wave velocity for the effective-pressure increase at every perforated sand is calculated. Then, the changes to the original sonic log are added to create a modeled post-production sonic log. The modeled sonic logs and the density log are converted into zero offset synthetics.

4.4 Results

Four different post-production scenarios are modeled to see how the results vary:

- $\alpha = 0.55$ with pore-pressure scaled by the production log
- $\alpha = 0.55$ with no pore-pressure scaling
- $\alpha = 1$ with pore-pressure scaled by the production log
- $\alpha = 1$ with no pore-pressure scaling

The first scenario in the list has a low value of alpha and was scaled by the production log; thus, it represents the smallest change we would expect to see. The last scenario in the list represents the largest change we might expect. The other two scenarios are intermediate (Figure 4.5).

The modeled production changes are interpreted in two ways. The first is to calculate the time shifts between the synthetic without any production and the synthetic after production. This is accomplished by calculating a time shift via cross-correlation for every point on the modeled trace. The time shift algorithm, part of Hampson Russell's PRO4D software, cross-correlates the two traces over a user specified window. It then defines the shift as the time of maximum correlation. The, calculated time shifts using a 200 ms window, overlain by the produced effective-pressure curves are shown in Figure 4.6.

The time shift calculation indicates that even with all the zones producing at a maximum pore-pressure decline only a 1-ms time shift accumulates. This may be an over-estimate given that velocity increases in producing zones can be accompanied by velocity decreases in the surrounding zones. Also, the time shifts don't correspond in depth to the producing zones' depths. Thus, it does not appear that individual producing zones can be located via time shifts. The best time shifts can do is indicate that production is occurring in a spatial region.

Amplitude analysis is also useful for identifying time-lapse change. To do amplitude analysis the time shifts are removed from the modeled trace and the modeled

trace is then inverted using a colored inversion. Figure 4.7 shows the percent impedance changes calculated between the original synthetics and the modeled synthetics. The results indicate that production of individual zones may be monitored with amplitude data if the noise level is low enough. It appears that the changes in impedance will be very small: on the order of one percent.

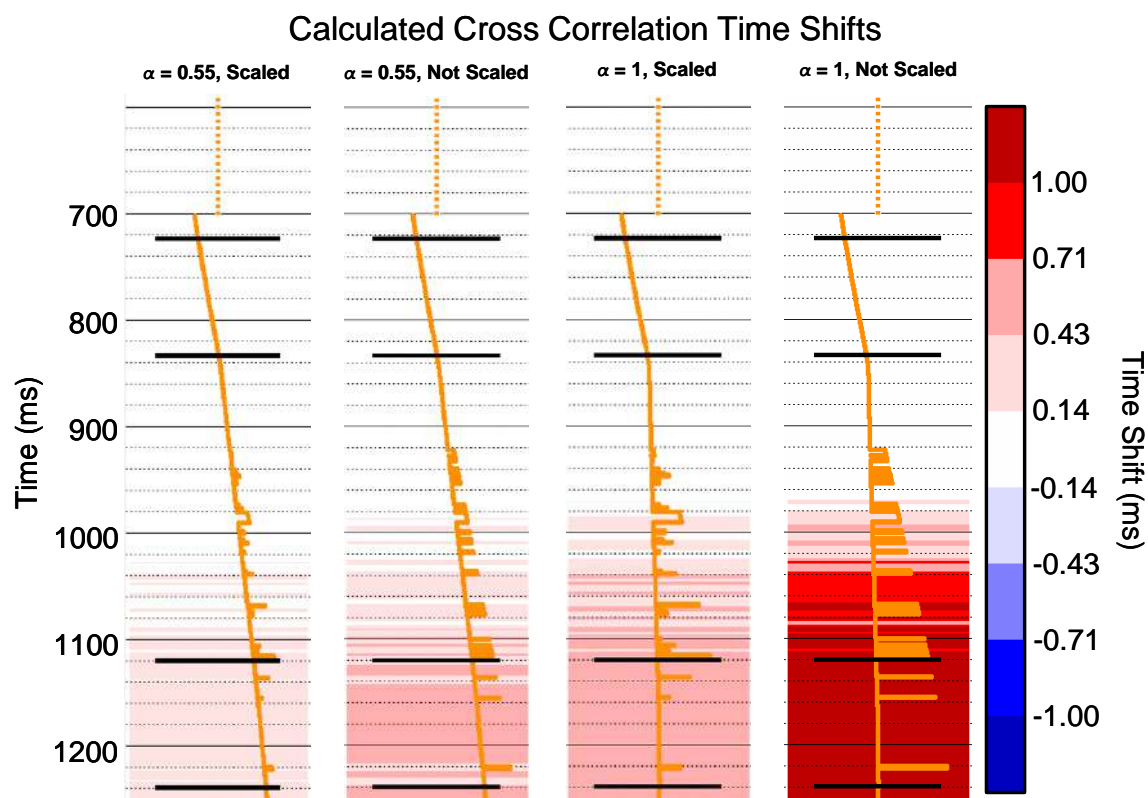


Figure 4.6 - The calculated cross-correlation time shifts between the modeled data and the original data. The results indicate that time shifts will be very small and cannot indicate individual producing zones.

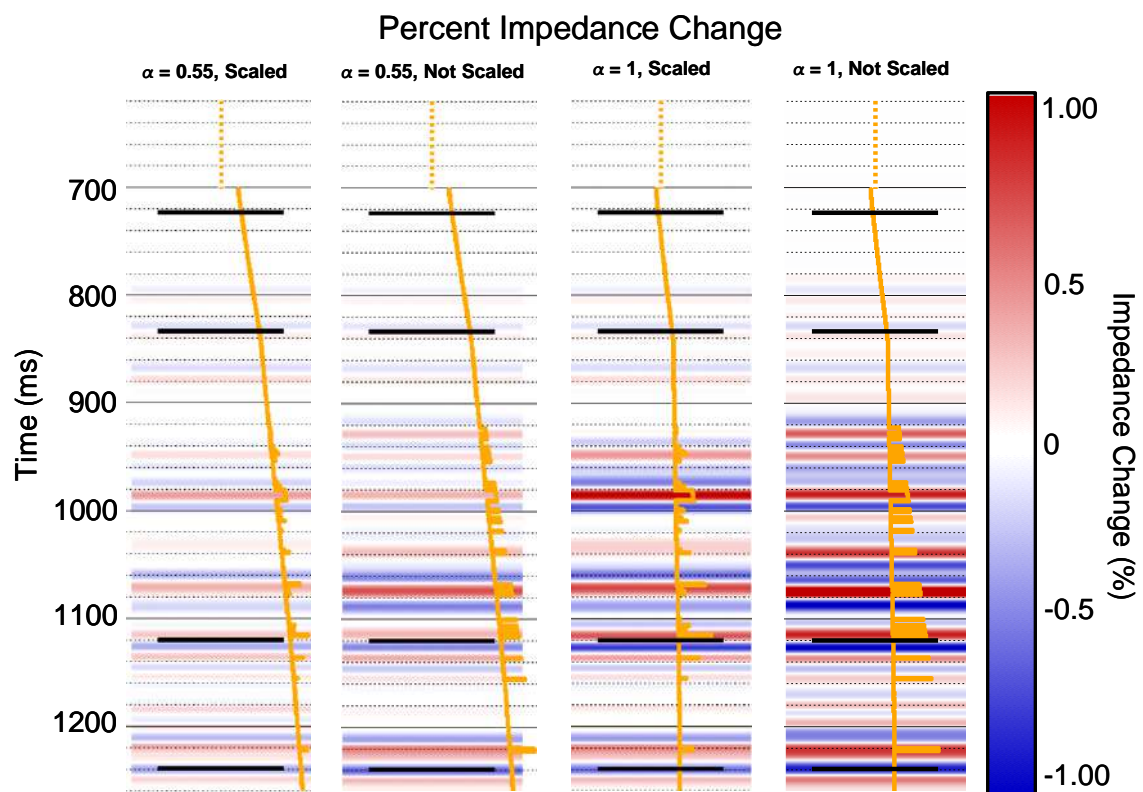


Figure 4.7 -The percent impedance change between the modeled and original data. The results indicate that impedance changes will be very small but will be able to identify large individual or groups of producing zones.

4.5 Model Assumptions and Shortcomings

In the words of Exxon Mobil 4D seismic specialist Dave Johnston, "All models are wrong." This model is no exception as it lacks several key features. First, it is only a zero offset synthetic model. In reality, different offsets would see different changes in impedance.

Another key shortcoming of this model is that it is based on ultrasonic measurements. The relationship measured at ultrasonic frequencies may not be the same relationship measured at seismic frequencies. One reason for this is dispersion: the variation of velocity with frequency. Though, in high-velocity rocks, like the rocks at Rulison, dispersion is less of a factor than in low-velocity rocks. Another concern is the scale of the volume of rock being sampled. For instance, ultrasonic data measures at wavelengths of millimeters while seismic data measures at wavelengths of tens to hundreds of meters. At these scales, core plugs cannot possibly include all the features in the subsurface that would affect seismic data: notably, faults and fractures. Therefore, macroscopic crack closure due to production could have a significant effect on seismic impedance; however, my model, based only on matrix production, does not include this effect (Hatchell and Bourne, 2005).

The model also assumes that changes are only occurring in sandstones. This is because the effective-pressure P-wave velocity measurements were only conducted in sandstones. While it is true that the sandstones are connected to the wellbore; it is not true that they will be the only formations affected by production. For instance, stress changes may affect adjacent formations through a process called stress arching. In this process, stress increases in producing zones are accompanied by stress decreases in the overlying and underlying zones. This causes large stress increases in the producing zone at the edges of production. Seismically, the result is that velocity increases in producing zones are surrounded by velocity decreases in adjacent formations. The same is true for impedance (Tura et al., 2005).

Lithologies other than sandstones may be producing. Fractures can extend beyond their intended boundaries into other units. At Rulison, this is not a problem since the gas bearing interval is huge and contains only bound water. Thus, out of zone fractures do not lead to the wells watering out. They may however lead to production from shale or coal and unexpected 4D effects.

Finally, the many assumptions about pressure and rock properties may not be correct. The mini-frac data has uncertainties, but it was calibrated with pressure buildup tests. The wellhead pressure decreases may not be directly attributable to pressure in the reservoir, but it is the only pressure data available in a time-lapse sense. Even if the pressure decreases are large enough to see, it is still uncertain whether one year is a large enough period of time for the decrease to spread far enough from the wellbore to see. Another problem is that α is difficult to determine accurately. While it's possible that it may be higher than my estimate, it may also be lower. An α of 0.2 would be devastating for time-lapse at Rulison; however, it is unlikely that it is this low given the results of Mahendra Kusuma's work.

Therefore, considering the limitations of the model, I expect that the 4D signal from matrix only production in the sandstones at Rulison should be very small. Given that data have noise and repeatability issues, it may even be too small to see. However, due to the shortcomings of the model it's possible that larger than predicted changes could also occur, especially given the fractured nature of the reservoir. Furthermore, if such changes are present and significant with respect to repeatability, it is reasonable to assume that they are not directly caused by production of gas from the rock matrix. Therefore, they must be caused by some other effect like fractures closure, stress effects, or production from other lithologic units.

CHAPTER 5: INTERPRETATION

5.1 Time Shift Analysis

The theory behind time shift analysis is simple. It is based on the fact that velocity is expected to increase in the producing sandstones between the two surveys. This increase in velocity is indicated by Eugenia Rojas's P-wave effective-pressure relationship (Rojas, 2005). I modeled its effect in the previous section. Because of the velocity increase, seismic waves take less time to pass through producing zones. One thin producing zone will hardly change the travel time of a wave, but a large stack of these zones will have a cumulative effect on the travel time of the wave. If the velocity increases are large enough, and the zone is thick enough, this travel time decrease will be seen as a pull up in reflectors below the zone of velocity increase.

This pull up is quantified by calculating the correlation time shift below the zone of interest or throughout the entire volume. The process for calculating the shift is exactly the same as was used in the cross-equalization flow. First, a window is chosen over which common trace pairs are cross correlated. The time shift at the value of maximum correlation is the correlation time shift. For a volume based calculation, a sliding window is chosen. The shift is calculated at one time sample, the window is advanced one time sample, and the shift is calculated again. This process continues for all time samples in the volume. The resulting time shift volume is used as an attribute to indicate velocity change and to precisely align two volumes in time before amplitude analysis.

It is important to realize that correlation time shifts are based on the maximum value of cross-correlation. This may sound trivial, but it has important implications for interpretation. For instance, if the correlation is low, the time shift may not be a real time shift induced by velocity change of the overlying strata. It may simply be a result of

comparing two wavelets of different shape and forcing them to align. In time-lapse data, this kind of information is still useful. Physical changes in the reservoir can cause changes in the character of a seismic wavelet over time. Thus, the maximum correlation volumes associated with correlation time shift volumes can be important time-lapse attributes themselves, but they can first be used as a check to make sure that calculated time shifts are real.

The correlation window length is also important. Short windows result in shifts that are large and associated with low correlation values. This is because only a small part of the wavelet is considered. If the window is extremely short, in the sense that it does not always include a minimum and a maximum, then the shifts will be extremely variable and will distort the wavelet. Long windows smooth shifts by averaging all the reflectors in the window. One large isolated shift will throw off the shift calculated in nearby zones because that large shift is within the large correlation window. I use a window of 200-ms based on experimentation with the modeled data.

5.1.1 Repeatability

Modeling indicates that the largest time shifts due to production in the Williams Fork will be approximately one millisecond, but what is the smallest shift that can be confidently observed? Using permanent sources and receivers pressure induced time shifts down to 50 μ s have been measured (Meunier et al., 2001). Using non permanent sources and receivers time shift accuracy is less.

There are several acquisition related factors that influence the accuracy with which time shifts can be observed. The first is that the recording equipment is capable of measuring accurately under a millisecond. The I/O System Four recording system accurately records samples to within 20 μ s and is therefore not a significant source of error (Elder, 2006). Another factor is that sampling interval is small enough to capture

the highest frequencies of the signal. Meunier et al. used a 2-ms sampling rate to observe shifts as small as 50 μ s (Meunier, 2006). The Rulison data has a sampling rate of 2-ms and therefore a Nyquist frequency of 250 Hz. The data do not contain much information above 80 Hz, thus this sampling rate is more than adequate to capture the frequency content of the signal (Figure 3.6). Finally, cultural noise contaminates the data and can lower time shift accuracy by making waveforms less repeatable. An oilshale processing plant in the northwest of the survey, a drill rig operating in the northwest corner of the survey, a garbage dump in the northern part of the survey, and the day to day operation of the field all contribute to this noise. The high fold of the RCP survey combats this problem.

Near surface velocity variations can also influence the accuracy of time shift interpretation. These variations shift traces forward or backward in time depending on the nature of the velocity change. The shifts do not influence the timing between reflectors that are below the near surface. However, stacking the data can introduce noise into the time shifts because at far offsets the early-time reflectors are muted. Due to this, the early-time reflectors are only present in the near offsets while the late time reflectors are present at all offsets. Slight shifts at far offsets are then stacked into the late reflectors but not the early ones. This results in noise in the time shift calculation between early and late-time reflectors. Statics corrections and high fold compensate for this effect.

Small velocity variations in the near surface are present between the surveys. These may be caused by rain during the 2004 survey. Also, they may be caused by slight differences in recording geometry or man-made changes in the near surface. For instance, a pipeline was built between the surveys that involved the creation of a road. This changes both the near surface and shifts source and receiver positions.

Examination of the final statics solutions indicates they are generally consistent between 2003 and 2004 (Figure 2.7). Nearly all the differences between the shifts are less than 1-ms (Figure 5.1). Crossplots of the statics solutions between the two years indicate a strong correlation ($R^2 = 0.99$). However, a difference map of the statics

solutions between years indicates that there are isolated differences up to approximately 5-ms (Figure 5.1). These differences may be indicative of residual statics differences that remain in the data. The high fold of this survey (up to 220 in the center) should help to compensate any time shift noise induced by residual statics that remain in the data. A pre-stack correlation time shift may also be a way to improve time-shift accuracy (Roche, 1997).

There are many sources of noise that can influence time shift accuracy. It is difficult to know how much noise each source contributes, and in many cases there is not enough information to calculate it. An estimate of the total noise in the time shifts is therefore the most effective way to gauge the noise level. However, even making this estimate is problematic. If the survey encompassed an area where absolutely no production occurred and no change was expected, the shifts in traces in this area, over the depth range of the productive interval in productive areas, would be the noise. There is no such area at Rulison. Another method is to assume that, based on the modeling in Chapter 4, only positive time shifts (velocity increases) are expected. There are, however, mechanisms that can cause velocity decreases. Stress increases in the producing zones can be accompanied by stress relief (velocity decreases) in surrounding zones in a process called stress arching (Tura et al., 2005). Therefore, it cannot be assumed that all the negative time shifts are noise.

Thus, I cannot think of a way to accurately estimate the noise in the time shifts. This does not mean it cannot be done, and it would be valuable future work. However, knowing the potential causes of time shift noise can still be an aid to interpretation.

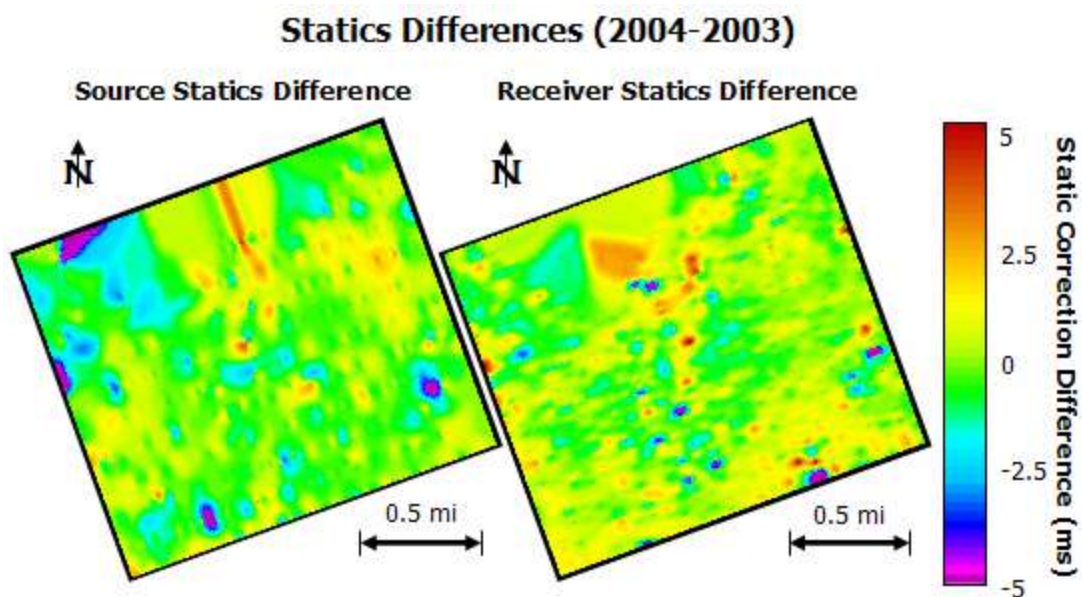


Figure 5.1 -Difference maps of the statics corrections between years indicate that the solutions are generally consistent, but that there are isolated differences up to 5 ms.

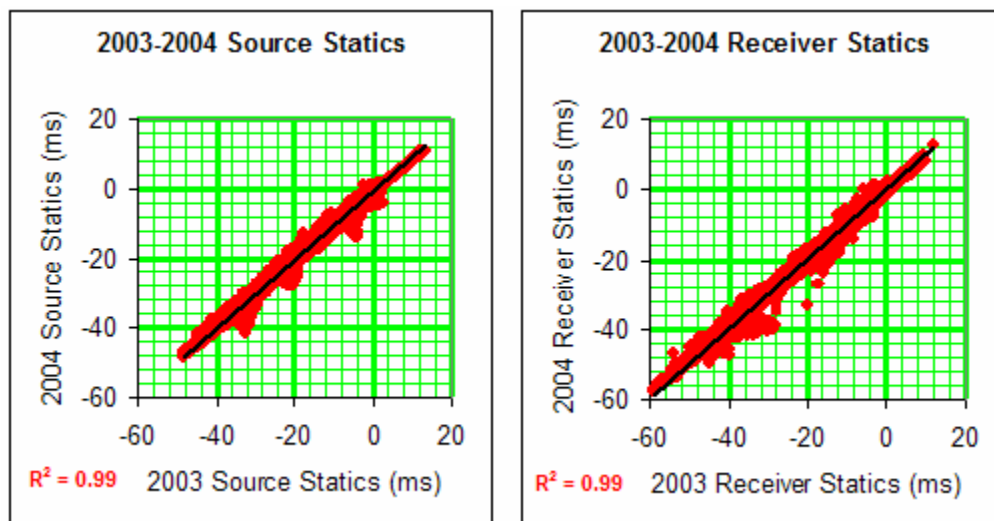


Figure 5.2 - The source and receiver statics crossplots indicate that the statics are consistent between the two years even though they were calculated independently.

5.1.2 Observations and Interpretation

Time-lapse anomalies are identified and investigated using a time-variant time shift volume, the modeling results, and production information. These data show that there are time shift anomalies that are generally consistent with modeling. I observe that the magnitude of the anomalies is not directly related to production, though there are several reasons for this lack of correlation. Also, the anomalies are located near wells of varying ages, indicating that production and the corresponding time-lapse response, is complex.

The time-variant time shift volume created using Hampson-Russell's PRO4D software package contains the time shifts that must be applied to the 2004 volume to align it with the 2003 volume. Prior to the creation of this time shift volume, the 2003 volume is aligned to the 2004 volume at the static section. Thus, the shifts in this time shift volume should represent production induced effects.

The calculated shifts generally agree with the modeling. Most are a millisecond or less and the majority are positive. A positive shift indicates that an event in the 2004 volume arrived earlier in time than in the 2003 volume. This implies a velocity increase. The opposite is true for negative time shifts. In section view, the shifts accumulate with depth starting at about 6000-ft. An overlay of the modeled scenario with production scaled and $\alpha=1$ indicates that the modeled and real data are consistent in the magnitude and distribution of time shifts (Figure 5.3).

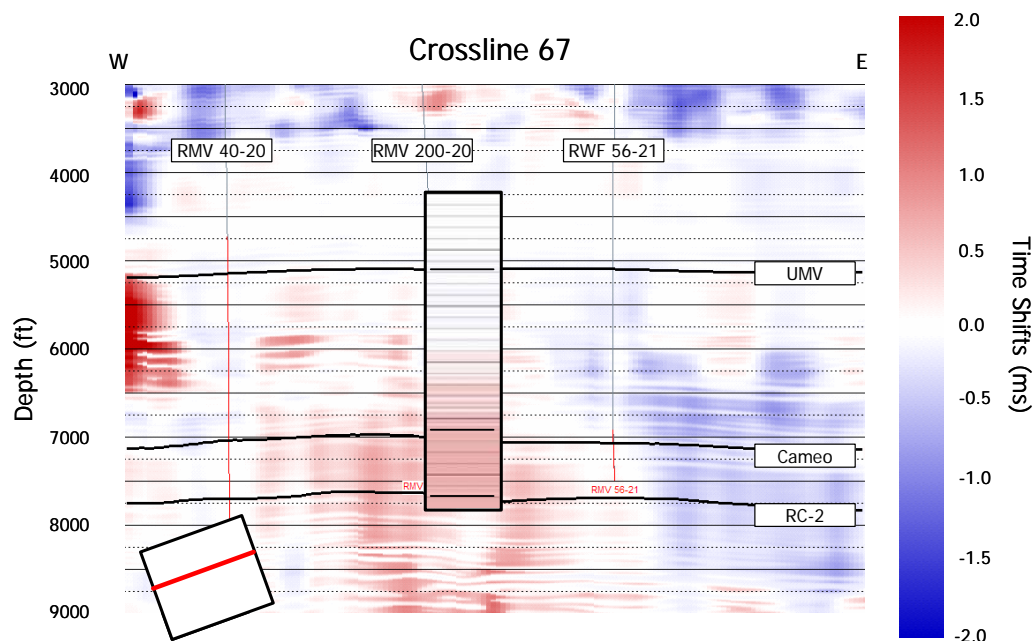


Figure 5.3 - A section through the time-variant time shift volume indicates that there is an accumulated positive shift of nearly 0.7-ms. An overlay of one of the modeled scenarios shows that it is consistent with modeling where the shifts are positive.

There are also negative time shifts of up to a millisecond. A map of the time shifts at the Cameo level shows that most shifts within the high fold region of the data are either zero or positive (Figure 5.4). A map of the maximum correlation values calculated with the time shift indicates that the waveforms are highly repeatable because the correlation values within the high fold portion of the survey are all above 0.95 (Figure 5.5). Therefore, the dominant shift is positive and is not due to low correlation values. The negative shifts are also not due to low correlation values. Since there is no reason to invalidate them, the negative shifts may be real time-lapse signal that indicate a mechanism not included in modeling. A Rulison specific time-lapse geomechanical model, like the kind employed by Hatchell and Bourne in 2005, may aid in the understanding of these negative time shifts. It is also possible that they represent the noise level, and in that case, the significance of the positive time shifts is questionable.

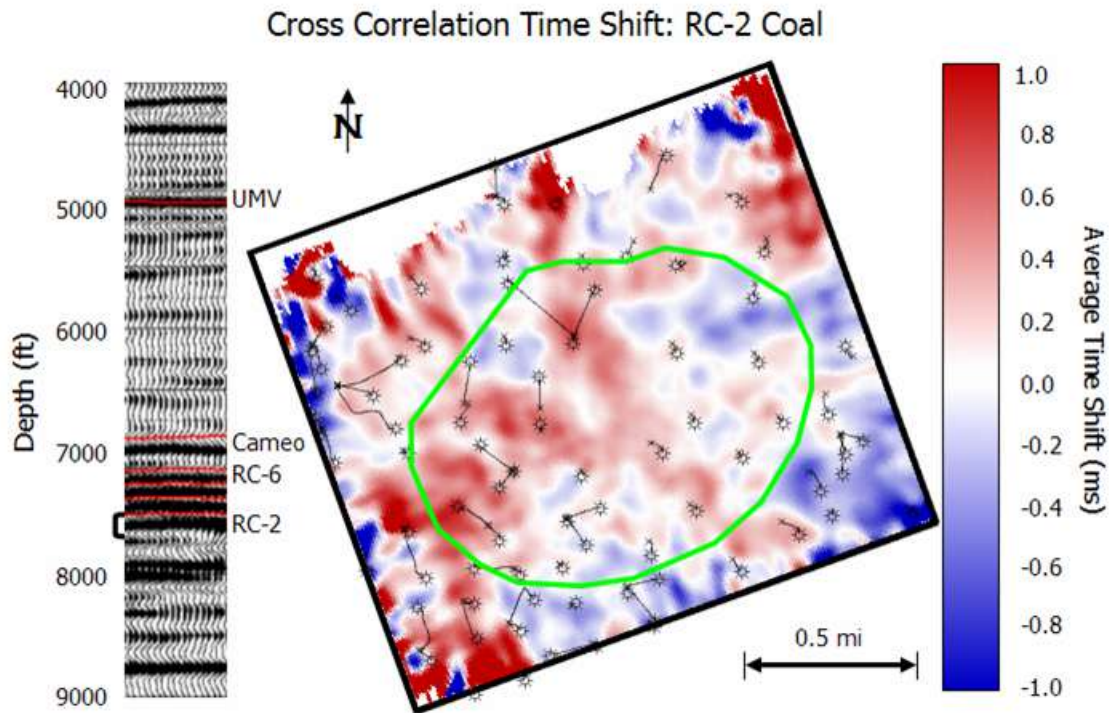


Figure 5.4 - A map of the derived cross-correlation time shifts shows that within the region of high fold, the time shift is predominantly positive.

Applying a 0.5-ms threshold to highlight the largest anomalies and makes clear that the largest shifts in the high fold regions are approximately 0.7-ms (Figure 5.6). There are nearly no negative time shifts in the high fold region with a magnitude greater than 0.5-ms. Therefore, the largest time shifts are positive indicating velocity increases in those areas. This is consistent with the modeling of time shifts due to matrix production in sandstones. Most of the anomalies in this figure are associated with wells in the western portion of the survey. These wells, Clough-19, RMV 33-20, RWF 433-20, and RWF 532-20, are circled with black dashed lines.

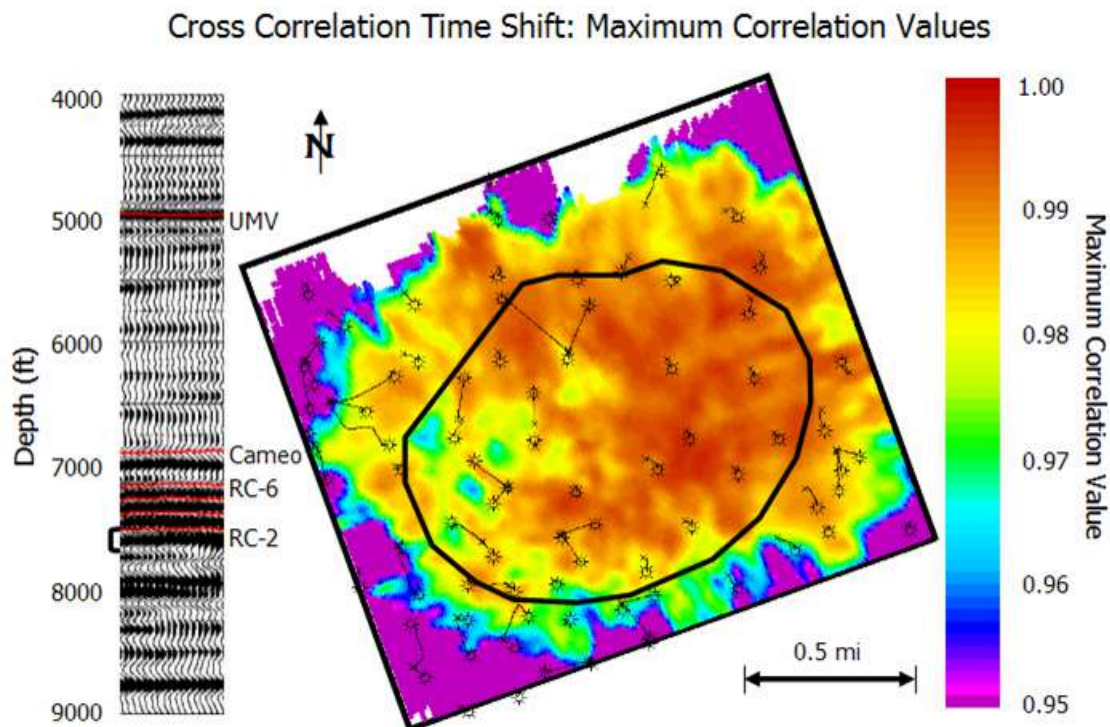


Figure 5.5 - The shift does not appear to be the result of low correlation values as the correlation values are nearly all above 0.95.

The time shift anomalies are not correlated with production volume. The largest anomalies indicated in Figure 5.6 have varied production in the time lapse period (Figure 5.7). The five highest producing wells show no significant time shift anomalies. Thus, it is apparent that production volume is not directly linked to the presence of large time shift anomalies. An overlay of production on the time shift anomalies shows this (Figure 5.8). Proof of this lack of correlation is shown in Figure 5.9. The plot shows the time shifts from Figure 5.4, averaged over a 350 ft radius at each well in the high fold area's bottomhole location, plotted against the production during the time-lapse interval. The correlation coefficient is zero, indicating no simple relationship between the two. Changing the averaging radius does not improve the correlation.

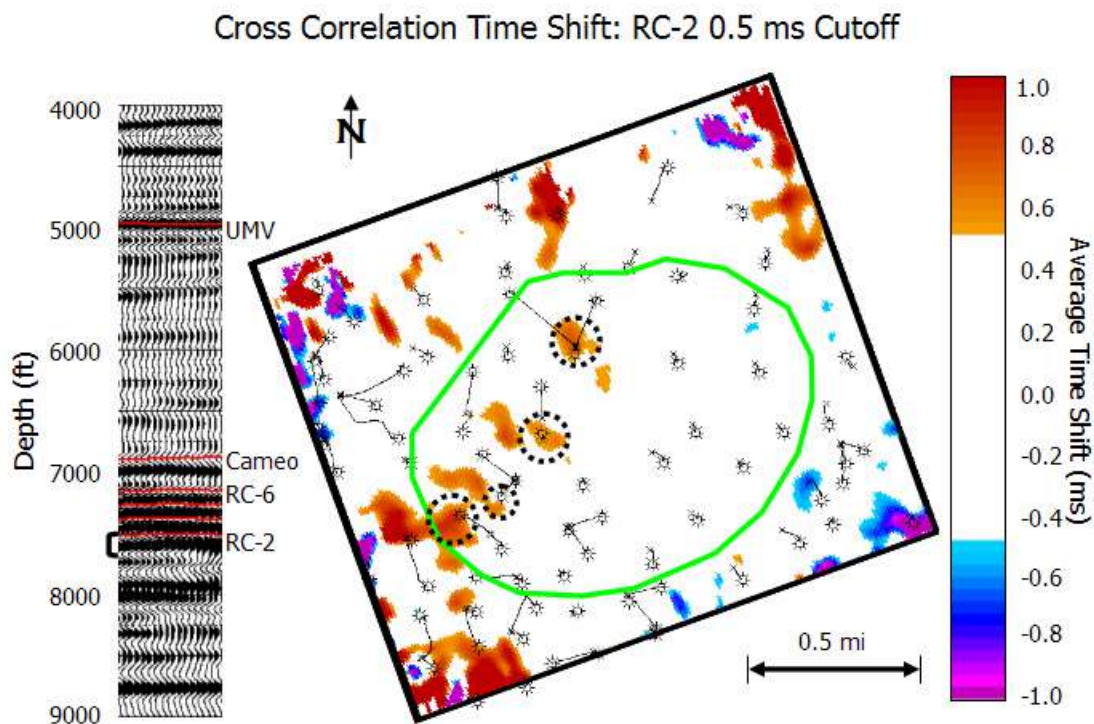


Figure 5.6 - The time shift at the RC-2 with a 0.5-ms mask indicates that there are very few shifts over 0.5-ms. All wells that produced in the time-lapse interval are shown. The high fold zone is shown in green. The wells associated with anomalies are circled.

The time shift magnitudes may not correspond to produced volumes for several reasons. First, the noise may be too high to accurately determine the production related time shifts. However, even with shifts above the noise level production may not correspond to large time shifts. This is because the time shift response is dependent upon the number, thickness, and pressure decline of each producing zone. The total production from a well during the time-lapse period is the sum of the production volumes of each of these individual zones. The pressure decline is related to production volume, but the relationship is not necessarily a simple one. The volume of the productive zone, the permeability, and other factors play a role in this relationship.

For instance, a few thin zones with large pressure decline have the same time shift response as many thick zones with a moderate or low pressure decline. This is illustrated in Figure 5.10. It shows zero offset time shifts calculated using varying thicknesses of producing sands and pore pressure declines. The curves are calculated using the following equation:

$$\Delta T = \frac{2x}{V_o + \Delta V} - \frac{2x}{V_o}$$

The relationship used for the change in P-wave velocity (ΔV) due to the change in effective pressure is shown in Figure 4.3. The initial P-wave velocity (V_o) is assumed to be 14500 ft/s, the average log P-wave velocity in the sandstones in RWF 332-21. The sum of the thicknesses of the producing zones is denoted by x and α is assumed to be one.

These curves show that the shift for a 200-ft producing interval with a 2000-psi pore pressure decrease will be nearly a millisecond. The same is true for a 400-ft producing interval with a 1000-psi pore pressure decrease. Thus, with a stack of thin producing sands that have variable total thickness, like at Rulison, the cumulative time shift response is not unique. The picture is complicated by the fact that the production and pressure decline in each reservoir unit is not likely to occur at the same rate. Highly permeable zones may dominate production initially and keep tighter zones from flowing until later. Also, the pressure decline in any zone is a function of the permeability, reservoir unit volume, and flowing pressure: not simply production volume alone. Further complication may occur if mechanisms other than production from the matrix of sandstones are causing 4D effects. These mechanisms may include production occurring from lithologies other than sandstones, fracture closure, or stress arching.

Therefore, in order to relate the time-shift anomalies back to production or pore pressure decline, engineering knowledge and data are necessary. If pore pressure decline is the driving force behind time-lapse changes at Rulison, it is important to understand

how it will behave under realistic production scenarios and what this implies for 4D changes. For instance, knowing how quickly the pore pressures are expected to drop and the rate at which the pressure front spreads from the wellbore are crucial to understanding how large changes should be and when to shoot repeat surveys to optimize monitoring. This means that pressure data over time at individual producing zones, or a realistic reservoir simulation of the field or individual wells are necessary to fully understand the time shift anomalies.

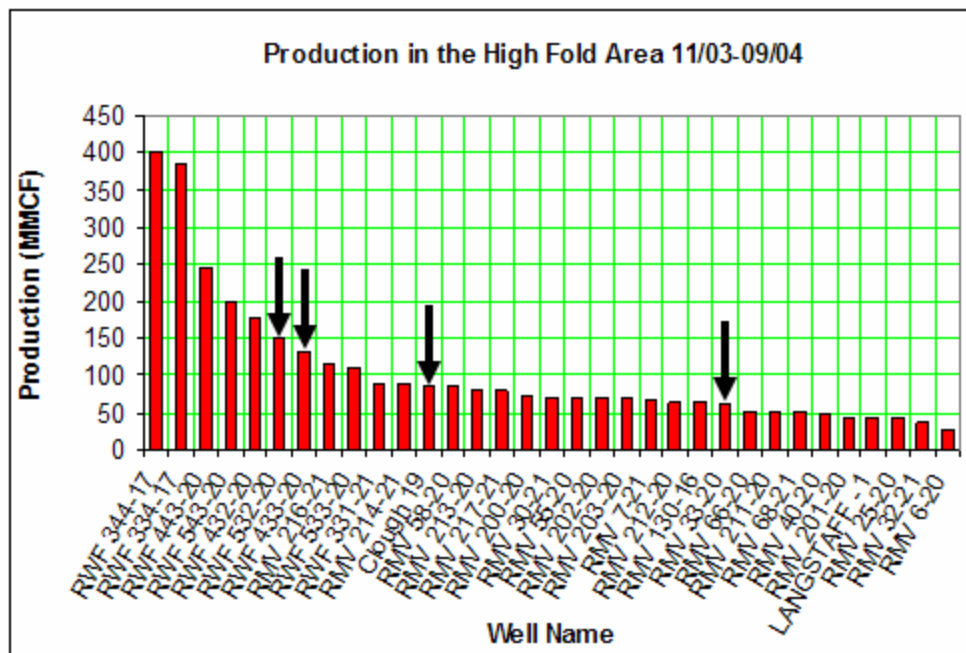


Figure 5.7 - The production at each well in the high fold zone during the time-lapse interval shows that the four wells associated with the largest time-shift anomalies (black arrows) are not the highest producers.

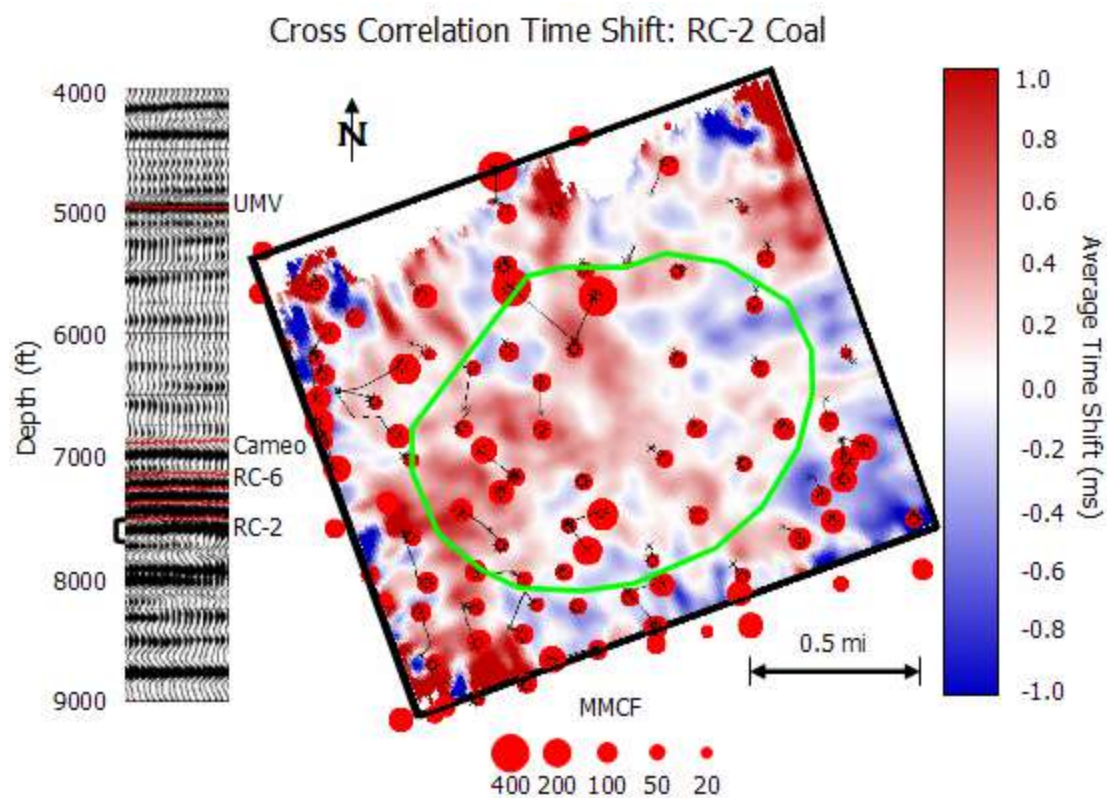


Figure 5.8 - The time shift at the Cameo with the total production during the time-lapse period indicated in red dots. There is a general correlation, but there is not a direct correlation between high production and high time shifts.

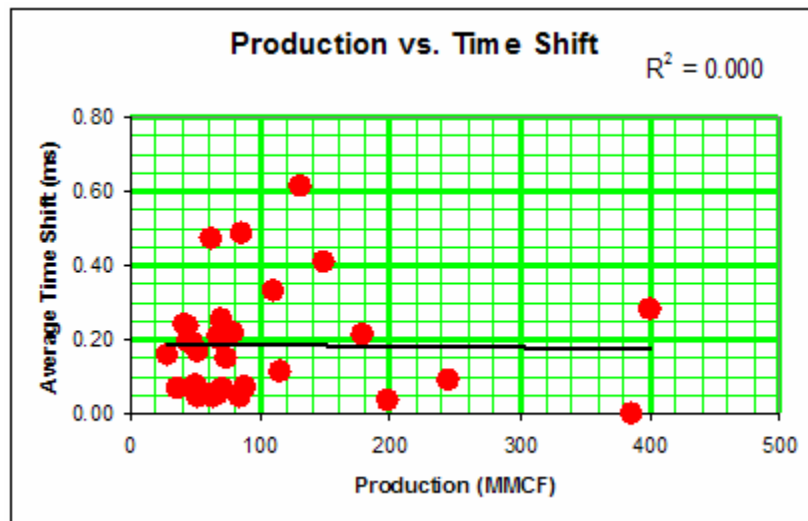


Figure 5.9 - A cross plot of production vs. the time shift averaged over a 350-ft radius around each well location shows that there is no relationship between the two.

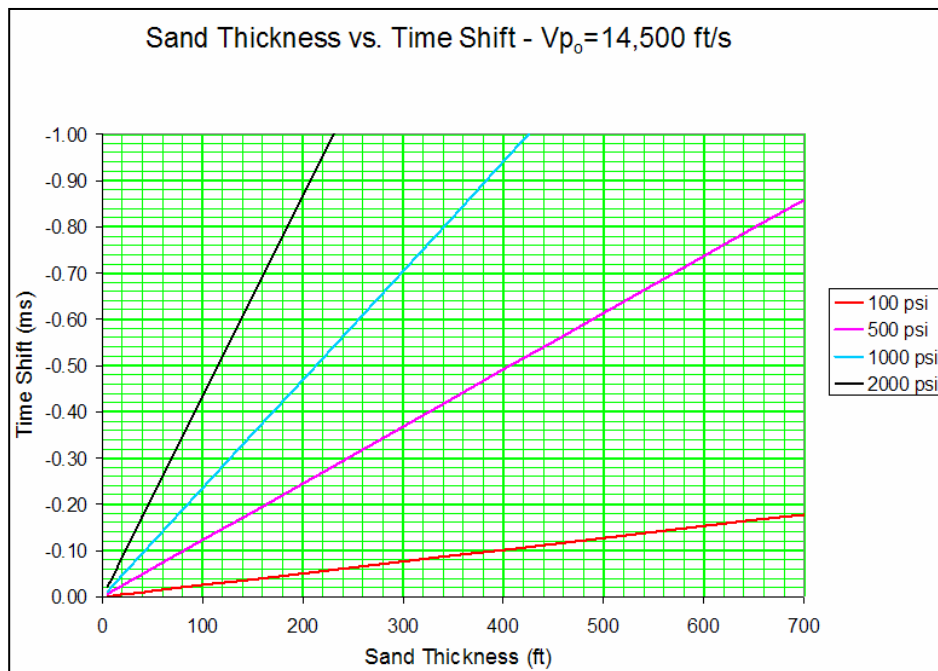


Figure 5.10 - The calculated time shifts for varying sums of producing sand thickness for different pore pressure declines indicate that time shift interpretation is complicated at Rulison.

5.1.3 Conclusions

The time shift interpretation showed that there are time shifts on the order of a millisecond in the Rulison data. These shifts are consistent with modeling in that they are generally positive and accumulate with time. However, there are also negative time shifts that either imply noise or mechanisms of 4D change that were not included in the modeling.

The magnitude of the time shifts does not correlate with production volumes between the two surveys, though the largest anomalies are associated with producing wells. However, time shifts are dependent upon the thickness and magnitude of velocity changes in the reservoir. These factors are related to the engineering properties of the reservoir; therefore, to fully understand the cause of the time shifts, integration of the 4D seismic with engineering data is necessary. Because the shifts are related to production and pressure decline which may vary zone to zone over time, repeat surveys may pick up larger time shifts and indicate whether some zones undergo pressure decline later than others.

5.2 Amplitude Analysis

The concept of amplitude analysis in time-lapse data is simple: find changes in the amplitude of reflectors between the two surveys. Reflection strength is determined by the reflection coefficient, which is a function of the impedance contrast at the reflecting boundary. Any change in that impedance contrast will manifest itself as an amplitude change in seismic data. Therefore, changes in seismic amplitude indicate an impedance change in the earth between the two surveys.

In practice amplitude analysis is not that simple. First, care must be taken in acquisition and processing to preserve seismic amplitudes so that differences are not obscured or new differences created. Chapter 3 explains that the Rulison data are acquired and processed for time-lapse purposes, meaning that whenever possible, the exact same procedures and parameters are applied to both data sets. Only the statics, surface consistent amplitude equalization, and deconvolution were applied independently.

Even with careful acquisition and processing, unwanted differences in amplitude still occur. Cross normalization procedures are used to lessen these differences, though these corrections can be problematic. Cross normalization calculates the ratio of the RMS amplitude over a time window of common trace pairs. These ratios are applied to the traces of one volume to scale them to be more comparable to the traces of the other volume. The process can also be applied over several windows to calculate a time varying scaling function. In order to avoid removing time-lapse signal, it is important to calculate the gain function using reflectors in which no amplitude change is expected. Typically, these are reflectors well above or below the reservoir. Sometimes, a large window over the reservoir is used. In any case, this method makes the assumption that the scaling between the two traces is a simple function of time. While this may generally be true, even slight variations in trace scaling can introduce amplitude anomalies on the order of the expected time-lapse signal. Thus, it is important to understand the noise associated with the amplitude changes.

It is also important to characterize the changes and try to determine their physical cause. This is done through acoustic impedance inversion. A reliable inversion, combined with knowledge of the production and geology of the field indicates in what lithology the changes occur, whether it is an impedance increase or decrease, and what process caused that change to occur.

5.2.1 Repeatability

Modeling indicates that impedance increases due to production will be approximately 1%. In order to see such a small change highly repeatable data is necessary. It is also necessary to understand the noise level and limitations of the data in order to be confident that the amplitude changes are time-lapse signal.

The first limitation can be the recording equipment. At Rulison, the data are 24-bits and sampled at 2-ms. The receivers use accelerometers that can record signal up to $\pm 3.3 \text{ m/s}^2$ and have a dynamic range of 118 dB at 2-ms sampling. This translates to a minimum signal of $5.23 \times 10^{-12} \text{ m/s}^2$. The equivalent input noise of the receivers at 2-ms sampling is $5.95 \text{ } \mu\text{m/s}^2$. This will translate to a base noise level in seismic amplitude, but I do not have the information to calculate this.

Non-source generated random noise is also a cause of amplitude non-repeatability. At Rulison, there are several sources of random noise. Primarily these sources are in the northern part of the survey. A drill rig noise is present in the northwest corner of the 2004 survey. Also, in both surveys there is noise due to an oil-shale processing plant in that same area. The northern center part of the survey contains a garbage dump that was active during both shoots. Finally, there are the standard natural sources of random noise like wind and weather, etc... Random noise is alleviated through the high fold of stack (up to 220) present in this survey. The amplitude of the random noise in the stacked data is difficult to separate out and it will vary depending on fold.

The positioning differences between the source and receiver locations between years are also a source of error. These errors cause the surveys to sample different parts of the earth from each other. In a homogeneous earth, this is not a problem, but in the real earth, scatterers are present. These scatterers cause what appears to be noise, but actually, is quite repeatable provided the near surface has not changed. Therefore, closely repeating the geometry closely repeats this scattered noise. This is important because scattered noise, unlike random noise, is coherent over short distances. Stacking does not attenuate it as quickly as random noise, and therefore, for 4D purposes, it is critical to repeat it (Calvert, 2005).

At Rulison, traces with source and/or receiver deviations up to 55-ft were allowed into the stacked data, though there were few deviations that high. Nearly 95% of source and receiver positions are within a tolerance of 2.5-ft: an estimate put forth by Rodney Calvert as a tolerance that would provide excellent scattering repeatability for land data. Thus, provided the near surface has not changed, scattering is probably not a major cause of noise (Calvert, 2005).

If the near surface changes, some source generated noise may not be repeated exactly. Slight differences in the statics corrections indicate near surface velocity changes occurred (Figure 5.1). This causes phenomena like ground roll and scattering to not be repeated exactly and can induce amplitude differences between the surveys. A detailed pre-stack analysis is necessary to estimate this effect, and therefore I do not attempt to estimate it.

It is possible to estimate the total noise in the post-stack amplitude data using the static section. Ideally, in the static section, there should be no amplitude differences. Thus, after cross equalization, amplitude changes in the static section should serve as a rough estimate of the noise level. A map of the maximum absolute percent impedance changes over the static section (700 to 925 ms) indicates the largest changes in that section (Figure 5.11). A subjective low noise area is encircled in the solid black line. This is not a strict boundary, especially because noise will change with time, but it serves

as a guide for interpretation at deeper levels. Of interest in this map is the high noise section in the northwest. This is likely due to the drilling, oil-shale plant, garbage dump, and low fold in this region. Also, the largest changes in the statics corrections between surveys are in this northern part of the survey.

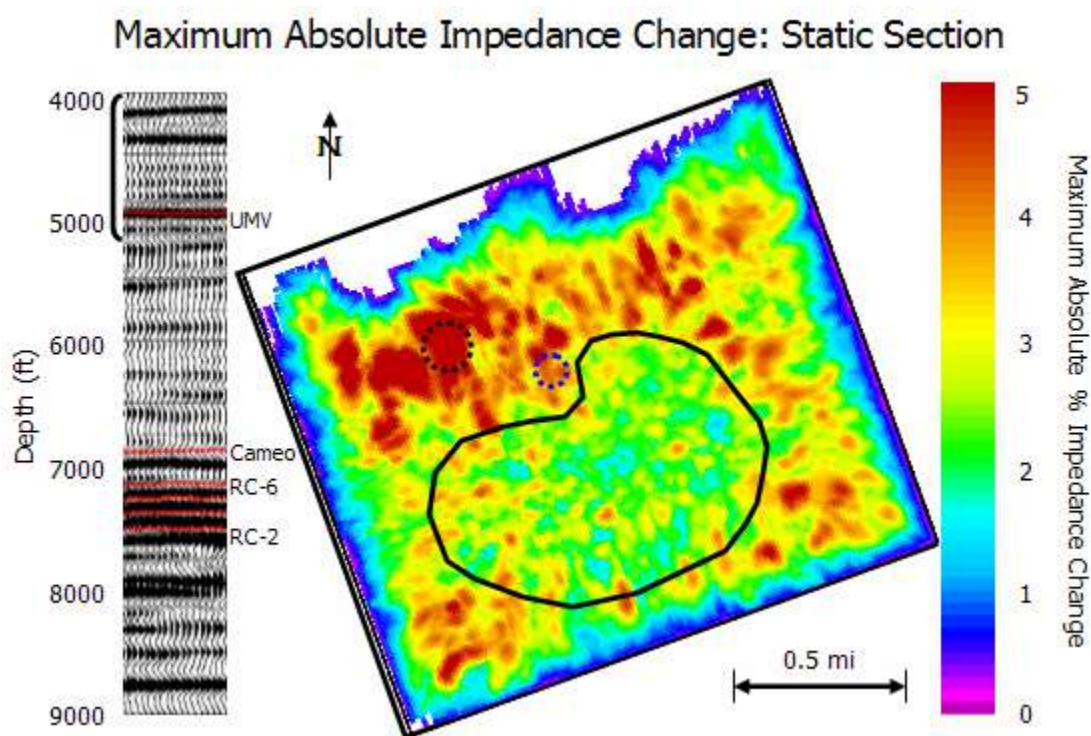


Figure 5.11 - The maximum absolute impedance changes over the static section indicate the noise level to be approximately 4% in the highest fold portion of the survey. The solid black line indicates the low noise zone. The black and blue dashed circles indicate the approximate locations of the oil-shale plant and garbage dump respectively.

It is also necessary to keep in mind the systematic amplitude changes that were removed during the comparison gain process mentioned in Chapter 3. While these changes are assumed to be removed from the data, they may not be removed perfectly. Artifacts could still remain, especially in areas where the corrections were especially large. The percent seismic amplitude differences before the application of the comparison gain process at the UMV and Cameo horizons are shown in Figure 5.12. They indicate significant differences are removed in the north. Thus, artifacts may remain in the north, though for interpretation purposes it is assumed that the differences have been removed.

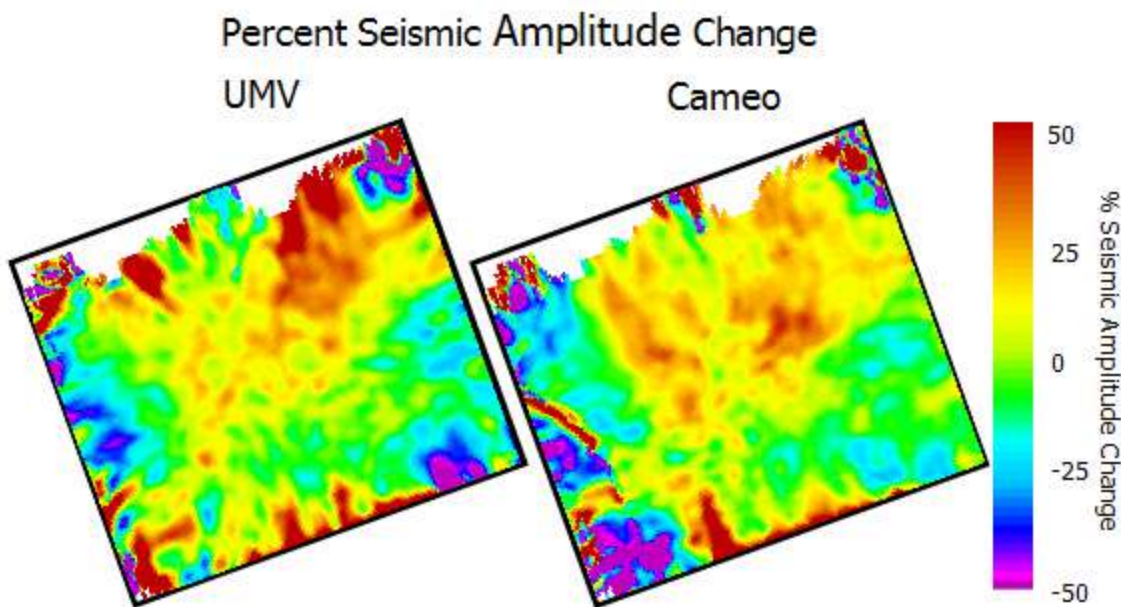


Figure 5.12 - The percent seismic amplitude difference maps at the UMV and the Cameo before the application of the comparison gain process.

Having an idea of the magnitude and sources of noise is important in trying to validate time-lapse anomalies. The factors identified in this section are therefore used to judge the validity of anomalies discussed in the next section.

5.2.2 Observations and Interpretation

A maximum percent impedance change map over the UMV to Cameo interval shows that this zone is similar to the static section (Figure 5.13). There, are almost no changes bigger than what are observed in the static section. There is a localized anomaly near the Clough-19 well (circled in black) that attains a maximum of 4.6%. This is significant compared to the noise in the static section.

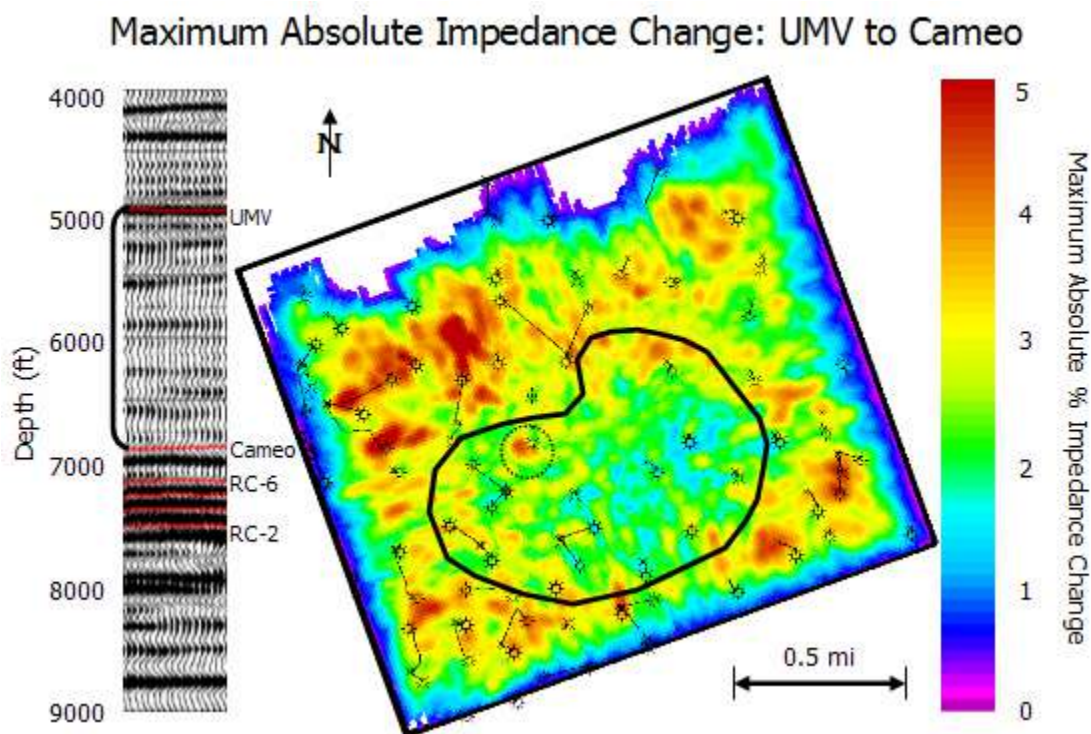


Figure 5.13 - The maximum absolute percent impedance change from the UMV to the Cameo is very similar to the same map over the static section indicating that the changes are at or below the noise level. There is one significant anomaly at the Clough-19 well (circled in black).

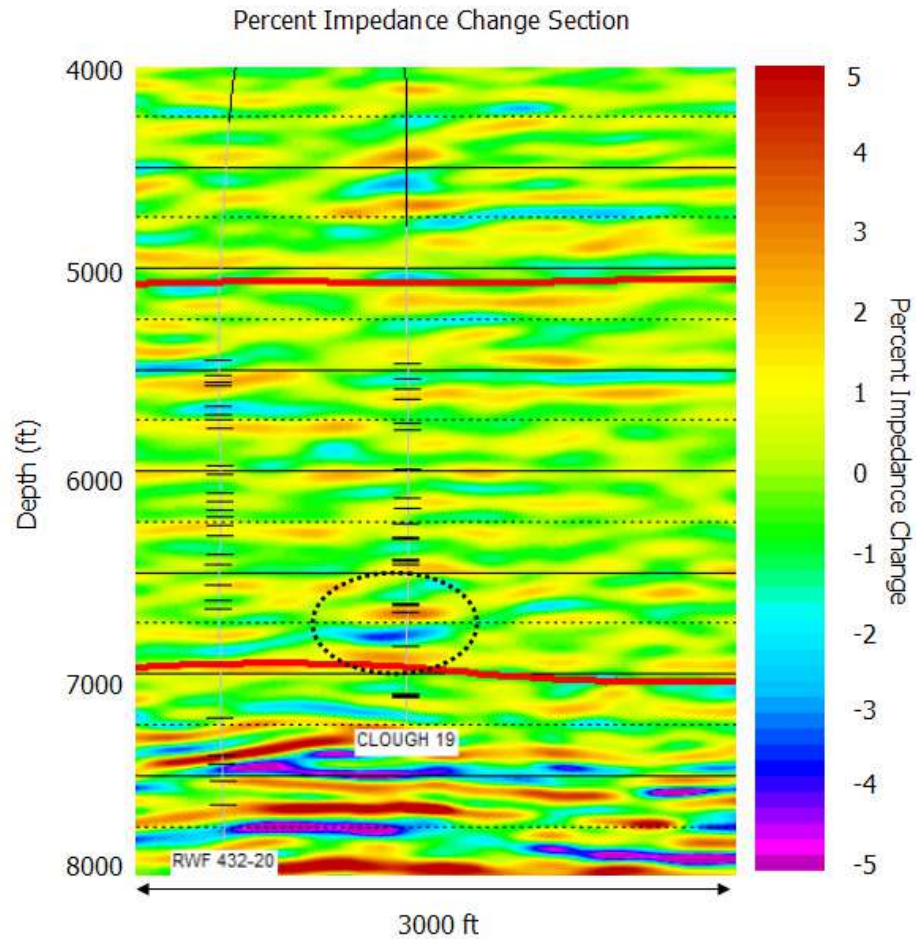


Figure 5.14 - The anomaly at the Clough-19 is associated with perforations. The perforations are the black lines perpendicular to the wellbore.

A cross section through this anomaly reveals that the apparent impedance increase is associated with perforations Figure 5.14. It is also larger than the background fluctuations in this area. These facts support the idea that this anomaly is real time-lapse signal. The Clough-19 is a relatively old well. The completion at the level of the anomalies is from 1995.

A comparison of Figure 5.13 with production reveals that the highest producing wells are not associated with significant anomalies in the Upper Williams Fork (Figure 5.15). This is not surprising given that there is only one anomaly that is significant compared to the changes in the static section. However, that anomaly is not associated with high production.

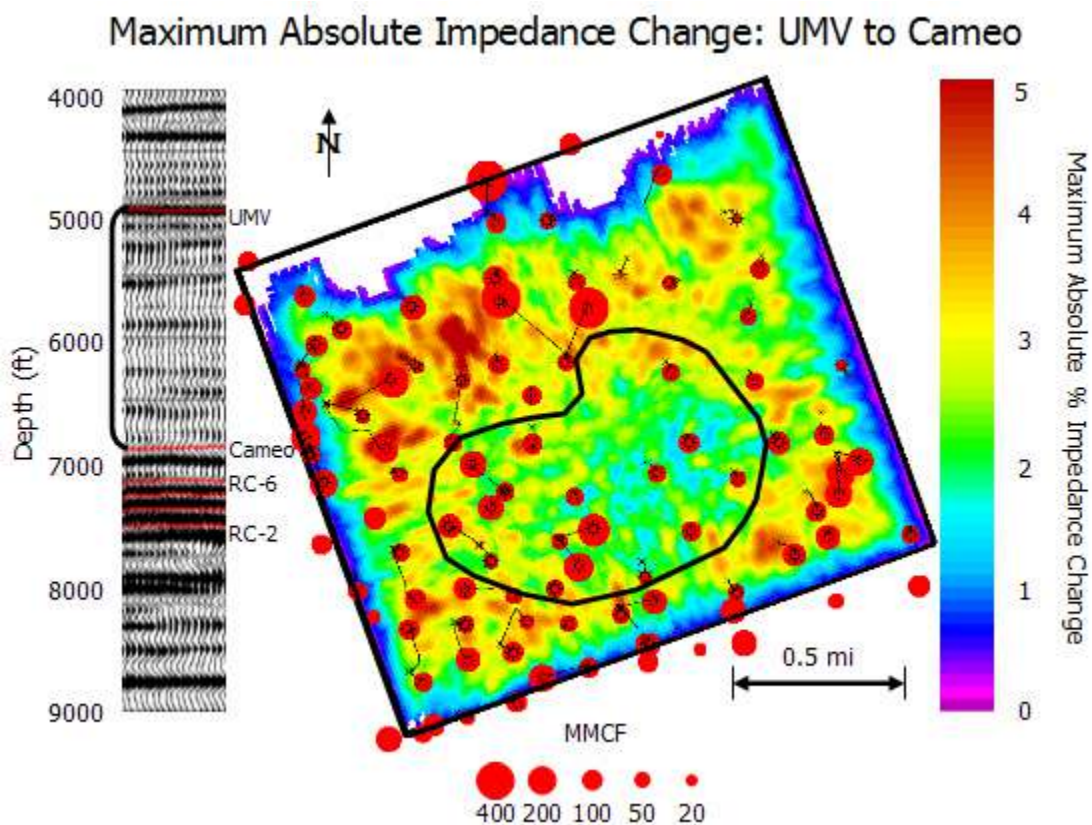


Figure 5.15 - The maximum absolute percent impedance change from the UMW to the Cameo has no relationship to production.

There are several possible ways to explain the observations of the impedance differences in the Upper Williams Fork. First, it may be that the pressure decline in this section of the reservoir is not large enough to cause observable amplitude changes in this seismic data, even if it is producing large volumes of gas. Mahendra Kusuma's work with the 1996 DOE survey and the 2003 RCP survey indicates that the rocks show an amplitude response to production. The anomaly near the Clough-19 well also seems to be indicating that. However, Kusuma's survey has a 7 year time interval while this survey has only a one year interval. Over one year, it is possible that the pressure decline is simply not large enough to provide a time-lapse signal in most producing zones.

Another way to explain the observations is that the Upper Williams Fork is not producing enough gas to cause large time-lapse anomalies during this survey. This is not to say that it is not producing, but it is possible that the Lower Williams Fork produces more gas, and therefore has larger pressure declines, than the Upper Williams Fork. Evidence supporting this idea is seen in map of the changes at that level.

A map of the maximum absolute percent impedance changes in the Lower Williams Fork indicates larger changes at that level (Figure 5.16). Impedance changes over ten percent are present. In the north the changes are as large as 30%, and are unrealistic according to modeling. These extreme changes are probably noise from the sources mentioned in the previous section or artifacts of the comparison gain process.

There are some changes within the low noise region that are separated from the northern region of unrealistically high change. In fact, nearly every well is near a change larger than 4% (the noise level derived from the static section). The Clough-19, RWF 432-20, RWF 532-20, and RMV 202-20 are all in an area of especially large change (shown with black dashed circles).

A closer inspection of the anomaly near the Clough-19 well indicates it is at the level of the RC-3 coal. A percent impedance change slice through this level indicates that the anomaly is an impedance decrease (Figure 5.17). The slice is created by making an RMS impedance slice for both years over a window hung 100' below the RC-3 coal.

The 2003 slice is subtracted from the 2004, divided by the 2003, and then multiplied by 100. The Clough-19 anomaly is circled in black. The two large changes in the north are probably indications of noise in those areas.

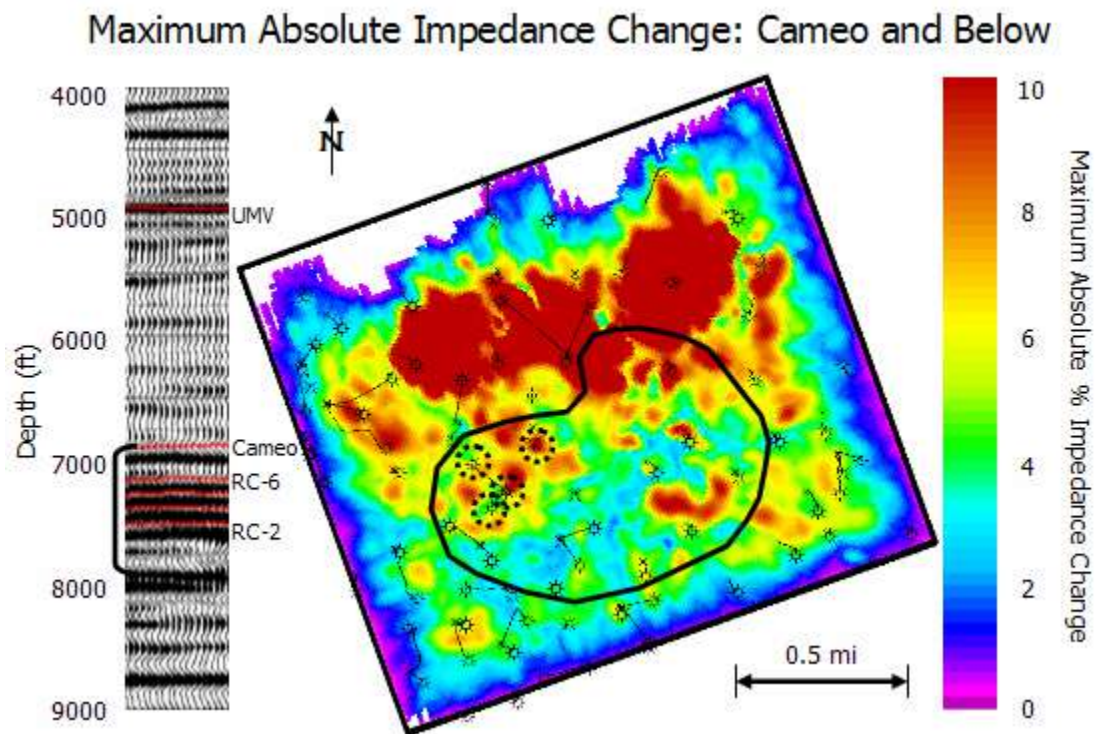


Figure 5.16 - The maximum absolute impedance changes in the Lower Williams Fork are significantly larger than the changes in the Upper Williams Fork. The black circles indicate wells that began production during the time-lapse interval.

Sections through the impedance volumes near the Clough-19 are also instructive (Figure 5.18). They also show that the anomalies are impedance decreases in the low impedance zones and impedance increases in the high impedance zones. These changes indicate, that the faults, interpreted by Kjetil Jansen's coherency work (shown in red), are possibly acting as a conduit for production since the well is not drilled to this depth (Jansen, 2005). This is reasonable given that the fault is only approximately 700' away

from the wellbore. Completions at Rulison can produce fractures over 1000' away from the wellbore and are nearly east-west. Therefore, it is possible that the fault is connected to the well and is allowing gas to be drawn up from below (Figure 5.19).

It is also possible that well RWF 432-20, which is perforated at that level, is drawing in gas from under the Clough-19 well. However, the anomaly is not centered at that wellbore. In that case, the anomaly may indicate enhanced natural fracturing due to the proximity of the fault. In any case, the proximity of the anomaly to the fault is interesting, and indicates that faulting and its associated fracturing must be accounted for in reservoir models.

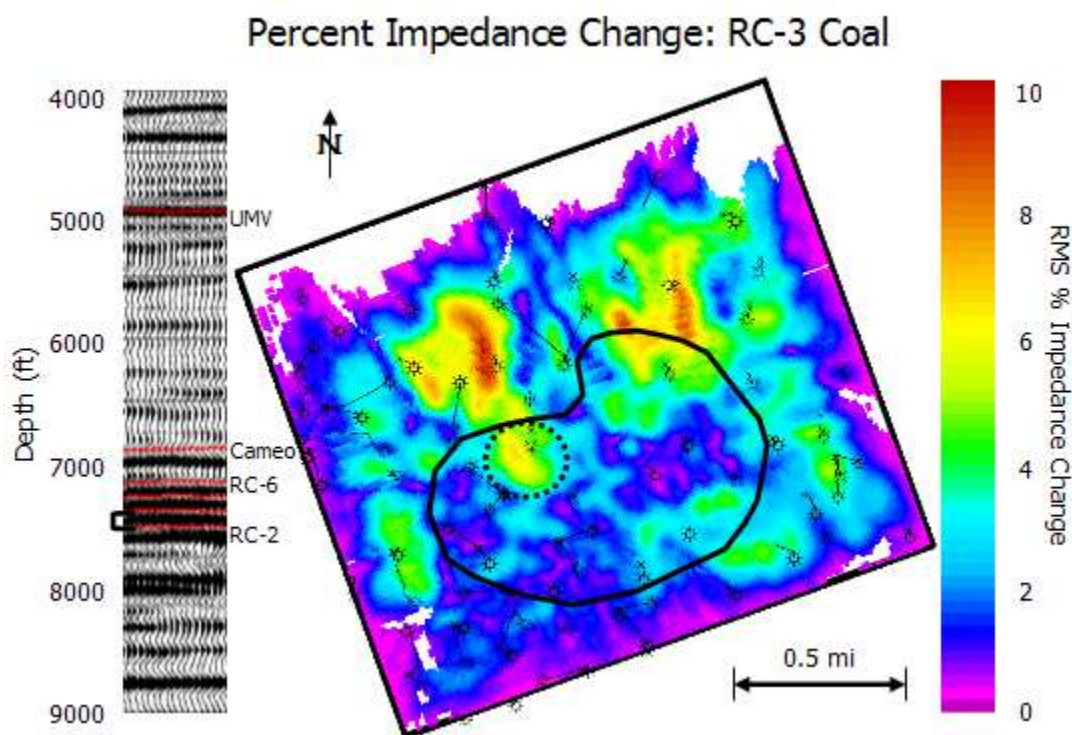


Figure 5.17 - An impedance change map from the RC3 level of the Lower Williams Fork is shown above. The dashed black circle indicates a possible real anomaly.

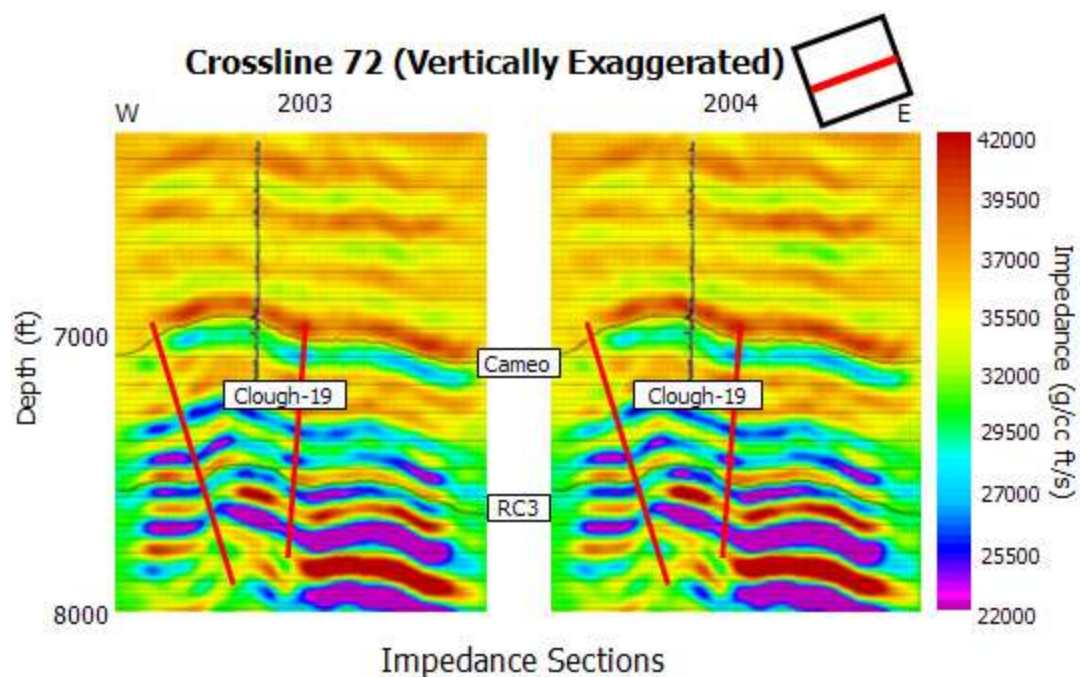


Figure 5.18 - Cross sections through the impedance volumes between years 2003 and 2004 indicate some impedance changes in the Lower Williams Fork.

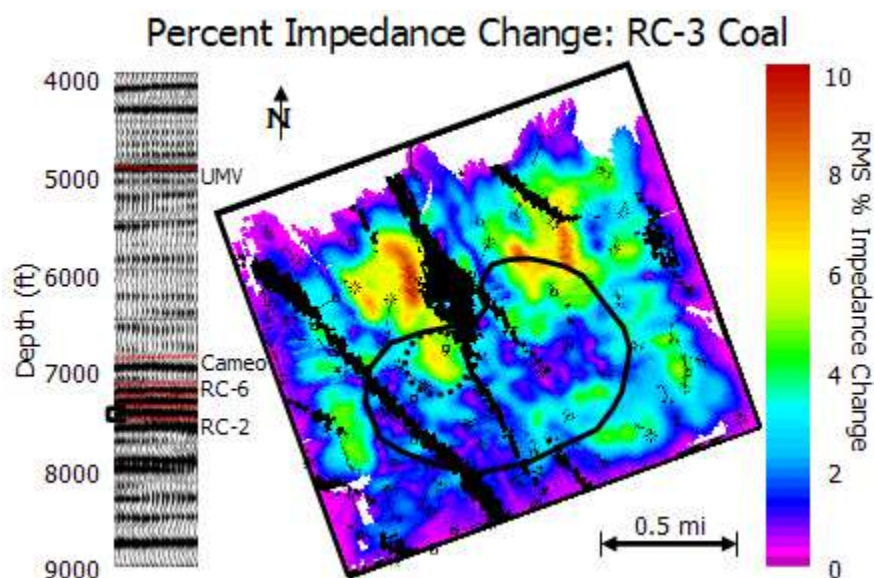


Figure 5.19 - The impedance changes in the RC3 coal are located near faults interpreted from coherency volumes.

It is apparent from the impedance change maps and sections that there is little change in the Upper Williams Fork and relatively large change in the Lower Williams Fork. As mentioned earlier, this may be because there are larger pressure changes and greater production in the Lower Williams Fork. It is also possible that the rocks in the Lower Williams Fork are more sensitive to time-lapse changes than the rocks of the Upper Williams Fork. In any case, why should there be any difference at all between these two sections?

Geologically, the major difference between the Lower and Upper Williams Fork is the presence of coal in the former. These coals may be causing the large discrepancy in time-lapse response. Coals experience large velocity changes with changes in stress, especially if the coals are dry and highly pressured with gas (Yu et al., 1993). The gas in the coals of the Lower Williams Fork is dry. Also, the Lower Williams Fork can be overpressured with gradients up to 0.8-psi/ft (Koepsell et al., 2003). Therefore, it makes sense that any stress changes in the coals could yield a large time-lapse signal. These changes could be due to stress arching from production in the sands (Tura et al., 2005). Also, production could be occurring from the coals. Production from coals can lead to the closing of the cleat system through an increase in effective pressure. However, it can also lead to the opening of the cleat system due to shrinkage of the coal matrix from desorption (Cui and Bustin, 2005). An opening of the cleat system could explain the observed impedance decreases in the coal reflectors. Prior to 1996 the coals were targeted for production and produced gas. Thus they have the potential to produce. Also, image logs indicate that they can be highly naturally fractured Figure 5.20. Therefore, it is possible that even sands completed adjacent to the coals are connecting the coals to the wellbore.

More work is necessary to completely explain the time-lapse response in the Lower Williams Fork. Rock physics measurements on Rulison specific core samples would be ideal; however, this is somewhat unrealistic. Coring coals is difficult and expensive. Samples from the MWX site exist, but may be too altered from their original

state to be of value. Modeling based on coal properties derived from the MWX study and other sources may be useful. Specifically, a geomechanically coupled reservoir model that included coals could provide insights into the details of the time-lapse response. Also, pore pressure measurements in the Williams Fork, at individual producing sands, over time would be invaluable. These are expensive, but they can show what zones are producing, how pressure decline varies from zone to zone, and how quickly pressure declines in individual zones. Information like this would be incredibly valuable for tying the time-lapse response to the production of the field.

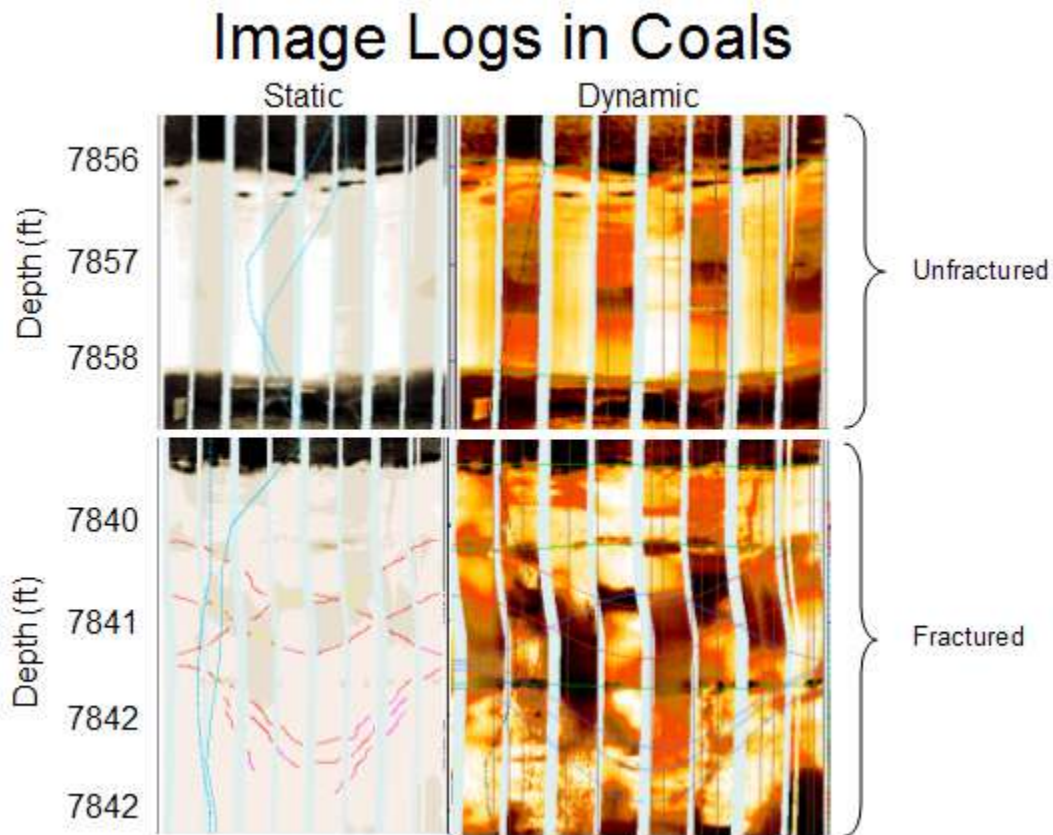


Figure 5.20 - Image logs indicate that the coals can be fractured or unfractured.

CHAPTER 6: CONCLUSIONS AND FUTURE WORK

6.1 Conclusions

One conclusion that can be drawn from this research is that the time shift data indicate that velocities in the Williams Fork are increasing near some wells. The magnitude of these shifts is not correlated to production volume, though the shifts may still be due to production near those wells. Determining what zones are producing to cause those time shifts is difficult. A better understanding of production and how it relates to pressure decline in individual zones is necessary.

Another conclusion that can be drawn is that the velocity changes due to production in the Upper Williams Fork are too small to be seen with these data. There is only one small anomaly in the section that is barely above the noise level estimated in the static section. This may be due to low pressure decline or low production during the time-lapse interval. Another survey should be shot in order to see if a larger time interval, and possibly a larger pressure decline, will cause anomalies above the noise level in this section.

The amplitude analysis also shows that there are significant amplitude changes in the Lower Williams Fork. The changes are larger than the changes in the Upper Williams Fork, and may be due to the presence of coal. Coals can be fractured and very sensitive to stress changes. These stress changes can come from production in the coals or stress changes in the coals due to production in the sands. A better understanding of the properties of the coals at Rulison, and the production in the Lower Williams Fork is necessary to determine the exact cause of the time-lapse response at that interval.

This work also showed that production from the deeper zones may be along faults and their associated fracture zones in some areas. The anomalies in the Lower Williams Fork near the Clough-19 well are below the depth at which it was drilled. They are

however, adjacent to a fault mapped by a previous RCP student Kjetil Jansen (Jansen, 2005). The well is close enough to have tapped into this fault and pulled up gas from depth.

In all, this work indicates that the Lower Williams Fork is showing the largest time lapse change. Therefore, future interpretations and logging programs should concentrate on this interval to find out if it is exhibiting a large change due to high production or high sensitivity. The role of the coals should be more clearly investigated. If the larger response is in fact due to high production, the interval should be aggressively targeted for production with focus on the coal bearing zones.

6.2 Future Work

A recurring theme in this work is that more work is necessary to tie the time-lapse response to production in the field. Primarily, this involves understanding the relationship between reservoir pressure, production volume, and time. A reservoir model that could be used to simulate time-lapse data may be a way to do this. Pore pressure measurements at individual reservoir units over time are another way, but they are very expensive. Of special interest would be pore pressure and production measurements in the Clough-19 well. If there is a deep zone that is still producing at a high rate and has little pressure decline, the argument that gas is migrating from depth will be strengthened.

More work needs to be done to understand the time-lapse response of the coals at Rulison. Measurements on the coals in the MWX cores may be useful. Also, geomechanical modeling of the Lower Williams Fork under different production scenarios, including coal production, may yield insights into the large amplitude changes in that zone. Specifically, a model of the area near the Clough-19 or RWF 432-20 well would be interesting since that area shows the largest changes in the Lower Williams Fork. In such a model it is important to consider the decrease in permeability due to

increases in effective stress, and an increase in permeability due to a shrinkage of the coal matrix (Cui and Bustin, 2005).

Pre-stack analysis of the P-wave time-lapse data may see some production induced effects more clearly. For instance, near or far offsets stacks may be more sensitive changes in the reservoir. Also, if fractures are closing, comparing traces of different azimuths may show this better than stacked data. In the coal intervals, near wells Clough-19 and RWF 432-20, this technique may be especially effective if the cleat system is closing. Pre-stack data may also be used to better estimate the repeatability of the seismic data and what can be seen with it.

A higher quality inversion may also improve the interpretation of the data. Since the producing intervals can be very thin, on the order of 5- to 10-ft thick, improved seismic resolution could aid in determining exactly what the time lapse anomalies mean. This will be critical for attempting to estimate pressure declines in individual sands based on seismic data.

Analysis of the S-wave time-lapse data may also help to better understand the response of the reservoir to production. Changes in anisotropy can indicate whether or not fracture closure is playing a large part in the time-lapse response. This may be especially useful in the coals if a well developed system of cleats is closing. S-wave data may also be more sensitive to effects like stress arching than the P-wave data if the directions of the principle stresses are altered.

All this work will help to better understand the nature of production at Rulison field. Ultimately, if successfully integrated with the engineering data, it would allow pore pressure prediction and monitoring from seismic. Seismic, could then be used to more efficiently place wells and produce the field. At a cost of only approximately \$100,000 per P-wave survey, and a cost of nearly \$1.5 million per well, the surveys would be more than paid off by saving only one well. Therefore, every effort must be made to integrate the seismic and engineering data at Rulison so that tight gas sands everywhere may be produced at a lower cost.

REFERENCES

-
- Akintunde, O.M., 2005, Monitoring Coal Bed Methane Production: A Case Study from the Powder River Basin, Wyoming, United States of America: SEG 2005 Expanded Abstracts.
- Blakey, R.C., 2003, Paleogeography through Geologic Time, 4/4/06, http://jan.ucc.nau.edu/~rcb7/global_history.html
- Boyd-Gorst, J., et al., 2001, 4-D Time Lapse Reservoir Monitoring of Nelson Field, Central North Sea: Successful Use of an Integrated Rock Physics Model to Predict and Track Reservoir Production: The Leading Edge, v. December.
- Calvert, R., 2005, Insights and Methods for 4d Reservoir Monitoring and Characterization: Tulsa, OK, Society of Exploration Geophysicists.
- Cole, R., and Cumella, S.P., 2003, Field Trip Guidebook Stratigraphic Architecture and Reservoir Characteristics of the Mesaverde Group, Southern Piceance Basin, Colorado, *in* Peterson, K.M., Terrilyn, M.O., and Anderson, D.S., eds., Piceance Basin 2003 Guidebook: Denver, CO, Rocky Mountain Association of Geologists, p. 385-443.
- Cui, X., and Bustin, M., R., 2005, Volumetric Strain Associated with Methane Desorption and Its Impact on Coalbed Gas Production from Deep Coal Seams: AAPG Bulletin, v. 89, p. 1181-1202.
- Cumella, S.P., and Ostby, D.B., 2003, Geology of the Basin-Centered Gas Accumulation, Piceance Basin, Colorado, Piceance Basin 2003 Guidebook: Denver, Rocky Mountain Association of Geologists, p. 171-193.
- Davis, T.L., 2003, Integrating Dynamic Data into High Resolution Reservoir Characterization: Golden, CO, Colorado School of Mines.
- Eastwood, J., et al., 1998, Processing for Robust Time-Lapse Seismic Analysis: Gulf of Mexico Example, Lena Field: 1998 SEG Expanded Abstracts.
- Eastwood, J., et al., 1994, Seismic Monitoring of Steam Based Recovery of Bitumen: The Leading Edge, v. 13, p. 242-251.

- Elder, K., 2006, Inquiry to Customer Support, *in* Keighley, D., ed.: Golden, CO, Input Output, Inc.
- Evans, L., 2006, Williams Meeting: Denver, CO.
- Gabriels, P.W., et al., 1999, Time Lapse Seismic Monitoring of the Draugen Field: SEG 1999 Expanded Abstracts.
- Hatchell, P., and Bourne, S., 2005, Rocks under Strain: Strain-Induced Time-Lapse Time Shifts Are Observed for Depleting Reservoirs: The Leading Edge, p. 1222-1225.
- Hettinger, R.D., and Kirschbaum, M.A., 2002, Stratigraphy of the Upper Cretaceous Mancos Shale (Upper Part) and Mesaverde Group in the Southern Part of the Uinta and Piceance Basins, Utah and Colorado: USGS Geologic Investigations Series, v. I-2764.
- Hofmann, R., et al., 2005, Effective Pressure or What Is the Effect of Pressure?: The Leading Edge, p. 1256-1260.
- I/O, 2006, I/O System 4 Brochure, 1/11/06,
http://www.i-o.com/content/includes/pdfs/system_four_brochure.pdf
- Input/Output, I., 2005, I/O System Four Datasheet, 4/18/2006,
http://www.i-o.com/Resources/Product_Information/Datasheets/
- Jansen, K., 2005, Seismic Investigation of Wrench Faulting and Fracturing at Rulison Field, Colorado [Masters thesis]: Golden, Colorado School of Mines.
- Koepsell, R., et al., 2003, Applications of Borehole Images in the Piceance Basin, *in* Peterson, K.M., Terrilyn, M.O., and Anderson, D.S., eds., Piceance Basin 2003 Guidebook: Denver, CO, Rocky Mountain Association of Geologists, p. 233-251.
- Kragh, E., and Christie, P., 2002, Seismic Repeatability, Normalized Rms, and Predictability: The Leading Edge, p. 640-646.
- Kusuma, M., 2005, Analysis of Time-Lapse P-Wave Seismic Data from Rulison Field, Colorado [Masters thesis]: Golden, Colorado School of Mines.
- Lancster, S., and Whitcombe, D., 2000, Fast-Track 'Coloured' Inversion: SEG 2000 Expanded Abstracts, p. 1-4.

- Meunier, J., 2006, Re: Time Shift Accuracy, *in* Keighley, D., ed.: Golden.
- Meunier, J., et al., 2001, Reservoir Monitoring Using Permanent Sources and Vertical Receiver Antennae: The Cere-La-Ronde Case Study: The Leading Edge, p. 622-629.
- Rickett, J., and Lumley, D., 2001, Cross-Equalization Data Processing for Time-Lapse Seismic Reservoir Monitoring: A Case Study from the Gulf of Mexico: Geophysics, v. 66, p. 1015-1025.
- Roche, S., 1997, Time-Lapse, Multicomponent, Three-Dimensional Seismic Characterization of a San Andres Shallow Shelf Carbonate Reservoir, Vacuum Field, Lea County, New Mexico [T-5050 thesis]: Golden, Colorado School of Mines.
- Rojas, E., 2005, Elastic Rock Properties of Tight Gas Sandstones for Reservoir Characterization at Rulison Field, Colorado [Masters thesis]: Golden, Colorado School of Mines.
- Tura, A., et al., 2005, Monitoring Primary Depletion Reservoirs Using Amplitudes and Time Shifts from High-Repeat Seismic Surveys: The Leading Edge, p. 1214-1221.
- Walden, A.T., and Hosken, J.W.J., 1985, An Investigation of the Spectral Properties of Primary Reflection Coefficients: Geophysical Prospecting, v. 33, p. 400-435.
- Winarsky, R., 2006, Processing Questions, *in* Keighley, D., ed.: Golden.
- Yilmaz, O., 1987, Seismic Data Processing, Investigations in Geophysics, Volume 2: Tulsa, OK, Society of Exploration Geophysicists, p. 103-105.
- Yu, G., et al., 1993, The Influence of Confining Pressure and Water Saturation on Dynamic Elastic Properties of Some Permian Coals: Geophysics, v. 58, p. 30-38.